MILLIMETER WAVE GENERATION TECHNIQUES FOR FUTURE COMMUNICATION SYSTEMS

By

Fawziya Al Wahaibi

For the degree of

DOCTOR OF PHILOSOPHY

College of Engineering, Design and Physical Sciences

Department of Electronic and Electrical Engineering

Brunel University London

London, England

2021

Abstract

Millimeter-waves (mm-wave) can be an attractive candidate for providing capacity improvements beyond 5G. Since mm-wave generation is the main factor in mm-wave communication, this thesis aims to generate high-quality frequencies in the mm-wave band using a cost-effect and straightforward design. The mm-wave generation converges with the Radio over Fiber (RoF) communication system through the data transmission.

A 60 GHz is generated based on carrier suppression using an external modulation method; for the first time, an inverted optical filter is used to suppress the carrier; the performance of the obtained signal worked effectively up to 10 Gb/s for 20 km.

A high-quality 72 GHz mm-wave signal based on carrier suppression is generated based on the quadrupling frequency technique; the Optical Suppression Sideband Ratio (OSSR) improved by 29.1dB. The performance of the resulting mm-wave signal is compared with two optical modulators, The Electro Absorption Modulator (EAM) and Mack Zehnder Modulator (MZM), along with two different types of photodiodes Avalanche Photodiode (APD) and PIN-PD. The resulting performance of the EAM is higher than the MZM, with a Q max factor of 20. Additionally, the power of the received 72 GHz signal is improved by 35% with APD.

A novel approach is introduced to generate an upper band of mm-wave frequencies through the 12 frequency tupling technique using parallel DD-MZM's only. In addition, the max Q factor of various transmission distances for the obtained frequencies is measured. The max Q factor for 300 GHz with 20 Gb/s over a 10-km transmission distance is 8.22 with a minimum BER of 1.97 × 〖10〗^(-28).

A performance of 300 GHz over free-space optics (FSO) over various distances was investigated using two FSO channel models, gamma-gamma and log-normal, with different attenuation levels.

The resulting performance is highly desirable with a max Q factor of up to 80 dBm / km to a 2000-m FSO link.

Therefore, mm-waves generated using the proposed designs could be implemented beyond 5G for future indoor and outdoor communication networks.

Acknowledgement

I want to thank my supervisor Professor Hamed Al-Raweshidy, knowing that I won't thank him enough for his fantastic professional and friendly support throughout my research. If it weren't for his professional and sharp level of guidance, I wouldn't be able to make it. I acknowledge the tremendous support out of my family as they were always by my side. I especially thank my lovely son, who always motivated me and kept me going through this special journey. I would specially thank my partner, who helped me to correct and proofread my thesis.

I would also thank all the Electronics and Electrical Engineering staff for engaging in discussions and assessments throughout my research. Finally, I would like to express my deep gratitude to all my friends and colleagues who made my PhD journey much more enjoyable and enlightening throughout the years.

Declaration

I declare that I carry out all the work in this research during my time at Brunel University London. This declaration is to be used as my statement for the work done in this research. The work done is not submitted to achieve any degrees or promotion unless otherwise stated.

Table of Contents

Table of Figures

Table of Tables

Publications And Presentations

1. Al-Wahaibi. Fawziya, Al-Raweshidy. Hamed, Nilavalan. Rajagopal, Advances in Information and Communication, Investigate the Performance of 240 GHz Millimeter-wave Frequency over Fiber with 10 and 20 Gb/s, vol 2, 2020, DOI 978-3-030-39445-5_3.
2. Al-Wahaibi. Fawziya, Al-Raweshidy. Hamed, Intelligent Computing, Downlink High Quality 72 GHz Millimeter, Intelligent Computing, DOI 978-3-030-22868-2_25, 2019.
3. Al-Wahaibi. Fawziya, Hamed. Al-Rwashidi, Nilavalan. Rajagopal, Study the Performance of Optical Millimeter-Wave Based on Carrier Suppressed by Using an Inverted Optical Filter, Intelligent Computing, July 2019, DOI: 10.1007/978-3-030-22868-2_26.

List of abbreviation

APD	Avalanche Photo Diode
BSs	Base Stations
BW	Bandwidth
CS	Central Station
DD-MZM	Dual Drive –MZM
CW	Continuous Wave
EAM	Electro Absorption Modulator
EDFA	Erbium Doped Fibre Amplifier
FBG	Fibre Bragg Grating
FSO	Free Space Optics
Gb/s	Giga bit per second
GHz	Giga Hertz
GVD	Group Velocity Dispersion
LO	Local Oscillator
LoS	Line of Sight
MZM	Mach-Zehnder Modulator
mm-wave	Millimeter-Wave
OC	Optical Coupler
OSA	Optical Spectrum Analyser
PD	Photo Detector
PIN-PD	P-Intrinsic Photo Detector
QoS	Quality of Service
RAUs	Radio Access Units
RF	Radio Frequency
RoF	Radio over Fibre
RFLO	Radio frequency of a local oscillator
RX	Receiver
SMF	Single Mode Fibre
THz	Tera Hertz
TX	Transmitter
UHF	Ultra-High Frequency

Chapter 1 Introduction

1.1 Overview

Recently, there has been much research to meet the future demand and capacity congestion issues in future wireless communication networks. In particular, national-level 5G research organisations and missions have been proposed one after the other to achieve the 2020 technical targets, including the introduction of small cells, having mm-wave frequencies, and introducing massive MIMO in the wireless communication systems. These targets were adopted by the European Union (EU) 5GPPP/METIS, China IMT-2020 (5G) Promotion Group, Korea 5G Forum, and Japan ARIB [1]. The ITU-R later and officially released a recommendation on 5G frameworks where 5G devices became available. Service providers launched the 5G networks, including 13 million 5G subscriptions worldwide at the end of 2019. Moreover, low latency video and multimedia applications for wireless devices are limited to a carrier frequency spectrum ranging between 700 MHz and 2.6 GHz.

In the first five years, the 5G subscription uptake is expected to be significantly faster than that of LTE-A, which was operated in 2009. However, there is a projection that 5G subscriptions might reach 2.6 billion by the end of 2025 [2]. Therefore, hiring a new frequency of mm-wave bands can become an essential solution to support various new applications beyond 5G wireless communication. Mm-wave frequencies are critical beyond the fifth-generation (B5G) mobile networks and wireless communication systems. B5G enables the wireless communication system to handle a massive amount of data and very high throughput per device from multiple Gb/s up to several Tera-bps (Tb/s).

Mm-wave bands operated between 30 GHz and 300 GHz could be suitable for various applications of mobile communication systems. Different frequencies and bandwidths are available in other mm-wave bands. For example, the Local Multipoint Distribution Service band (LMDS) is named for 28–30 GHz, 57–64 GHz, and the E-bands, which is called for 71–76 GHz. 81–86 GHz band, and 92–95 GHz [1][6][7]. The upper band of mm-waves is considered the lower band of the terahertz frequency (THz) in the range (0.1 THz to 0.3 THz) [3]. Many researchers and engineers have recommended the mm-wave band to provide higher bandwidth to handle massive capacity and data rate [4][5]. Mm-waves meet users' demand for services at high speed and high capacity [6][7][8][9][10].

Mm-waves over ROF have two essential processes: mm-wave generation and downlink data modulation [12]. The optical generation of an mm-wave signal is one of the main stages in mm-wave over fibre technology to obtain a high-quality signal. In addition, they are generating mm-wave at higher frequencies by using an external modulation technique to realise frequency-tupling. Optical generation of mm-waves using the external modulation technique is expected to have the advantage of being more accurate, with such schemes having shown the most potentiality for high-frequency signal generation owing to the sizeable tunable range, excellent stability, high spectral purity and lower system cost.

In addition, radio-over-fibre (RoF) technology provides a method for the convergence of wireless and Optical networks by merging the technical advantages of both networks. RoF has introduced system flexibility and enlarged the coverage area without increasing the cost and complexity [12][13][14]. Several Bell studies have reported that the fibre transmission link could carry up to 15.5 Gb/s over 7000 km. Therefore the advantages of ROF, including low propagation loss, large bandwidth, and low cost, and its immunity to electromagnetic interference, makes it one of the promising technologies for future mobile communication systems.

Based on the following limitations, extensive research has been conducted on developing mm-wave signal generation and transmission technologies. The electronics devices such as; a local oscillator (LO) with a higher frequency own a higher price and are harder to produce.

Additionally, the maximum frequency obtained from LO is 100 GHz. Therefore, a frequency-tuple technique with a frequency multiplication aspect could be a proper solution for generating mm-wave using a low input frequency local oscillator.

Despite the advantages of radio-over-fibre (RoF) technology, the demand for greater bandwidth used in the backhaul of the network and that for various applications by the subscribers have meant that the research industry needs to utilise higher frequencies; which consider as a limitation in the RoF system. Hence, mm-wave frequencies have become a solution to increase the power of the RoF technology, as a high bandwidth could be offered in wireless communication systems, and high-speed operation can be obtained [11][12][13][14]. Thus, integrating the features of mm-wave frequencies and those of fibre systems, which deliver a massive data rate and capacity, would lead to improved systems to meet the demand from wireless communication systems.

Large operational bandwidth can be offered to users and operators in the mm-wave bands. However, they have a significant propagation loss in the free space and metal cables [4]. By considering the characteristics of the mm-wave bands, the short coverage of free-space links with photonic links can integrate through optical fibre links. Furthermore, researchers have proposed to incorporate mm-wave signals over different transmission links like; free-space optics, fibre transmission links, and wireless systems, as is shown in Figure (1-2) [15] [16][17] [21].

As shown in Figure 1-2, this proposal highlights that mm-wave frequency generation should be considered critical for beyond 5G technology. In addition, FSO will also be another promising backhaul solution, as it offers both a high data rate and a relatively low cost [18].

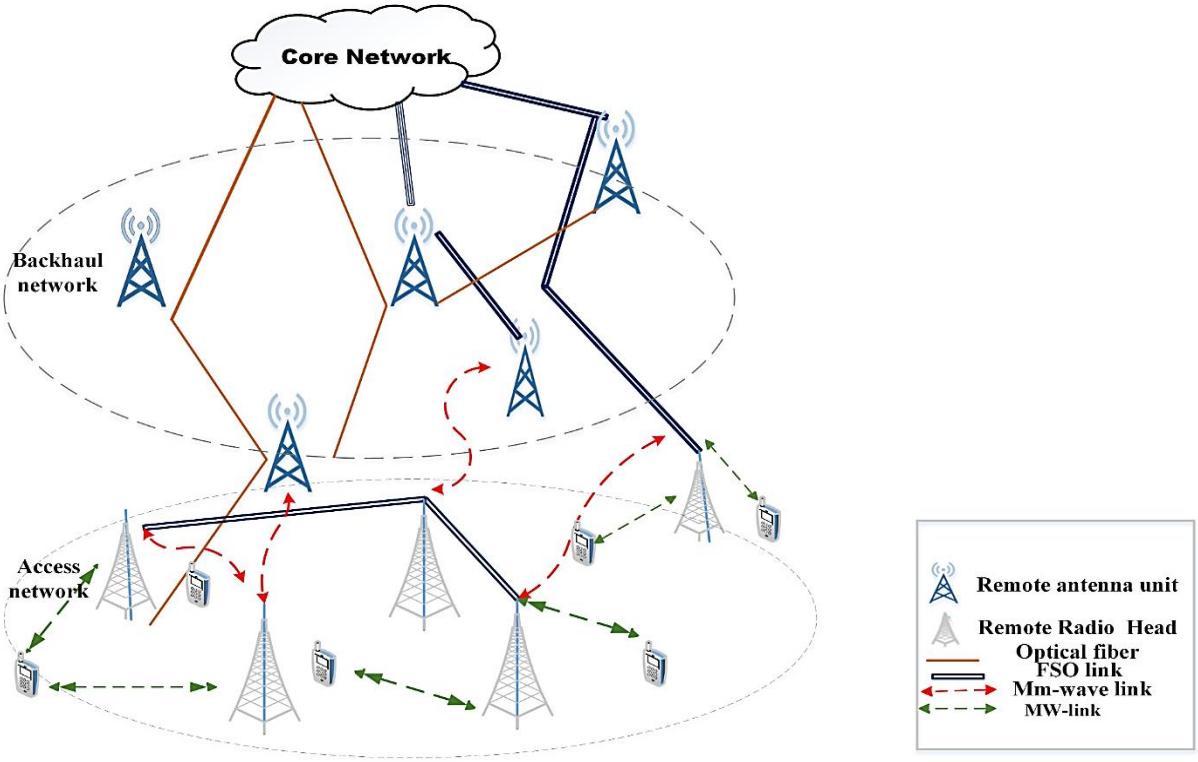

Figure 1-1: Proposal for mm-wave communication network beyond 5G [19]**.**

However, some challenges are still related to the integration of mm-waves in the RoF system, such as generating high-quality signals at mm-wave bands to overcome fibre issues, including dispersion and attenuation.

1.2 Motivation

It has been predicted that the global monthly traffic of mobile devices will be approximately 50 petabytes in 2021. The global mobile traffic volume was 57 EB per month in 2020, and this traffic is predicted to be 4394 EB per month in 2030, as shown in Figure 1-3. A [22]. Moreover, the data traffic per subscriber is predicted to increase about 48 times in 2020, as shown in Figure 1-3. B. This Figure shows that mobile traffic is estimated to grow at an annual rate of around 54% in 2020-[20][21], since the wireless communication toward a society of fully automated remote management systems.

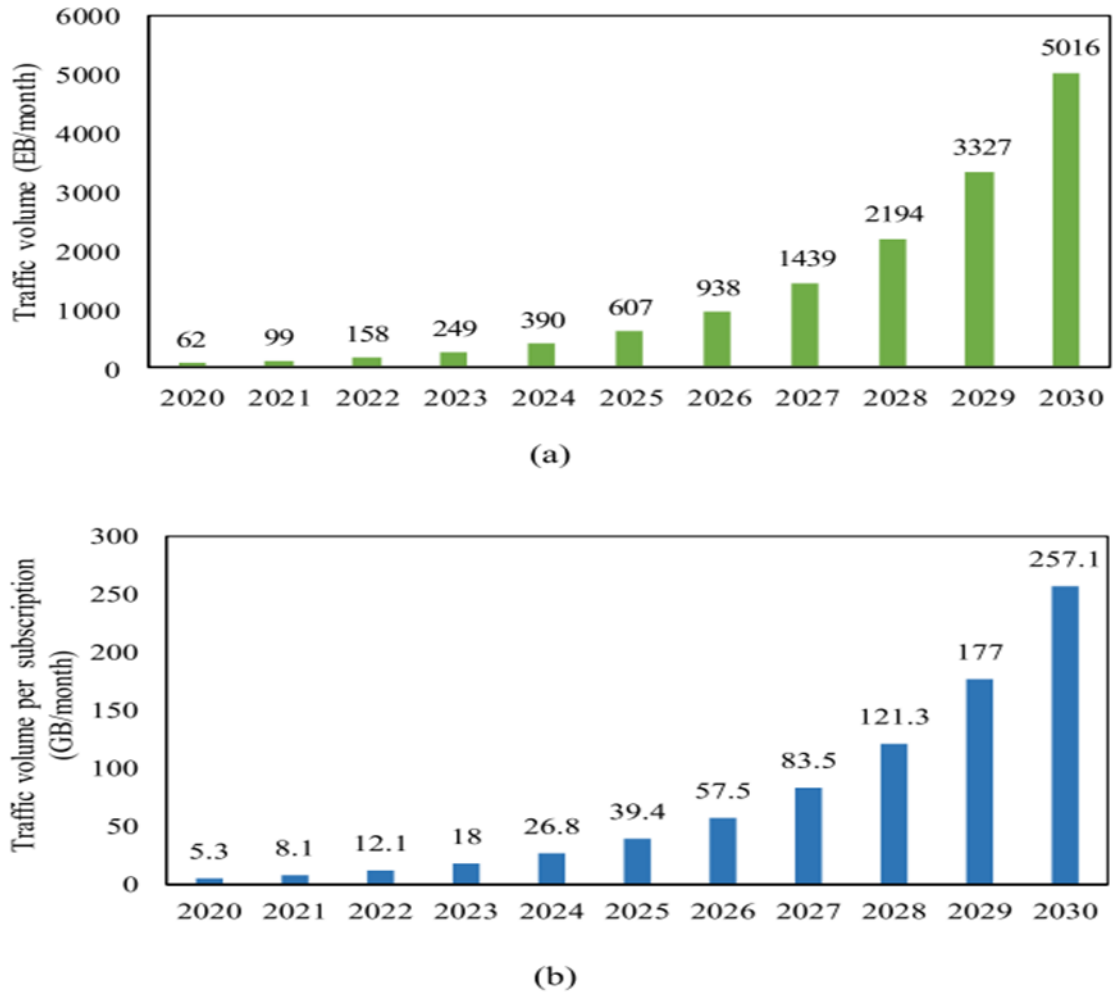

Figure 1-2: The predicted growth of global mobile connectivity during 2020-2030 [33]. (a) total global traffic volume, (b) traffic volume per subscription [23]

To conclude, the considerable volume of data and the number of devices will continue to grow exponentially in B5G, related to many new applications beyond personal communication [3][5]. Future wireless communication networks are expected to have higher frequencies. The mm-wave band is considered a promising spectrum for a futuristic wireless

communication system, which can compensate for the lack of bandwidth of the current wireless carriers. The compensation for the lack of bandwidth is because the mm-wave frequency bands are less crowded than the lower-gigahertz radio frequency bands and have wider license-free RF bandwidth available, such as 7 GHz bandwidth in the 60 GHz. Having mm-wave frequencies is a solution to handle more data traffic and resolve the current issues by increasing the communication system capacity. The mm-wave transmission still has some challenges, and many issues must be addressed when considering mm-waves for future wireless communication networks.

The first is the generation of mm-wave signals (30 GHz to 300 GHz), which implies that obtaining this relatively high frequency is challenging in the electronics generation domain; consequently, the optical generation method is preferred for obtaining this band. Additionally, the generation of high-frequency signals with high quality poses issues in electronics components and limits our ability to get frequencies in these bands [22][12] [23].

Regarding the cost, a local oscillator (LO) with a higher frequency is expensive and more challenging to fabricate to generate high frequencies [23]. Additionally, the maximum frequency can be obtained from LO is 100 GHz. In recent years several methods for an mm-waves generation were proposed. However, the application of mm-waves in communication systems still needs feasible and cost-effective ways to simplify the system setup. Therefore, the development of circuitry that operates at mm-wave frequencies optically is possible.

The integration between mm-wave and RoF systems is needed to generate and deliver mm-wave signals. Moreover, the mm-wave transmission through fibre cables will be advantageous in overcoming the high path losses of mm-waves in wireless propagation. Unfortunately, the transmitting of mm-waves over RoF systems also faces some limitations because of the fibre nonlinearity effects; this drives the necessity of developing new photonic generation methods with the RoF system to reduce these effects.

Realising a low latency communication link is essential for future communication networks to support massive and various delay-sensitive applications. Latency in fibre-optic networks comes from three main parts: the fibre itself, the optical components, and the optoelectronic components. The applications of a long fibre link will increase the latency and add additional complexity to the networks. In addition, a long fibre link needs to add more components to improve the performance of the communication system, such as amplifiers, dispersion compensators, and repeaters. As a result, the further use of fibre will not support the 5G

requirements for achieving low latency (below 1 ms)[24] [14][14][25]. However, there is still a need for a comprehensive investigation to apply these systems for future networks.

Moreover, laying fibre cables is not possible in some areas with natural obstacles; therefore, applying an FSO link will increase the network coverage area to reach the last mile. The application of free-space optical (FSO) systems can provide a low-latency communication link because of the possibility of applying a direct optical communication link. Considering the high bandwidth of the FSO transmission link with a short-range distance is beneficial to obtain low-latency communications. In addition, there is a crucial need for verifying an efficient communication link; therefore, applying an FSO system can provide a robust solution in these cases. The latest studies have investigated the use of such a system to transmit a high data rate between two fixed points over a long distance[16] [17], [18][18]. Studying the collaboration between the mm-wave frequency and the FSO link is still an ongoing issue [23][25]. These issues have raised the importance of designing a new system that integrates mm-wave frequencies with the RoF system and the FSO link (as explained in the second contribution).

1.3 Aim and Objectives

This study aims to generate high-quality mm-waves at different frequencies in mm-wave frequency bands and reduce the number of devices used in the design. The reduction will make the procedure a cost-effective and straightforward method that can be utilised for future networks.

The objectives of the research are summarised as follows.

1. Generating a photonic mm-wave carrier at different frequencies in a cost-effective and straightforward setup to obtain high-quality mm-wave.
2. Investigating the multi-Gbits/s data transmission at the generated frequencies by transmitting the generated mm-waves over the fibre system. This process tenses a practical mm-wave generation method and downlinks data transmission. The proposed approach was demonstrated using the Optisystem software.
3. Investigating the availability of the utilised system to generate a lower band of terahertz frequencies to carry a high data rate. This process includes proposing a novel mm-wave generation and transmission system over a hybrid fibre/FSO link.

1.4 Contributions

There are two main original contributions presented in this thesis, and two studies in different techniques were used to generate different frequencies within the mm-wave band.

There are two main original contributions presented in this thesis, and two studies in different techniques are used to generate different frequencies within the mm-wave band.

The two studies are summarised below:

1. Generate mm-wave by using a single MZM only.

- Generating 60 GHz using the quadrupling technique.
- For the first time, Suppressed the carrier by using an inverted optical filter.
- Investigate the performance of generated signal with data of 2.5Gb/s to 10 Gb/s over fibre.

2. Generate high-quality photonic mm-waves using the quadrupling technique.

- Achieve high-quality mm-wave at 72 GHz at the transmission side of the (CS).
- Achieve Downlink data transmission over a fibre link using different data transmissions.
- Use of two external modulators to choose the better one.
- Use two photo-diodes at the receiver (RAP) to compare the performance of the generated mm-waves.

The two contributions are summarised below:

1. A novel system is proposed to generate a lower band of THz frequency at a low-cost and effective method.

- The performance of the generated frequencies is investigated by transmitting the modulated signals with 10 Gb/s and 20 Gb/s between the CS and RAP at different optical fibre lengths.

2. The performance of the lower band of THz frequencies is investigated by transmitting the modulated signals with 10 Gb/s and 20 Gb/s between the CS and RAP at different optical free-space (FSO) link distances.

1.5 Thesis Outline

The organisation of the thesis is described below:

Chapter One: Introduces the elements of the work presented in the thesis, provides detailed background about the mm-wave communication system and the mm-wave generation techniques. A discussion of the RoF and the FSO systems is also included.

Chapter Two: Presents a systematic literature review.

Chapter Three: Introduces the proposed method for generating mm-wave signals at 60 GHz, based on carrier suppression modulation. The design principle used for developing this frequency is explained. The effectiveness of this approach is studied in different data modulation schemes, and the simulation results are presented.

Chapter Four: Presents study in the proposed design of the generation of a 72-GHz mm-wave, discusses the design principle and the simulation setup of generating the frequency over an RoF system.

Chapter Five: Presents the first contribution and shows the method used for generating the upper band of mm-wave signals, the performance of the transmission of these signals over a fibre link, and the impact of achieving a high-capacity communication link.

Chapter Six: Presents the second contribution in transmitting the upper band of mm-wave signals over the FSO link, simulation setup, and the effectiveness of the transmitted signal over FSO considering its different factors.

Chapter Seven: Presents the thesis conclusion and the future work-related.

Chapter 2 Literature review

2.1 Overview

Many researchers have studied Millimeter-wave (mm-wave) signal generation for radio over fibre (RoF). The extensive research is due to the future demand for the mm-wave band, a communication system primarily used in wireless local area network applications involving wireless local area networks (WLANs). RoF is a methodology where high-frequency microwave transmissions are sent through optical fibre connecting the central station (CS) and the base stations (BSs). The application of optical fibre in mm-wave radio communication, signal distribution is critical.

Communication systems have been extensively examined to deliver high-bandwidth connectivity and compact cell sizes (picocell). Additionally, they have the potential for a low cost. Infrastructure is required to facilitate the development of broadband mobile services. This essay will discuss the overall picture of RoF technology is followed by configurations of RoF links where radio frequency (RF) signals can be conveyed directly over fibre, either at the RF or an intermediate wavelength signals of intermediate frequency (IF). The review is mainly concerned with generating mm-waves for radio over fibre, including heterodyning optically, external modulation, transceiver optical, and up-and down-conversion.

2.2 Initial Research Questions

This chapter organised to answer four research questions:

Q1 What are the definitions, concepts and conceptualisations of mm-wave communication systems? The radio of Fiber (RoF) technologies? And mm-wave generation techniques?

Q2 What is the current state of the art of the concepts for the present frequencies utilised over fibre?

Q3 What are the research issues of the present mobile systems?

Q4 What are the directions for future research?

The chapter is then structured into two main phases; the first phase will cover methodology and the scope of the literature.

The second phase of this chapter will cover (1) the literature review where the techniques of generating mm-waves, definitions, concepts, and the scope of RoF and communication systems are reviewed (2) the literature analysis and results (3) presents potential directions for future research.

2.3 Overview

Human life has been significantly impacted by information and communication technology. Nowadays, most daily life activities can be accomplished through Internet services [1]. Fifth-generation (5G) is a mobile networking standard that aims to provide significantly more data bandwidth and speeds than the preceding Long-Term Evolution (LTE) generation [2]. 5G infrastructure enables innovative technologies across multiple industry sectors because of its exceptionally low latency and excellent reliability [3]. This generation's services include expanded mobile broadband (eMBB), central machine-type communications, ultra-reliable low-latency (URLLC) communications, and fixed wireless connectivity, such as fibre.

Wireless communication networks are overgrowing to provide anywhere and anytime communication among various emerging applications in current life. With unlimited increases in mobile user devices and high demands for higher data rates, a massive amount of data traffic is essential. v. Data traffic is predicted to reach 50 Petabytes in 2021, about 12 times in 2016 [33].

Since the current frequency bands for 5G has to be licensed as presented in [8], AT&T confirmed that progress 5G in Sub-6 GHz Band [35] [36]. The 5G was initially launched in Europe and Asia to transmit signals over longer distances while giving up raw speed. However, Huawei Telecom Company introduced a new 5G base station that depends on third-generation massive MIMO antenna technology promising considerably faster 5G uploads and downloads over large areas. The company announced its speed hit a record of 3.67 Gb/s on sunrise's live 5G network [37]. In addition, regardless of handling the increase in data capacity for present wireless communication systems having been reached by improving the spectral efficiency by implementing advanced modulation schemes and signal processing technologies [38] [39] challenging to achieve 10 Gb/s or more.

Mm-wave communications Bandwidth expansion is a successful approach to accommodate the increasing surge in data throughput, notably in 5G devices [6]. Today, most filled cellular networks run below 3 GHz, confirmed in [7,8]. Bandwidth shortages prompted the discovery

of the rich mm-wave frequency range from 3 to 300 GHz [9]. Massive Multi-Input Multiple-Output (MIMO) is a developing technology [10]. Massive MIMO uses hundreds of antennas to service thousands of user terminals simultaneously. Massive MIMO seeks to exploit all of MIMO's advantages, but on a larger scale [11]. Single-User MIMO (SU-MIMO) is used in LTE to optimise spectrum usage in multiple antenna time and frequency division modes. LTE-Advance uses 8x8 MIMO to meet the IMT-A Advanced Criteria [12,13].

To fulfil the growing demand for increased channel capacity expanded service coverage, and broadband mm-wave access systems in the future, technology must be developed to match those criteria. RoF technology is the most promising approach for increasing the capacity and mobility of base stations (BSs) while also lowering their costs. Most signal processing functions such as RF generation, coding, multiplexing, and modulation can be performed at the central station (CS). Additionally, given the restricted availability of RF bands, it was anticipated that the mm-wave bands would be used to address the requirement for increased signal bandwidth and alleviate frequency congestion in future RoF-based optical-wireless access networks.

Modulation can be performed directly on the RF or intermediate frequency signal (IF). This approach is appropriate for the backbone of a wireless access network. This architecture has several advantages, including the potential to reduce complexity at the antenna site, dynamic allocation of radio carriers to the various antenna sites, and network transparency and scalability. As a result, the cost of establishing a microcellular antenna site can be significantly lowered. A distributed antenna network has several benefits: low RF power remote antenna units (RAUs), frequency reuse, increased coverage, high capacity, high-quality signal, and minimal fibre attenuation. These advantages contribute to RoF's attractive technology for various radio signal applications, most notably mobile communication systems.

It is evident; there is a demand to have more spectral resources for futuristic systems. Extensive research is being undertaken in developing telecommunications, especially mobile networks, to handle massive amounts of data with very high throughput per device of up to several Tera-bps (Tb/s) for beyond the fifth generation (B5G). Thus, it is necessary to get higher carrier frequencies within the frequency spectrum for future utilisation in wireless communication systems [26]. Utilising Terahertz will appear an attractive candidate for a wideband futuristic communication system.

There are several positive trends of owing a higher band of mm-wave frequencies, which consider a lower band of THz frequencies (100 GHz to 300 GHz) for future wireless communication networks[10] [27][28]. Firstly, a higher band of the frequency spectrum is needed to offer higher capacity wireless access networks to serve the increasing demands for mobile traffic and the internet of everything's application. Massive traffic is expected for future emerging applications in wireless communication systems like; extensive data analysis, artificial intelligence, 3D media and the internet of everything, as shown in Figure (1-3) [1].

Besides the increasing demand for data traffic, video traffic is also expected to experience increasing demand. Moreover, mobile communication applications will reach 70% of total mobile traffic in 2020 [1]. Hence, there is a pressing need for the upper bands of mm-waves to be exploited to handle the vast demands of data and video traffic for beyond 5G (B5G) applications. In particular, the bandwidth of the lower bands of mm-waves (26 GHz to 100 GHz) is limited to less than 7 GHz, which will not meet the stated demand.

It is anticipated that the upper bands of mm-waves (200-300) GHz could have applications similar to 60 GHz but with a higher bandwidth [29]. Secondly, the attenuation of the upper band of mm-waves (200 GHz to 300 GHz) can be countered in wireless communication systems at below 10 dB/km, as indicated in Figure (5-2), making them suitable for backhaul communications and future short-range wireless technologies[28]. Thus, utilising this band will address the spectrum shortage and capacity limitation of current 5G systems [30]. Thirdly, owing the upper band of mm-waves will increase the ability of wireless communication networks to serve the demand of the expected tremendous amounts of data. The massive throughput per user device could reach several Tera (T) bps at these bands.

Regarding that, the higher the frequency, the greater the bandwidth. Hence, Utilizing Terahertz (THz, 100 GHz to 3 THz) carrier frequencies is a potential solution to meet the increase in data demands. The high data rates involve the deployment of high-density small cells.

Providing backhaul connectivity to the small cells with a high data rate is appealing to use hole carrier waves in the frequency range to support multi-gigabit data rate[31]. These rates have garnered increased interest because of the vast bandwidth offered in wireless communication, and it has not been allocated for any application in these systems [32]. There has been a lot of researches that have shown the potential of THz communications, which

will deliver ultra-fast future wireless communication systems accomplishing rates of 10Gb/s and 20Gb/s [33][28][34][35][36].

Picocells, femtocells, and small cells occupying 100s to tens of metres are used to describe microcells. The restricted coverage area of the primary technology, particularly in 5G networks, enables higher data transfers and better network flexibility for smartphone users [18,19]. For a tiny cell, the simple approach is to locate the access cells as close as possible to the smartphone users [20]. Due to insufficient coverage, these tiny cells reach smartphone consumers with limited transmission capability [21]. As a result, small cell base stations can be located in streets, trees, and lampposts. The tiny cell principle's central tenet optimises spectrum reuse to increase network availability [22] thousands of properties in waves. Millimeter waves are electromagnetic waves with a range of 30 to 300 GHz. Typically, the range is (3–30) GHz, just below the mm-wave range [23].

This paper reviews the latest and most efficient methodologies used by researchers in the last five years to study 5G in many domains. The method's details, including algorithms/techniques, procedures, and findings, are summarised. The researcher also highlighted the most widely used ways.

2.4 Literature Methodology

Many articles and authors highlight the importance of carrying out the relevant literature study in all scientific research [37], [38] to add new knowledge to the existing scientific knowledge. The literature review identified what work was done relative to the area of research. It is essential to avoid duplication of research and credit the authors who carried out the previous work. This study started with the central questions related to the generation of the mm-wave frequencies. The author of this paper introduced the initial questions to guide the route of the literature research. The questions were directed towards the major scientific publishers, and to avoid bias with specific scientific publishers, more sources were used like google scholar. This method of research was suggested by [39] [40]. This research considers this literature method appropriate and enough for this research in line with Webster & Watson 2002. Although the time was not strictly specified, the literature started in November 2019. The study focused on "generation of mm-wave" and "transmission of mm-wave over optical communication" to reach the main aim of the research.

2.5 Procedure

The research will have a deep examination of the concept, maturity, creation, values, applications, techniques, and technology behind the generation of mm-wave signals to identify and create the most suitable way to enhance and increase the capacity of communication systems. The first step is to collect good quality publications, and with practical screening through at least the last ten years, [39] identified further three steps to refine the articles obtained.

2.5.1 Refinement of Articles

2.5.1.1 Step 1: Suitable publications and screening

Publication related to the study area was collected for the last ten years, including articles, thesis and conference papers. However, working and commentaries will be excluded for the quality of the publications collected. At the same time, the author identifies the keywords closely related to the mm-wave communication systems, such as 5G technology and beyond, Free Space Optical (FSO) technology, and RoF. The main aim of looking closely at the keywords is to fit the purpose of the scope of the study. So, when using the keywords, the databases resulted in more than 500 outcomes, the results articles were taken for further refining and analysis.

2.5.2 Step 2: Suitable screening process

This step focuses on the selection benchmark regardless of the time of the publication. Therefore, the author will not consider whether the paper was published in the present or past. However, the author focuses on the generation of the mm-wave frequencies and their transmission over fibre. The benchmark is summarised below:

- Optimisation of the applications and scenarios
- Providing a comprehensive overview of trends to review the mm-wave frequencies and framework

2.5.2.1 Step 3: Reference analysis

The reference analysis is the last stage where reference is examined; the original reference for the articles closely related was 165, after further investigation, it yielded 24 more articles. The generation of the mm-wave and its transmission were created as a category for article analysis to fit and match the focus of the study; through the research, ten more references

were added to make the study more solid in the understanding and concrete in concept. The Figure below summarises the literature procedure.

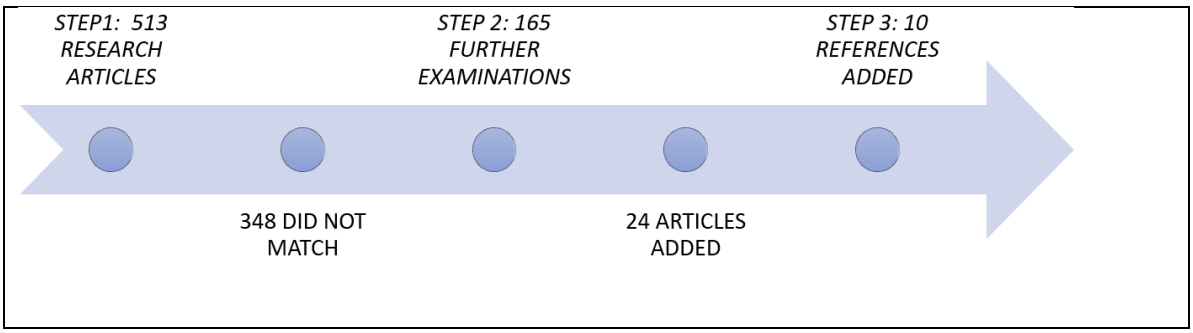

Figure 2- 1 Summary of the literature procedure

2.5.3 Scope of the review

The first step in any review is to determine the scope to determine the study's limitations, boundaries, and targets. [16] specified six dimensions to be followed while deciding the size of the literature. The author of this research will determine the area in line with [16] as follows:

Focus: With this reference, the author will focus the study on the concept, applications, methodology and the results

Aim: Concerning the second dimension, the author carrying out this study to identify limitations, gaps and issues which eventually lead to failure of the accurate and correct use of the technology

Perspective: The author of this research is presenting the literature from a neutral point of view and avoiding being bias

Coverage: This literature study will have the characterisation of being representative, and the author is determined to make sure this study should cover all areas around the focus to reach the aim

Organisation*:* Based on the coverage and perspective, the organisation is conceptual

Audience: The author presents this study to engineers, academic scholars specialising in engineering, technology scientists, and specialists in the telecommunication industry.

2.6 Literature review

This section will go over the most critical findings of some of the most current research in greater depth.

On the topic of 5G mm-wave communication system needs and radio frequency (RF) architecture design considerations, Chen in [38]provided an overview of the subject. He tackled the issues of design and growth patterns for the 5G mm-wave front-end module in this project. Mm-wave 5G base station and user equipment were equipped with four antennas (8/16/32/64) in a hybrid beamforming architecture he developed (UE). He also utilised a beam-tracking system to enable mobile transmission at speeds of up to 100 kilometres per hour. As a result of the growth of 5G technologies and the rapid introduction of new technologies, the Millimeter-wave wideband platform created by the Research Institute of Industrial Technology (ITRI) has been a highly scalable and versatile solution. Furthermore, a beam-tracking system has been designed to permit cell transmissions at speeds of up to 100 kilometres per hour.

Al-Ogaili and Shubair demonstrated the capability of the mm-wave expansion channel. The critical challenges connected with the usage of mm-waves were highlighted with the advantages and solutions related to their use [39]. Their explanation for the attenuation problem caused by atmospheric absorption, rain, and vegetation was to deploy Ultra-Dense Networks (small cell deployment) and Massive multiple-input multiple-output (MIMO) devices to overcome the problem. The findings suggested that the integration of massive MIMO, mm-wave, and tiny cells might be evaluated for inclusion in the major technology solutions for 5G mobile communication systems.

About [40] the generation of mm-wave frequencies by using external modulation based on tupling technique at the CS has shown its capability to generate mm-wave carriers with high spectral purity and reduce the dispersion effect.

Qi provided an outline of the Over-The-Air (OTA) measurement issues that would be encountered by the upcoming fifth-generation (5G) wireless communication technology [41], [42]. They also demonstrated many major 5G OTA measurement technologies that might be employed more widely, such as anechoic chamber absorbers, sampling antennas, and transition from near-field to far-field measurement techniques. The essential Devices Under

Test (including user equipment, chipsets, and active array systems) for 5G OTA include the following: (DUT). The difficulties associated with OTA measurements may substantially impact electromagnetic compatibility (EMC). The Radio Frequency (RF) and Electromagnetic Compatibility (EMC) testing are both conclusive in the case of 5G systems. In the end, the results provided a summary of the present success of the 5G OTA test and its future directions and current status. It is expected that the EMC group will be well-positioned to capitalise on both possibilities and challenges.

According to Ansari et al. [43], a detailed survey of existing parts-related approaches such as network identification, Device-to-Device (D2D) network protection, disturbance management, and proximity services. The findings revealed the investigated methods were in the sense of a resource-efficient and stable D2D network has provided some of the changing aspects of D2D networks have been shown. They addressed the difficulties connected with 5G D2D networks, influencing system implementation as mobile device density increases and data rate requirements increase simultaneously. It has been demonstrated that the zero-forcing approach may be utilised to eliminate intercom interference between a Cellular User (CU) and a D2D user using Coordinated Multipoint (CoMP) technology.

Zhang et al. described the current state of the art, associated obstacles, and research possibilities for mm-wave communication with unmanned aerial vehicles (UAV) [44]. Additionally, it discussed its modelling challenges and demonstrated the Channel's characteristics. Additionally, prospective solutions for UAV mm-wave cellular networks and difficulties were prepared, including spectrum sharing, UAV-to-base-station communication, and UAV-to-user communication. They overcame the substantial channel difference challenges by employing a UAV MIMO system under line-of-sight (LOS) situations. The findings of the emulation demonstrate that the received signal strength (RSS) is consistent with a modest number of scatters in the two-ray propagation model. However, simulated studies indicate that RSS changes rapidly under dense dispersions and a high-altitude urban climate. The findings suggest that UAV and mm-wave communications analyses provide enormous stability, endurance, and spectral performance benefits.

Reference to [45] [46], they obtained mm-wave frequency using modulation technique directly, but the maximum frequency obtained by this method is 30 GHz,40 GHz, as reported in reference [47]. In addition to this, the signal performance is limited by impairments such as

frequency chirp, significant non-linearities, and poor frequency stability, making this technique inappropriate for generating an mm-wave for RoF.

Polese et al. presented the most current standardisation activities on Integrated Access. Backhaul (IAB) clarified architectures without IAB in mm-wave implementations and architectures without IAB [48]. In addition, the IAB conducted end-to-end system-level simulations to demonstrate the benefits of cell edge throughput, which was previously discussed in detail. To overcome mm-wave restrictions like penetration losses and extreme routes, they used high gain antennas while simultaneously boosting the connection budget. The findings suggested that the IAB is a viable solution for the efficient conveyance of cell edge traffic, even though the benefits for more crowded networks have diminished.

Zugno et al. provided an analysis of the current standardisation efforts at waves for vehicular communications reveals parallels and differences between IEEE 802.11bd and (3GPP NR V2X) 3rd Generation Partnership Project standardising next-generation networks for vehicular applications the authors [49]. They employed the End-to-End (E2E) strategy to develop mm-wave Vehicle-to-Vehicle (V2V) networks to handle the issues of expanding from the application levels to the physical layers of the network. The results revealed that a preliminary E2E execution estimate of the mm-wave E2E communication system was present, which considered varied spread environments, coding schemes (MCS), modulation, and carrier frequencies, among other factors.

Yang et al. examined numerous hardware restrictions in [50] to determine their significance. They proposed new device architecture to alleviate these hardware constraints while enhancing performance for future mm-wave communication systems. They were successful. More importantly, these analogue elements are often flawed since they add many hardware defects and manufacturing faults to the process. Aside from that, hardware restrictions and vulnerabilities will significantly impact the performance of mm-wave systems in general. Traditional hardware restrictions such as phase noise, PA non-linearities, and IQ imbalance were addressed by incorporating a small number of high-precision phase shifters into the mixed beamforming network, which was previously impossible. The findings revealed that the design of the hardware-aided system, which contrasts the consistent relationship between software and hardware units and adaptability, provides higher flexibility for state-of-the-art when compared to other techniques.

Busari et al. established the combined influence of the three major technologies (UDN): massive MIMO, mm-wave (and/or terahertz) communications, and mm-wave (and/or terahertz) communications [41]. They also used machine-level simulations with 3-Dimensional (3D) channel models from the Third Generation Partnership Project (3GPP), which they found helpful. They make predictions about the performance of two-tier cellular networks comprised of mm-wave small cells and mm-wave microcells that are densely distributed. Compared to only large cell environments, the results showed that UDNs could achieve significantly higher capacities than previously thought possible. The results also show that increasing the mm-wave bandwidth used does not result in a proportional increase in execution speed. Because of the broader bandwidths, the signal-to-interference-plus-noise ratio decreases due to the consistent growth in noise (SINR).

Huo et al in [52] Presented the critical 5G User Equipment (UE) hardware design; the design shows the DPA-MIMO system architecture, a new and highly reconfigurable 5G cellular user equipment (UE) system architecture, has also been proposed in addition to the DPA-MIMO system architecture. Using a novel DPA-MIMO architecture and design process, they overcame the limitations of cell phone design, such as high path loss, human blocking, and self-heating problems. Results revealed that wireless UEs based on DPA-MIMO could be implemented using cutting-edge antenna, device, and circuit technologies to provide a reliable wireless experience. Therefore, this design will make it possible to achieve a peak throughput of more than 10 Gb/s while maintaining the slim form factor of mobile station devices.

Zhang et al. in [53] investigated the challenges involved in designing the antenna array structure for future 5 G mm-wave systems. Zhang et al. As an alternative to the traditional rectangle, the antenna components can also be propagated in the shapes of a cross, a circle, or a hexagon. In some outdoor applications, communication protection, forest growth, and hardware growth are significant drawbacks to mm-wave technology. They employed highly dense relays and massive MIMO systems to overcome these difficulties. The circular antenna array demonstrated its advantages in this experiment because of its robust misalignment of the beam and flat gain fluctuation. There has also been discussion of optimistic candidate solutions, such as multi-hop relaying and distributed antenna system solutions, to maintain mm-wave networks' connectivity and efficient coverage vulnerable to repeated blockages (DAS).

The carrier was suppressed by employing the OFM technique with an optical double sideband (ODSB) [61] [54] [55]. The used techniques show the mm-wave frequency is generated by beating the two sidebands and resulted in an optical mm-wave signal as the double frequency of the LO mm Carrier. The technique can be suppressed by either using a notch filter or an optical interleaved [56]at the output of EM with biasing voltage onto null-transmission point.

Feng et al. developed a new framework for 5G mm-wave transporters that is centred on global and manageable device architecture and is centred on global and manageable device architecture [57]. In the system under consideration, high-layer routing and scheduling schemes are used in conjunction with ambitious physical layer strategies, such as hybrid beam formation and full-duplex transportation. More specifically, they solve the challenges of transport channel selection and time distribution in mm-wave transporters by providing an optimisation study. They perform the same algorithmic analysis in the process. The outcome demonstrated that the advantages of proposed design process were advantageous. The routing and scheduling schema incorporates a modern mm-wave physical layer strategy, has shown significantly higher productivity, shorter latency, and a lower packet loss ratio than the previously presented 5G backhaul system.

Lee and his team defined the spectrum status for 5G using below and above 6 GHz. in both the organiser and technical components and the available spectrum status for 5G in both the organiser and technical details [58]. A particular focus was placed on the technological shortcomings of 5G support in the mm-wave range, such as the lack of coverage of problems and application-related issues. They used beamforming techniques to solve the coverage issues they were experiencing at the time. Furthermore, by improving hardware design, it was possible to overcome the limitations of the execution system. The findings showed that advanced antenna solutions are essential enablers for base stations and mobile systems. The results are consistent with previous research.

Yu Liu and Cheng-Xiang Wang Presented that various circumstances and frequency bands were used to define the behaviour of the High-Speed Train (HST) channel measurements and advanced HST channel models [58]. In addition, a new frequency non-stationary version of the HST channel model is currently being investigated. A combination of mm-wave and massive MIMO was used to overcome the (frequent and quick handover, broad Doppler spread) limitation and provide seamless connectivity for 5G and beyond high-speed transport

networks (HST). Results revealed that technologies of opportunity like massive MIMO, Millimeter-wave, and beamforming are believed to be capable of supporting reliable broadband high-speed transmission services (HST).

The principles and structures of collaborative multi-satellite transport strategies in 5G were demonstrated by [40] in their research paper. Furthermore, two multi-satellite relay transmission systems based on Time-Division Multiple Access (TDMA) and Non-Orthogonal Multiple Access (NOMA) architectures have demonstrated their effectiveness (NOMA). Hybrid terrestrial satellite backhaul networks used the routing algorithm to address effective resource management and access to increase network capacity while maintaining low latency. The findings revealed that time scheduling based on Maximum Effective Capacity (MEC) outperformed the other two strategies under all quality-of-service requirements. As a result, when high-quality contact in a specific conversation is requested, MEC-based time management is preferred. The findings suggest that the MEC-based strategy for Multi-Satellite Relay Transmission (MSRT) systems outperforms the TDMA-based approach in terms of performance [59].

In references [60] [63], [64] [62] presented higher-order harmonics for generating higher frequencies. When generating mm-waves using the EM technique, the CW-laser is modulated with fmm, which is a subharmonic of the desired mm-wave frequency fmm, by using EM. Then, the output of EM comprises the higher-order harmonics and multiple sidebands separated by fmm if EM is set with appropriate biasing of the input voltage and a modulation index. However, the maximum order of the OFM is limited by the harmonic generation efficiency and depend on the chosen EM.

In [60] [63], and [64], the researchers generated an optical mm-wave signal in CS is transmitted over the fibre to be electronically extracted at the desired mm-wave signal at the BS to up-convert the downlink signal. However, the primary impairment of this method is the constraint of the EM bandwidth and high input radio frequency (RF) that can be obtained. Remote generation of mm-wave signals using broad bandwidth modulators and mm-wave frequency LO has been reported using EAM, MZM and PM.

While [62] investigated and highlighted how the blockchain uses 5G networks. Furthermore, a survey of the blockchain Distributed Ledger Technology (DLT) framework was provided, which included a description of the framework's main features and supporting elements. Apart from that, intelligent contracts, decentralised stores, and trusted oracles can all be used

to develop decentralised 5G applications, services, and ecosystems, according to the researchers. Blockchain is critical in addressing the security and scalability issues that arise in 5G networks, which are characterised by a large number of Internet of Things (IoT) devices and a large number of mobile devices that are widely distributed. The findings revealed that the value of combining high-level technical information about device designs and architectures with the 5G blockchain was beneficial in several ways.

In their paper, Davaslioglu and Gitlin discussed the energy efficiency aspects of massive MIMO (also known as Large-Scale Antenna Systems (LSAS)), mm-wave connections, and dense deployment of small cells in cellular networks [63]. Based on the findings, it was discovered that the grid's energy efficiency could be significantly improved by implementing a complementary and robust layout. Modulated interference suppression and spatial multiplexing are two examples of massive MIMO techniques that provide access to bands that are not fully exploited by mm-wave, reduce communication distances, and mitigate small cell coverage apertures in the diffusion zone. Using beamforming and interference patterns to solve system challenges, it is also possible to separate the device, allowing the high frequency to be reused.

In contrast, to fully utilise the capacity of mm-wave small cells, it is necessary to address specific technological issues. Many protocols and techniques (Base station (BS) discovery, Beam alignment, and significant premeditation of device design) were described by [68]. Their solution to the consumer BS discovery and beam alignment problems in the intended coverage areas was to use beamforming reference signal transport in those areas. The results revealed that the instructions for designing the physical layer with mm-wave waves for small cells could be applied in practice. With a BS, the total number of beam pairs required to cover the 60-degree sector for comprehensive analysis is 128; with a hierarchical study, the total number of beams needed is 16.

The technical difficulties in the Channel Reciprocity-based secret Key Generation the Channel Reciprocity-based secret Key Generation (CRKG) caused by multiple duplex modes, large MIMO and mm-wave communications and prototypes in the Internet of Things (IoT) strategy were presented by[40], [64]. Their solution to the resulting issues, such as path loss and standard key distribution protocols based on cryptography, was beamforming to solve the problems. The findings revealed that in 5G networks and beyond, the three aspiring technologies can support breakneck data speeds and many connected devices.

Martin-Vega et al. in [70] provided a comprehensive overview of the state-of-the-art architecture systems believed to be used for vehicular telecommunications. Following that, the primary technologies that will improve the appropriateness of mm-wave connections for autonomous leadership were discussed in detail. The approach in [70] included the integration of analogue/hybrid beamforming and a location-based beam search protocol. It also developed radio and physical layer full-duplex switch generation to address problems associated with autonomous driving, such as the mm-wave band and the reduction in vehicular techniques of channel measurement operation at mm-wave. The findings demonstrated that autonomous driving could meet the established criteria and highlighted its potential advantages: low latency, high resolution, protection, and support for unicast and broadcast connections.

Table 2.1: Summary of the literature related to the mm-wave generation techniques

Ref	Tupling techniques	Frequency (GHz)	Configuration	Simulation / experiments	OSSR	RFSSR	
[73]	16	60	Four-MZMs in parallel	simulation	35dB	55dB	Precise MI and complex bias control are required
[74]	16		Two Parallel Dual Parallel-MZMs with two tunable lasers and a Phase modulator for Feed-Forward modulation.		-	-	
[75]	8, 12,16		Two Parallel DP-MZMS with Polarization Multiplexing	Simulation	24dB	18dB	Two different MIs and careful selection of polarizer angle is required
[76]	16		Two cascaded Dual Parallel MZMs	Simulation	21.5dB	38dB	OSSR and RFSSR are sensitive to MI
[77]	Double		Two IM and IL	Simulation	30dB	25dB	OSSR and RFSSR are sensitive to MI
[78]	Tripling		IM and three IL		20 dB	-	Utilising three filters
[79]	Quadrupling		Three MZMs Two polarization controllers	experimental	30 dB	20dB	Number of optical modulators
	Quadrupling	36	Single MZM	Simulation	30 dB	24 dB	
[80]	Quadrupling	4-40	Two MZMs	Experimental	20 dB	15dB	Low RSFSR. So electrical filters or optical filters are required in this scheme

[81]	Quadrupling	36	Three dual-electrodes MZMs	simulation and experiment	35dB	30dB	More number of optical components
[82]	Quadrupling	60	DP-MZM	Simulation	32 dB	33dB	Low OSSR and RFSSR
[83]	Quadrupling	30 to 42.4	Two MZMs single polarization modulator (P	Experimental	23.90dB	17.05dB	Low OSSR and RFSSR
[84]	sixtupling	60	Two MZMs	simulation	29.9 dB	24dB	Low OSSR and RFSSR
[85]	sixtupling	66 to 114	Polarization modulator, polarisation controller optical notch filter	Simulation and experimental	24.1dB	20dB	
[86]	sixtupling	60	Three MZMs	simulation	30dB	25.10dB	Low RFSSR
[87]	octupling	60	4 MZMs	simulation		44 dB	
[88]	12 tupling	60	dual parallel polarization modulator (DP-PolM) power controller (PC)	Simulation	37.76 dB	31.67 dB	
[89]	24 tupling	72	4 MZMs	Simulation	33 dB	26 dB	
[90]	octupling	216-256	Quadruple doubler	Simulation	-	-	
[91]	12 tupling	60	2 MZMs		26.4 dB	20.3	Less OSSR and OSSR compared to previous work in generating 60 GHz
[73]	16	80	Four-MZMs in parallel	simulation	35dB	55dB	Precise MI and complex bias control are required
[74]	16	160	Two Parallel Dual Parallel-MZMs with two tunable lasers and a Phase modulator for Feed-Forward modulation.		-	-	
[75]	8, 12,16		Two Parallel DP-MZMS with Polarization Multiplexing	Simulation	24dB	18dB	Two different MIs and careful selection of polarizer angle is required
[76]	16		Two cascaded Dual Parallel MZMs	Simulation	21.5dB	38dB	OSSR and RFSSR are sensitive to MI

2.7 Literature Analysis

Q1 What are the definitions, concepts and conceptualisations of mm-wave communication systems? The radio of Fiber (RoF) technologies? And mm-wave generation techniques?

The optical generation of mm-wave using the external modulation (EM) technique has great potential for providing high-purity high-frequency mm-wave signals, excellent stability, high spectral purity and lower system cost [92]. Generating mm-wave signals using an external modulator was proposed by O'Reilly in 1992, where the signal was generated by biasing a Mach Zehnder modulator (MZM) to suppress even-order optical sidebands[93]. Different methods have been demonstrated to generate mm-wave using external modulation techniques to hide the optical carrier, mentioned in the following.

Atechnique was used to obtain frequency quadrupling and upconversion in radio over fibre (RoF) and experimentally demonstrated. This technique is achieved by implanting two cascaded Mach-Zehnder modulators (MZMs) biased at the minimum transmission point [79]. By adequately adjusting a pair of optical wavelengths with a wavelength spacing corresponding to four times the frequency of the microwave drive signal is obtained. The two wavelengths are sent to a third MZM for an intermediate-frequency (IF) signal to supers the carrier. At the output of the third MZM, a frequency-upconverted signal at the mm-wave band is generated.

The technique's advantages are that a relatively low-frequency local oscillator (LO) signal generates a high-frequency LO signal. The obtained signal at the electrical domain is 34.125 GHz in their experiment, which is displayed near the quadrupled frequency. The obtained electrical spectrum includes the harmonic components of 0–4 orders. Because of the optical carrier suppression, the power of the fourth-order harmonic is higher than those of the first-, second-, and third-order harmonics. The system is a little bit complicated since they have used three MZM.

The proposed approach uses an optical phase modulator to obtain a frequency-quadrupled electrical signal in [98]. A Fabry-Pérot filter was introduced to select the two second-order optical sidebands. The mm-wave signal with four times the input local oscillator frequency was achieved by beating the two second-order sidebands at a photodetector. The main advantage of that system is that an optical modulator with a maximum operating frequency of 15 GHz can be generated up to 60 GHz mm-wave signal. However, in that approach, an optical filter selects the two optical sidebands to generate tunable mm-wave signals, which increases the system's complexity and cost. In [99][92], an approach to develop an mm-wave signal based on frequency quadrupling using a Mach–Zehnder modulator MZM is verified.

The approach of a frequency quadrupling scheme for optical mm-wave signal generation is proposed and demonstrated based on a dual-electrode dual-parallel integrated Mach-Zehnder modulator (MZM) [81]. It consists of three dual-electrodes MZMs, and electrical or optical filters are not required. The simulation and experiment verification are conducted to investigate the performance of the proposed scheme. The input frequency was used is a 9GHz RF drive signal. The achieved optical sideband suppression ratio (OSSR) is 35dB. The mm-wave at 36GHz is generated with the RF spurious suppression ratio (RFSSR) of 30dB.

A cost-effective system is proposed to generate a high-quality quadruple frequency mm-wave signal using an integrated dual-parallel MZM without an optical filter. Mm-wave of 60 GHz is generated with an input frequency of 15 GHz RF local oscillator (LO) [100]. The OSSR as high as 32 dB and radiofrequency spurious suppression ratio (RFSSR) of 33 dB has been achieved when an integrated IDP-MZM with 30 dB extinction ratio is utilised. The system performance is good even after 60 km transmission. The approach for frequency-quadrupled microwave signal generation with a phase shift of 360 ° is proposed and experimentally verified in [83]. Two DD-MZMs is biased at maximum transmission point to suppress odd-order sidebands.

The researchers in [101] proposed parallel configuration of MZM generates frequency quadrupling with OSSR of 42.07 dB and RFSSR of 36 dB when the extinction ratio is set to infinite. The MZMs were biased at the minimum transmission point to suppress the carrier. In our case, both the MZMs are driven by in-phase and quadrature signals and biased at the maximum transmission point to generate even order sidebands with pages. A180 degree phase shift is applied between the MZMs output and combined using an optical coupler. The coupler output contains only the second-order sidebands, which results in frequency quadrupling at the photodetector with higher OSSR and RFSSR. Based on the cascaded intensity and phase modulators, J. Zhang demonstrated the 36 GHz mm-wave generation with a 6 GHz RF drive signal [16]. However, since the undesired optical sidebands are not well suppressed, only the lower OSSR can be obtained, which degrades the RFSSR between the desired frequency sixtupling mm-wave signal and other undesired RF components.

Ascheme is proposed for generating frequency sixtupling mm-wave based on a laser and an integrated dual-parallel Mach-Zehnder modulator (MZM) without an optical filter in [84]. It consists of the two sub-MZMs with an extinction ratio of 30 dB. The optical sideband suppression ratio (OSSR) is as high as 29.9 dB, and the radio frequency spurious suppression

ratio (RFSSR) exceeds 24 dB. Pan presented another method in generating frequency sixtupling by using a polarisation modulator and a wavelength-fixed notch filter[85].

Yai Qin proposed a frequency sixtupling technique to generate mm- wave [104]. The proposed scheme consists of two cascaded dual-electrode Mach-Zehnder modulators (MZMs), interleaved with a Gaussian optical band-pass filter (GOBF) with different biasing. The first MZM was favoured at minimum transmission, mainly for optical carrier suppression purposes. The second MZM, selected at maximum information, is used for even-order optical harmonic generation and data signal modulation.

The GOBF between two MZMs is cast-off to the high-order optical harmonics suppression from the first-order optical harmonics. Thus 60 GHz is obtained from an input microwave frequency of 10 GHz, which carries the data signal and drives the MZMs with an RFSSR of 36 dB. However, the received optical power signal Is around -40 dBm and obtained electrical signal is about -50 dBm. Esaki proposed a method in generating an mm-wave signal based on frequency 12-tupling using DP-polarization modulators.

In [23], two filterless frequency-tupling mm-wave generator schemes are theoretically studied. In [88], the researcher generated an mm-wave signal through frequency 12 tupling using a dual parallel polarisation modulator (DP-PolM). By setting RF drive voltage and proper polarisation angle of the DP-PolM, the frequency 12-tuples mm-wave is obtained with an OSSR of 37.76 dB and RFSSR of 31.67dB. Further, the impact of nonideal parameters on the OSSR, RFSSR and BER are also analysed and presented. The study is composed of two techniques. The first one is a frequency 12-tuples; the design consists of a dual-parallel Mach-Zehnder modulator (DP-MZM), capable of generating the six-order optical harmonic. The second one is a frequency 36-tuples which is consists of the proposed frequency 12-tuples and two intensity modulators, which can utilise the six-order optical harmonic to generate frequency 36-tupling mm-wave signal.

In the prosed sachem by tuning the RF driving signal from 1.75 GHz to 3.25 GHz, mm-wave signals of 63 GHz to 117 GHz has been achieved by the frequency 36-tuples. The OSSR and RFSSR are over 28 dB and 23 dB, respectively has been obtained The BER has been achieved over 20 km SMF distance.

Chen, proposed a new scheme to generate frequency 24-tupling mm-wave using two cascaded integrated dual-parallel Mach-Zehnder modulators, which mean 4 (DD-MZMs) without the need of optical filtering [89]. 72 GHz mm-wave is generated from a local input oscillator of a

3 GHz microwave signal. Thus, the way significantly reduces the modulator's high-frequency requirement and the oscillator. However, The OSSR of 33 dB and the RSSR of 26 dB has been achieved in their study.

In addition, for that, the obtained optical power signal is around -36 dBm while the received electrical power is around -44 dBm. 2.5 Gbit/s data distribution performances are also measured for 20 km SMF distance to achieve BER of State Of The Art For mm-wave Generation Techniques.

Q2 What is the current state of the art of the mm-wave generation techniques?

[103] developed and recommended using the concept matrix where more investigations and deeper analysis are needed for the current state of the research. In line with [104] characteristics, the meta-data and the meta-information about the used articles in the study will be included. In line with [105], the solid framework is used in the literature to expose the characteristics more the inductive and deductive methods are employed in line with [106]. It is impossible to evaluate the concept matrix in academia and industries within the limited extent of this paper; the author focuses on the characteristics that are only relevant during the process.

2.8 Research Issues

Q3 What are the research issues of the mm-wave generation techniques?

Despite the many positive developments towards mm-wave over fibre systems, there are some challenges in its implementation, the complexity of devices, the high cost of the optical components and the quality of the mm-wave frequencies transmitted over fibre. These challenges are all considered influential factors for obtaining a successful transmission system. In addition, mm-wave-wave generation procedures are measured more sophisticated than low-frequency radio waves' generation methods. Additionally, there is a need to increase the number of BSs, which broad bandwidth PDs should support, to cover the service area in wireless communication systems [31] [54].

The limitations of the different mm-wave generation techniques compare all the stated methods of the record cited studies to improve the generated mm-wave signal. This comparison shows that the most straightforward generation technique is developing mm-

wave with a directly modulated laser that provides a low-cost system. Still, the laser and the modulator bandwidth limit the frequency of the generated mm-wave.

Table 2.2: Summary of the limitations of the different mm-wave generation techniques

Techniques	Ref	Limitation
Directly modulated Laser	[107][108] [47][109]	• The highest mm-wave frequency can be generated limited. • Poor transmission performance because of the nonlinearities, noise, and frequency chirp. • High power consumption due to extra laser required and setup insertion losses.
Externally modulated Laser	[110][111] [112][113] [98][65] [6] [64]	• High cost for high frequency operation. • Mm-wave frequency and bandwidth are limited by EM harmonic generation efficiency. • Optical filters are needed to remove undesired harmonics.
Multimode Light Source	[114][115] [6][116] [117][118] [119]	• Mode selection depends on the Multimode Light Source. • Low scalability
Heterodyning two Laser	[120]–[125]	• Complicated and expensive configuration. • Achieved frequency is limited by laser linewidth.

2.9 Literature Gaps

From tables 2-2 and 2-3, generating mm-wave using external modulation methods is preferred; however, the technique has a few gaps as follows:

1. High-cost for generating higher frequency
2. Restricting mm-wave frequency and bandwidth by

a. External Modulator harmonic generation efficiency

b. Optical filters are needed to remove undesired harmonics.

3. The maximum frequency obtained was 160 GHz.

4. More than two MZM's are required to generate higher frequencies of high-quality performance.

5. Getting low suppression between harmonics in the electrical domain (20dB to 27dB)

This thesis contributes to overcoming the specified literature gaps through the following:

1. Generating 60 GHz using a single MZM.

2. Generating high-quality signal at 72GHz with OSSR at 70dB and RFSSR at 52dB using only one parallel DD-MZM. Therefore, no need to use filters.

3. For the first time, the upper band of mm-wave generated at 216 GHz, 240 GHz, 288 GHz and 300 GHz using only two MZMs based on 12 frequencies tupling techniques.

4. The design of using only two MZM's is tunable, filterless, cost-effective and straightforward.

2.10 Future work

Q4 What are the directions for future research?

Recently, significant research has been conducted on applying mm-wave frequencies in response to the growing demand for the services considered the most challenging for following generation networks. The mm-wave spectrum has a wider available bandwidth than any other wireless communication system currently in use. Beyond 5G, capacity will be increased by using new mm-wave bands for indoor and outdoor wireless propagation. We consider a network in which vehicles are served by mm-wave base stations (BSs) installed alongside the road.

1. Investigate the performance of the frequencies obtained in this work in wireless links. The focus is proposed to be on the performance of 60 GHz, 72 GHz, 240 GHz, and 300 GHz links between BSs and users in indoor and outdoor local area networks.

2. Evaluate the performance of 60 GHz and 300 GHz vehicular communication systems in a highway communication network, considering the following factors: fundamental link budget

metrics, with fixed BSs and a user travelling at high speed in a car, antenna height, penetration and diffraction losses (affect the user inside the car).

3. Additionally, the terahertz frequency band may be critical for future wireless communication networks beyond 6G. My future research objective is to investigate the performance of terahertz (THz) frequencies such as 600 GHz and 1 THz over fibre transmission links.

2.11 Summary

This literature review is structured and focused on the generation techniques for mm-wave for future communication systems in industries and academia and organised along with four research questions. This chapter presented comprehensive concepts (RQ1), then provided state of the art in response to (RQ2), highlighted the research issues in response to (RQ3), and for the classifications and recommenced directions for the future research in response to (RQ4).

Since this review was initiated with scattered work, the comprehensive perspective did not exist, and the contribution of the evaluation is abundant in knowledge for academia and industry. This review contributes to improving and enhancing transparency for understanding generation techniques of mm-waves concepts and highlighting the values for its use in different applications. This review still contributes to the industry and academia with new routes for future research and directions for improvements. Although the study in this review was carried out in line with [126], and the study has many restrictions. However, it can still not fully guarantee the coverage of all the existing techniques used in telecommunication technology, mainly because of the significant number of different concepts in academia and industries. This literature review guarantees clearance of the understanding and transparency for the decisions that took place along the check-in line [127].

Mm-wave networking, machine-to-machine communication, the Internet of Things, and other emerging wireless technologies have created new security concerns for 5G networks. Developing effective, secure transmission methods for 5G wireless communications that take advantage of radio channels' physical layer propagation features has recently grabbed academics' interest. In 5G technology, this is referred to as physical layer security. The encryption algorithms used at the physical layer are resistant to increasingly sophisticated passive and active eavesdroppers. They are adaptable for remote key generation physical

layer authentication in 5G networks. With careful monitoring and execution, conventional encryption approaches can be combined to produce a well-integrated security solution that successfully secures the sensitive and private communication data of 5G networks. The most important study on 5G technology has investigated and explored a variety of problems, including attenuation, OTA measurements, mm-wave penetration, severe path losses in mm-wave, antenna array architecture, security, coverage, and scalability, among others.

Chapter 3 Performance Of Optical Millimeter-Wave Based On Carrier Suppressed

3.1 Overview

This chapter investigates suppressing the carrier for an optical mm-wave signal using an inverted optical filter. Specifically, a simple and cost-effective design generates a single DD-MZM and inverted optical filter. This work has two simulation schemes; the first pertains to developing an mm-wave signal based on carrier suppression. The Optical spurious suppression ratio of 30.56 dB is achieved in the first. The power signal with carrier suppression is improved by 60 % compared with no carrier suppressed signal. Therefore, the quality of obtained 60 GHz mm-wave signal based on carrier supersession using an inverted optical filter is demonstrated. The second simulation scheme analyses the performance of downlink data transmission of 2.5 Gb/s with obtained mm-wave over a single-mode fibre transmission line. Two scenarios are considered to modulate the data with obtained optical mm-wave in the obtainable design.

The first scenario modulates the data directly with DD-MZM while generating the optical mm-wave. The second scenario is when the data is modulated with the obtained optical mm-wave signal. In this study, measuring the max Q factor for different bit rates are considered to observe the performance of the obtained mm-wave signal over the single-mode fibre. With the proposed design for 2.5 Gb/s, the max Q factors of 21 over 20 km fibre length are achieved. In addition, the Max Q factor of the obtained signal is measured with different bit rates at 2 km, where for 10 Gb/s, a max Q Factor of 8 can be achieved. This design approved that the mm-wave signal based on carrier suppression can be generated effectively using an inverted optical filter.

3.2 Introduction

Mm-wave over fibre is a promising technique that merges the benefits of mm-wave frequencies and fibre technology. That is, optical fibre technology provides high bandwidth and supports long transmission links. At the same time, the mm-wave frequencies offer large bandwidths in the wireless domain and overcome the problem of spectral congestion at lower frequency ranges that provide broadband wireless access services [128] [6]. Mm-wave signal generation for RoF is a critical technique that needs to continuously develop for high-

frequency ranges, mainly for the frequency beyond 30 GHz. Thus, different methods have been used to generate mm-wave; direct modulation, optical heterodyning, Four-Wave Mixing (FWM) and external modulation (EM) [27] [129]. The optical generation of mm-wave using the external modulation (EM) technique has great potential for providing high-purity high-frequency mm-wave signals, excellent stability, high spectral purity and lower system cost [92]. Generating mm-wave signals using an external modulator was proposed by O'Reilly in 1992, where the signal was generated by biasing a Mach Zehnder modulator (MZM) to suppress even-order optical sidebands [93]. He implemented the frequency doubling based on carrier suppression to get a signal of 36 GHz generated from a drive signal of 18 GHz.

As mentioned early in chapter 2, implementing EM to generate mm-wave involves a Continuous Wave (CW) laser followed by an EM that modulates the laser light with radiofrequency. The EM used in this technique can be an intensity modulator (Mach-Zehnder Modulator (MZM) or an Electro Absorption or Modulator (EAM)), or a Phase Modulator (PM) [4]. The EM generates higher-order harmonic required to implement Optical Frequency Multiplication (OFM) [12]. OFM technique has been proposed to produce mm-wave signals at frequencies above the EM bandwidth using electrical signals (fi). There are two main approaches to using the OFM technique. The first is to take advantage of the generation of higher-order harmonics with proper bias and modulation index. The second approach utilizes the OFM technique for suppressing the carrier [88].

Different modulation schemes by using EM have been deployed to generate mm-waves, such as single sideband (SSB), double sideband (DSB) and optical carrier suppression (OCS), with each having different resistance for the fibre dispersion [5-6]. It has been found that OCS is preferred due to its advantages. It can produce signals with high receiver sensitivity, low spectral occupancy, low bandwidth requirement for RF signals, and minor power penalty over long-haul transmission [94]–[96]. In addition, signals carried by dual-tone optical sidebands of OCS mm-wave are transmitted over the chromatic fibre; they are immune to the fading effect [97].

Many studies have demonstrated generating mm-wave using external modulation to suppress the optical carrier. For example, an mm-wave signal at 60 GHz is obtained using frequency six tuples techniques [76]. The system in this reference includes two cascaded Mach-Zehnder modulators (DD-MZMs). The first MZM is biased at the maximum transmission point, used for even-order optical harmonic generation. Second, MZM is biased at minimum transmission point, used for optical carrier suppression and data signal modulation. However, it used an Optical filter to get the desired signal. In [74], the system is complicated since it

uses four MZMs. In [82], A cost-effective method is proposed to generate quadrupling-frequency optical mm-wave based on integrated dual-parallel MZM, which comprises three sub-MZMs with an OSSR value of about 32 dB and the system we perform well until 60 km only. In [81], two cascaded MZMs with a Gaussian optical Bandpass filter (BPF) were used to suppress the optical carrier. MI-insensitive and filterless frequency octupling scheme based on two parallel dual-parallel Mach–Zehnder modulators (4MZMz) were used for carrier suppression purposes [73]. Whereby mm-wave signal at 60 GHz is obtained with RFSSR of 40dB. However, in [93], the mm-waves are generated using a single MZM only. In that study, the Fiber Brag Grating (FBG) is used to remove the carrier to obtain a tunable mm-wave signal of (32 GHz, 44.6 GHz and 49 GHz). However, the issue of using FBG is sensitive to temperature, which is required a complex control system to stabilize its operation.Furthermore, it is consumed due to the FBG reflection.

This chapter generates an mm-wave of 60 GHz. The carrier is suppressed using an inverted optical filter. Then, the generated mm-wave performance is investigated to validate the quality of the obtained signal by implanting different scenarios to modulated the obtained 60 GHz with data signal of 2.5 Gb/s.

3.3 The Principle Of Proposed Design of generating a 60 GHz mm-wave

The proposed design of generating a 60 GHz mm-wave with an inverted optical filter is shown in Figure 3-1. An electrical drive signal is applied to a single Dual Drive –MZM (DD-MZM), which is biased to suppress the odd-order optical sidebands. An inverted optical filter is connected at the output of DD-MZM to eliminate the optical carrier, and two second-order optical sidebands are obtained at the output of the inverted optical filter. A beat signal with four times the frequency of the electrical drive signal is obtained at the PD.

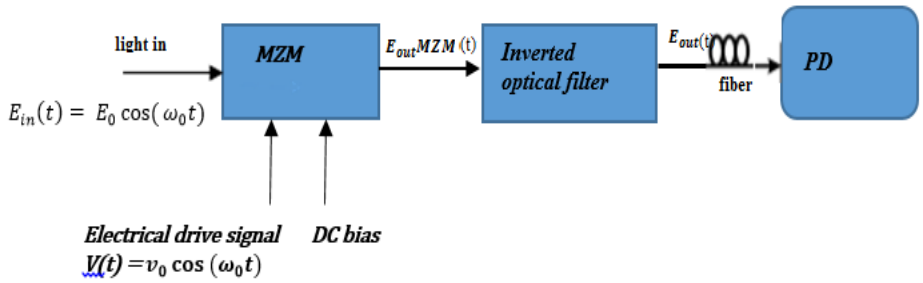

Figure 3-1: The principle of generating mm-wave based on carrier suppression

The conceptual diagram of 60 GHz Optical Carrier Suppressed mm-wave signal generations based on the proposed method is that the CW laser is emitted light into DD-MZM. It is based on 90^0 phase shifts introduced between the RF-driving signals applied to DD-MZM drive electrodes. The output of DD-MZM contains all nth-order sidebands except for n=4k, where k is an integer, as shown by solid arrows in Figure (3-1). Then, the optical signal is transmitted through an optical fibre to PD. Suppose all these optical sidebands are fed to PD. In that case, harmonics of the electrical drive signal will be generated and can be obtained higher order electrical harmonic like second order and third order sideband. The frequency-doubled electrical signal can be considered as first-order sideband is achieved at PD, which has more efficiency than other electrical signal orders like second-order sideband, which can be considered second order.

The proposed method in this paper, the dc bias of the MZM, is tuned to have 0, leading to removing all of the other order sidebands to improve the efficiency of obtained signal. However, when this generated signal is applied to a PD, a strong frequency, a double electrical signal (first-order sideband), is generated, and a weaker frequency quadrupled

electrical signal (second-order sideband) will be achieved. Then, these generated optical signals are composed of two sidebands. The optical carrier is transmitted over a single fibre, which will suffer from chromatic dispersion induced by the high-power penalty. In addition, the presence of the first order will cause interference to the process of the second sideband electrical signal in the system application. In this proposed method, a filter (Notch filter) is used to eliminate the first-order sideband and remove the carrier, as shown in Figure 3-2.
The input electrical field at the input of MZM can be expressed by

$$E_{in}\,(t)\text{audacious}\,cos(\omega_0 t) \qquad (3-1)$$

The output of dual-port MZM $E_{out}\,MZM(t)$ can be expressed by

$$\boldsymbol{E_{out}}\,\text{MZM}\,(\boldsymbol{t}) = \boldsymbol{E_0}\ \boldsymbol{cos}\left[\frac{\phi \boldsymbol{V(t)}}{\boldsymbol{2}}\right]\ .\boldsymbol{cos}(\boldsymbol{\omega_0 t}) \qquad (3\text{-}2)$$

Where electrical field amplitude is donated by $\boldsymbol{E_0}\ \boldsymbol{and}\ \boldsymbol{\omega_0}$ indicates the angular frequency of the optical input carrier, applied electrical drive voltage is indicated by V (t). $\phi\boldsymbol{V}(\boldsymbol{t})$ is the optical phase difference caused by V(t) between the two arms of the MZM. *If* the MZM is driven by a sinusoidal electrical signal and biased with a constant dc voltage $\phi\boldsymbol{V}(\boldsymbol{t})$ is expressed by

$$\phi\boldsymbol{V}(\boldsymbol{t}) = \ \emptyset_{\boldsymbol{0}}+\frac{\boldsymbol{\pi}}{\boldsymbol{V_\pi}}.\boldsymbol{V_m}\,\boldsymbol{cos}(\boldsymbol{\omega_0 t}) \qquad (3\text{-}3)$$

$\emptyset_{\boldsymbol{0}}$ does the dc-bias voltage determine a constant phase shift.

$\boldsymbol{V_\pi}$ is the half wave voltage.

$\boldsymbol{V_m}$ and $\boldsymbol{\omega_0}$ are amplitude and angular frequency of the electrical drive signal, respectively. Considering phase modulation index as β, which = $\frac{\boldsymbol{V_m}}{\boldsymbol{V_\pi}}\ .\ \frac{\boldsymbol{\pi}}{\boldsymbol{2}}$, while the Bessel function of the first kind of order n is noted as $\boldsymbol{J_n}$ .The electrical field of the output optical signal can be written when substituting (3) in (2), which will be equal

$$E_{out}\,MZM\,(t)$$

$$= E_0\ cos\left(\frac{\emptyset_0}{2}\right) J_0\,(\beta)\ cos(\omega_0 t) + \ E_0\ cos\left(\frac{\emptyset_0}{2}\right)$$

$$\times \left\{\sum_{n=1}^{\infty} J_{2n}(\beta)\, cos(\omega_0 t - 2n\omega_e\, t + n\pi) + cos(\,\omega_0 t + 2n\omega_e - n\pi)\right\}$$

$$- \ E_0\ sin\left(\frac{\emptyset_0}{2}\right) \ \times$$

$$\left\{\sum_{n=1}^{\infty} J_{2n-1}(\beta)\, c \begin{bmatrix} sin(\omega_0 t - (2n-1)\omega_0 t + n\pi - \frac{\pi}{2}) \\ - sin(\omega_0 t + (2n-1)\omega_0 t - n\pi + \frac{\pi}{2}) \end{bmatrix}\right\} \quad (3\text{-}4)$$

Equation (3- 4) indicates that the input power of the carrier will be spread out among first order, second order and third order higher-order optical sidebands. The amplitude distribution of these sidebands is directed by the variation of Bessel functions parameterized by and values of will affect their amplitude. Suppose all these optical sidebands are fed to PD. In that case, harmonics of the electrical drive signal will be generated and can obtain higher-order electrical harmonic like second order and third order sideband. A frequency-doubled electrical signal can be considered a first-order sideband with more efficiency than other electrical signal orders like a second-order sideband. In the proposed method, the dc bias of the MZM is tuned to have 0, which leads to removing all of the other order sidebands to improve the efficiency of the generated signal. The optical signal now can be approximately expressed as

$$E_{out}\,MZM\,(t) \cong E_0\,J_0\,(\beta)\ cos(\omega_0 t) - \ E_0\,J_2\,(\beta)\ cos(\omega_0 t - 2\omega_0 t) - E_0\,J_2\,(\beta)\ cos(\omega_0 t \mp 2\omega_0 t) \quad (3\text{-}5)$$

However, when this generated signal is applied to a PD, a strong frequency, a double electrical signal (first-order sideband), is generated, and a weaker frequency quadrupled electrical signal (second-order sideband) will be achieved. Then, these generated optical signals are composed of two sidebands. The optical carrier is transmitted over a single fibre, which will suffer from chromatic dispersion induced by the high-power penalty. In addition, the presence of first-order will cause interference in the second sideband electrical signal process in the system application. In this proposed method inverted optical filter (Notch

filter) is used to eliminate the first-order sideband and remove the carrier (see Figure 3-2). The electrical field of the optical signal at the output of the inverted optical filter (notch filter) will be expressed as

$$E_{out}\ (t) \cong -E_0\, J_0\ (\beta)\,[\cos(\omega_0 t - 2\omega_0 t) + \cos(\omega_0 t + 2\omega_0 t)] \qquad (3-6)$$

When these obtained optical sidebands are fed to PD, a signal that has four timed the frequency of the electrical drive signal will be generated (see Figure 3-3), which can be written as

$$\boldsymbol{V_{out}(t) = CJ^2\ (\beta)\, cos(4\omega_0\, t)} \qquad (3\text{-}7)$$

Where C is a constant related to the PD's responsivity.

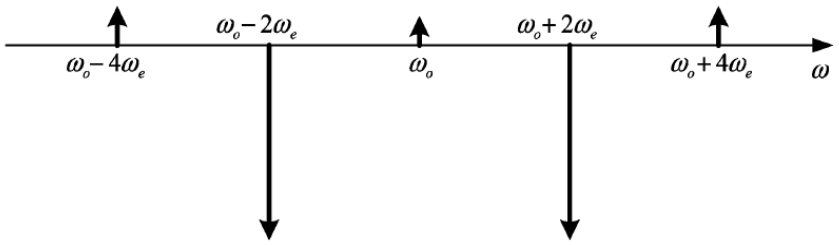

Figure 3-2: Optical spectrum at the output of the inverted optical filter.

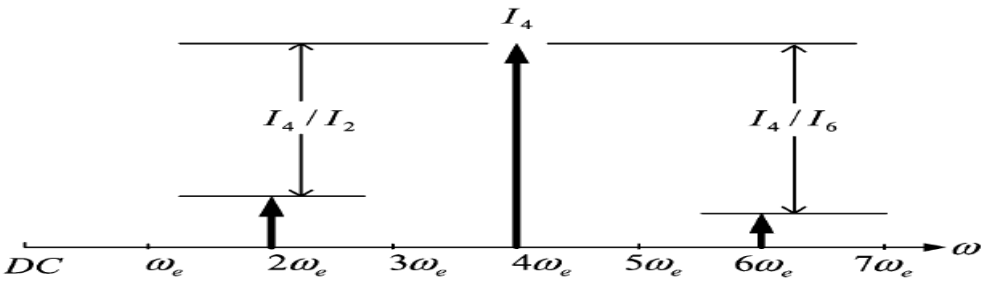

Figure 3-3: Electrical spectrum at the output of a PD

3.4 Simulation And Results

The proposed design is simulated using Optisystem software to generate an optical carrier suppressed mm-wave signal. Further, the performance of data transmission of generated mm-wave over fiber using data modulation schemes are also analysed.

3.4.1 Generating Mm-wave At 60 GHz

The proposed scheme regarding the generation of a 60 GHz mm-wave signal with carrier suppression can be seen in Figure (3-4). The entire system is simulated using Optisystem software (complete simulation design included in appendix 1). The simulation parameters setup for generating 60 GHz using an inverted optical filter are summarized in table (3-1).

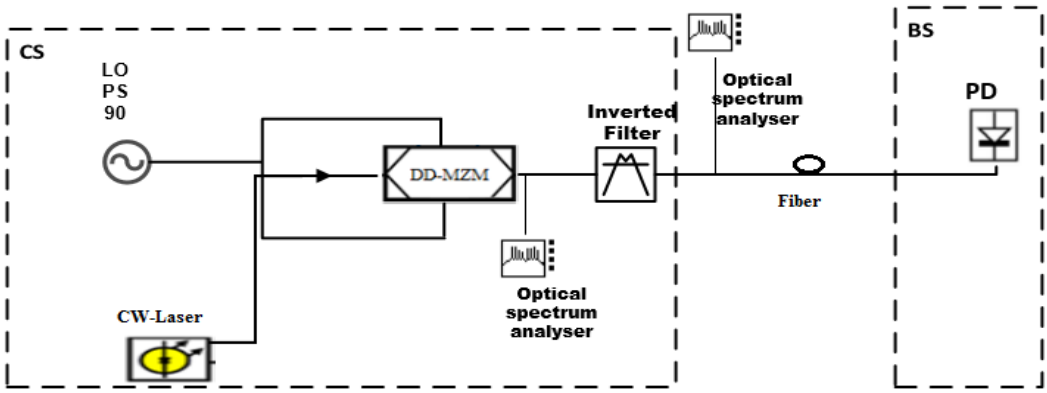

Figure 3-4: The proposed design to generate mm-wave of OCS 60 GHz.

LO: Local Oscillator, PS: Phase shift, DD-MZM: Dual Drive Mach Zehnder Modulator, PD: Photodetector.

Table 3.1: Simulation parameter setup for generating 60 GHz using an inverted optical filter

Device	Parameter	Value
(CW) Laser	Optical frequency	193.1THz
	Optical Power	Ten dBm
	Linewidth	10 MHz
LO	Radio frequency (RF)	15 GHz
Fiber	Fiber lengths	(0 -110) km
DD-MZM	Bias voltage	0V
	Extinction Ration	60 dBm
	Switching voltage	4V

PD	Responsivity	1 A/W

The obtained optical spectrum at the output of the DD-MZM is shown in figure (3-5. A). The optical spectrum analyser measures the measurement. The obtained optical spectrum comprises the carrier, first-order sideband, and second-order sideband. Whilst that of the optical filter as shown in figure (3-5. B). The optical spectrum obtained at the output of the inverted optical filter (notch filter) is composed of first and second-order sidebands. Thus, the input power of the carrier will be spread out among first order, second order and third order higher-order optical sidebands. It clearly shows that the optical spurious suppression ratio (OSSR) is 30.56 dB, which lead to avoiding using an electrical filter at the receiver. At the PD, when the system generates mm-wave without using an inverted optical filter, mm-waves are obtained, namely, 30 GHz, which is double the input frequency (15 GHz), 60 GHz, which quadruples the input frequency as shown in the figure (3- 6. A). That is measured by a Radiofrequency analyser connected at the output of PD.

The obtained mm-waves at the PD when using an inverted optical filter as shown in figure (3-6. B) are; double the input frequency (30 GHz), which is the first-order sideband, is removed, and the power level of quadruple the input frequency (60 GHz) is increased. In addition, 90 GHz is generated but with an RFSSR of 25.34dB.

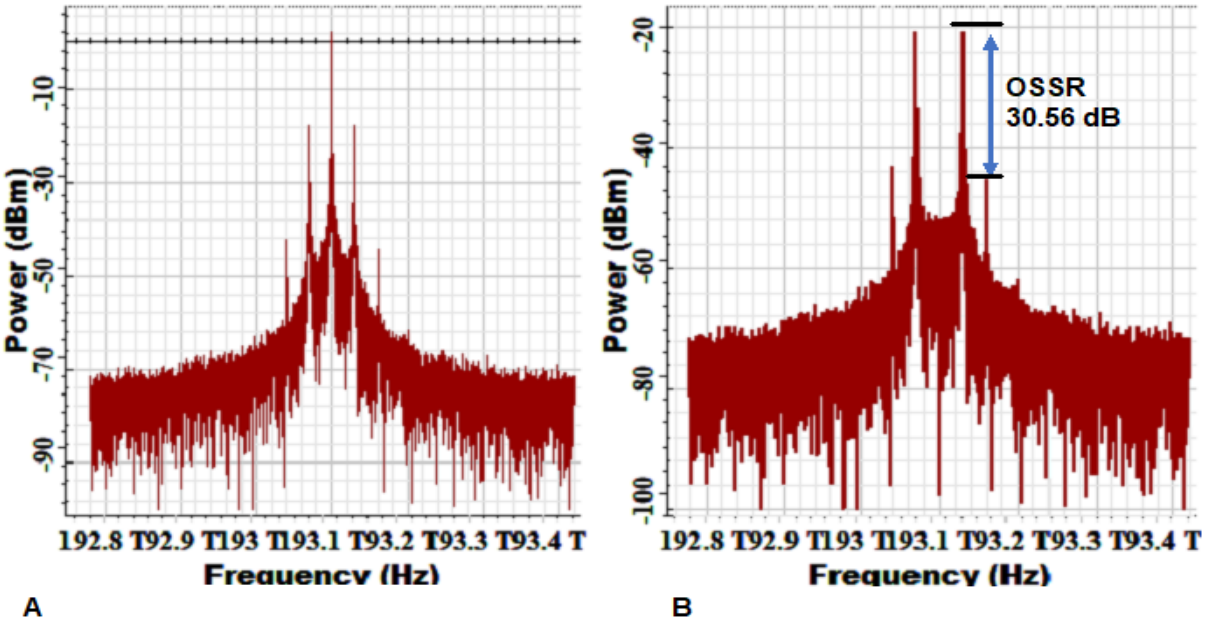

Figure 3-5: The obtained optical spectrum (a): At the output of DD-MZM (b) At the output of the inverted optical filter.

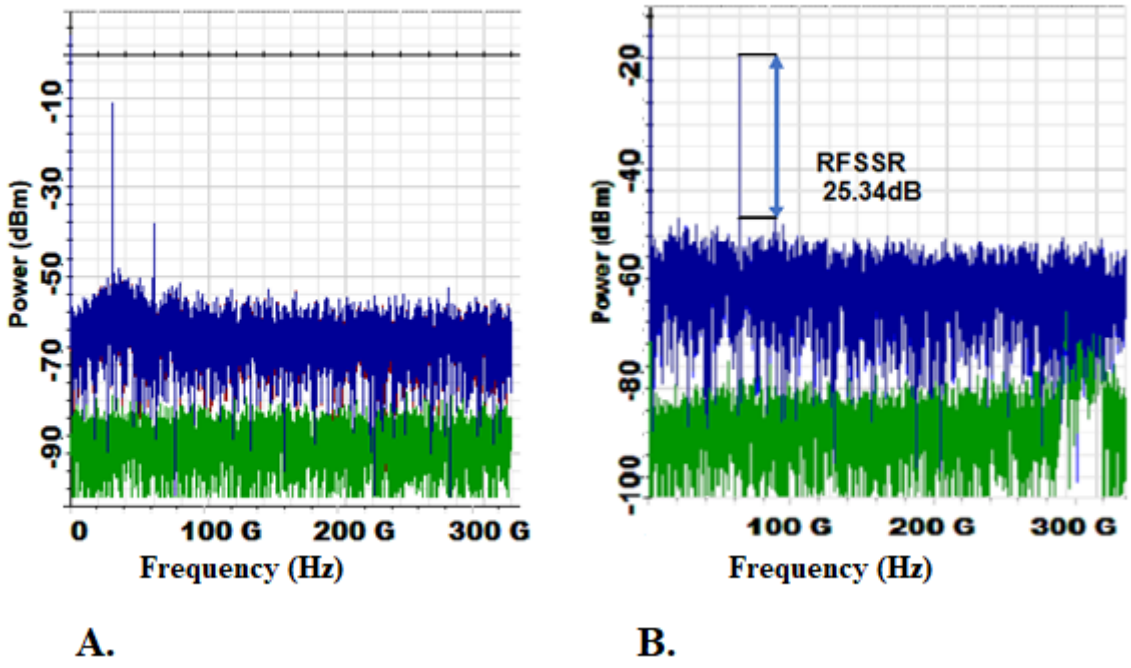

Figure 3-6: The obtained mm-wave signals at the PD (a): when the carrier is not suppressed; (b) when the carrier is suppressed.

While figure (3-6. B) Indicates that the received signal power of 60 GHz is increased from -58 dBm to -23 dBm to 25.34dB. Therefore, removing the carrier by using an inverted optical filter enhances the RFSSR. With the proposed design, the power of the desired mm-wave signal at 60 GHz is greater than that of other generated frequencies near -56 dBm.

3.4.2 The Data Transmission

The transmission performance of the obtained mm-wave signal over single-mode fibre (SMF) is evaluated by modulating the obtained optical signal with a baseband signal of 2.5 Gb/s. Firstly, data transmission performance is evaluated when the system does not use the proposed inverted optical filter, referred to as design A, as is shown in figure (3-7). Then two configurations are considered to modulate the baseband signal the data in the proposed design and compare the performance of the modulated mm-wave in each. The first configuration, when the data is modulated directly with DD-MZM while generating an optical mm-wave signal, namely, Design B, as shown in figure (3-8) and simulation set up design, is presented in appendix 2. The second configuration is when the data is modulated with obtained optical

mm-wave signal, namely design C, as is illustrated in figure (3-9). Its simulation setup is presented in appendix 3.

All designs are simulated using Optisystem software. The modulated signal is sent over the SMF transmission line at different distances stating back to the back system (B to B), 2 km, 20 km and 40 km. The SMF attenuation is set to 0.2 dB/km and 16.75 ps/nm/km dispersion. At the receiving part, PD is used to detect the modulated mm-wave signal at 60 GHz. Then, the data are recovered to evaluate the performance of the mm-wave by observing the eye diagram analyser for each design. An Eye diagram analyser is used in Optisystem to detect the obtained modulated mm-wave signal by monitoring the opening eye diagrams, which designate the quality of the obtained signals as shown in figures(3- 10) to (3-12).

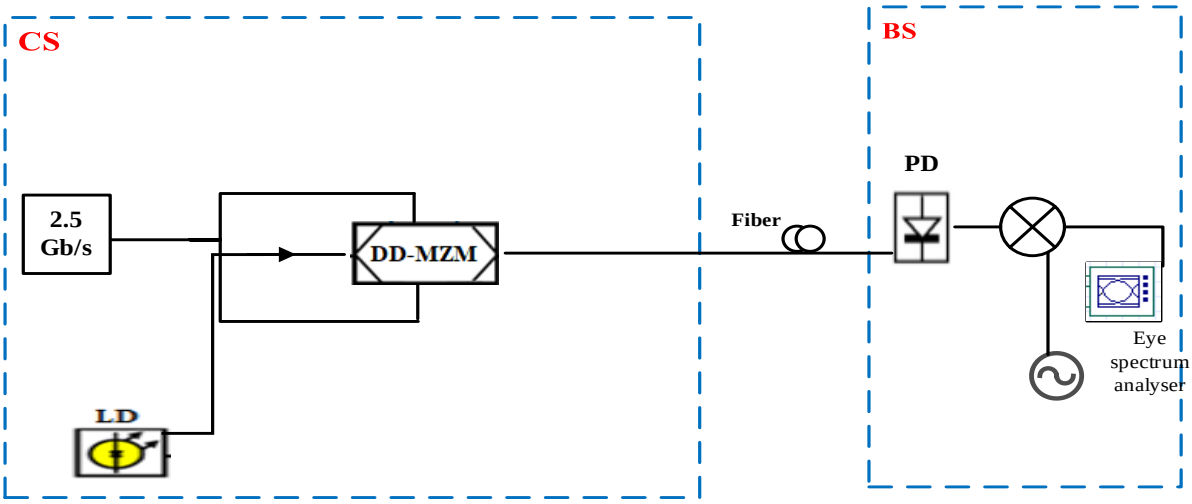

Figure 3-7: Simulation setup of design A

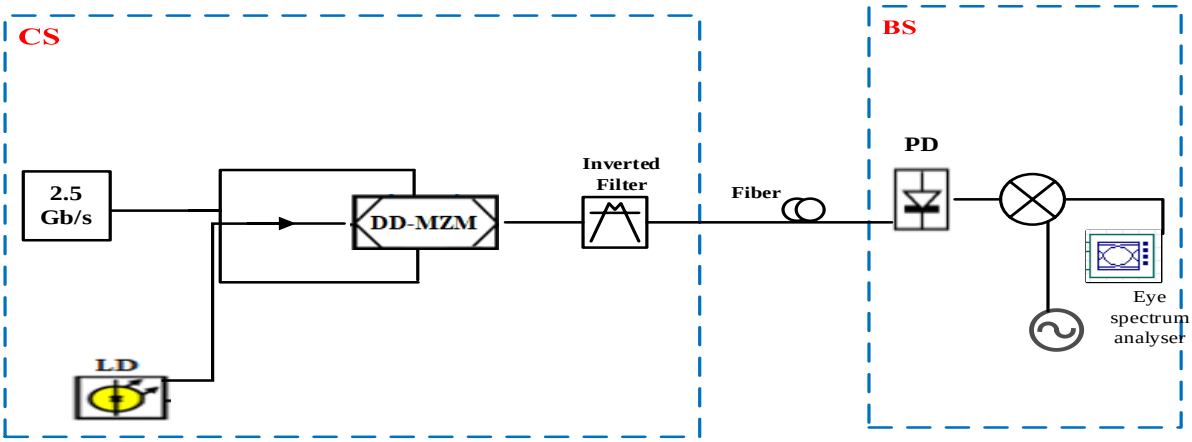

Figure 3-8: Simulation setup of Design B, where the inverted optical filter is used.

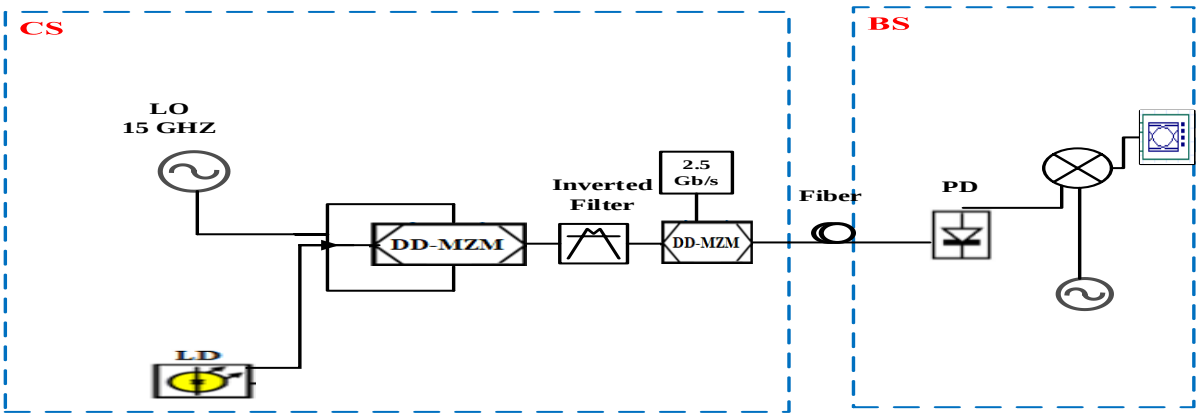

Figure 3-9: Simulation setup of Design C.

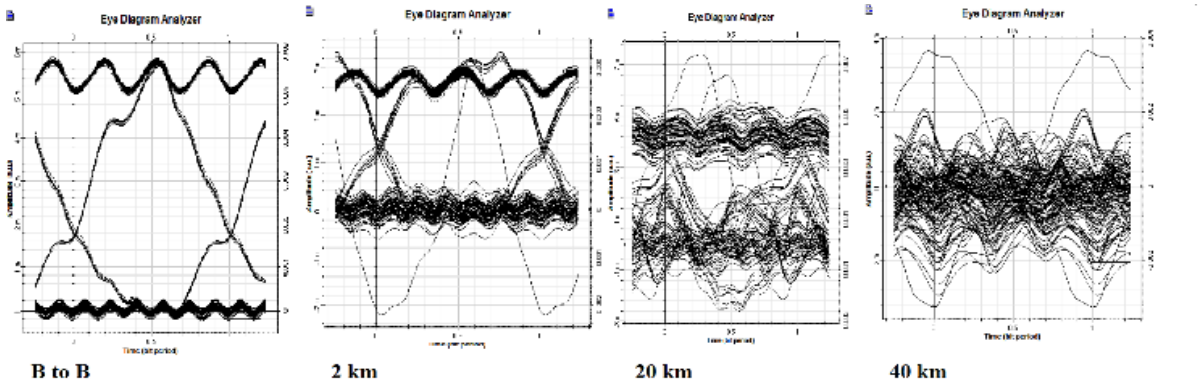

Figure 3-10: Eye diagram for design A.

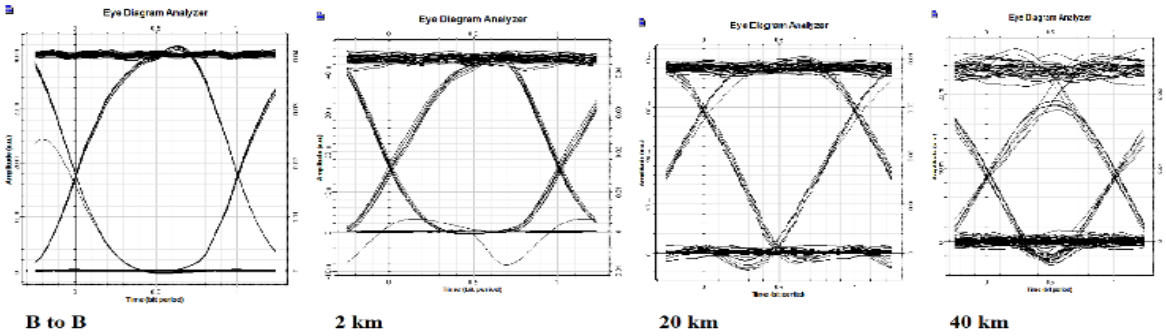

Figure 3-11: Eye diagrams for Design B.

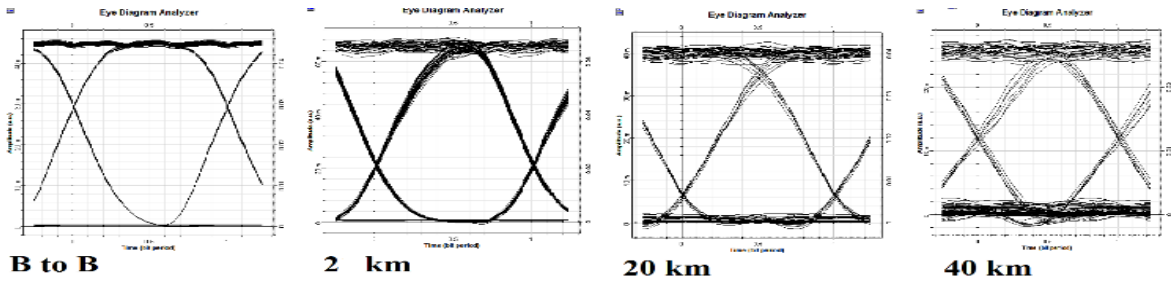

Figure 3-12: Eye diagrams for Design C

Figures (3-10) (3-11) (3-12) illustrate the eye diagrams that are obtained for designs A, B, and C, respectively. Figure 3-10 shows that the obtained signal from design A has extensive performance degradation where the carrier is not suppressed. Figure 3-11 indicates that the eye diagram of the received signal at 2 km is clear and widely opened. When transmission distance increases, eye diagrams become distorted due to optical fibre impairments such as; attenuation and chromatic dispersion. On the other hand, the eye diagrams obtained from design C are clear and wide open with less distortion than that in design B, which means has more capable to overcome the effect of attenuation and chromatic dispersion. Eye diagrams obtained demonstrated that removing the carrier benefits transmitting the data with obtained mm-wave more.

Moreover, the Max Q factor of the obtained signal for designs A, B, and C are measured over different SMF distances, as shown in figure (3-13). For design A, the achieved max factor is 10.04 for 20 km SMF length and 40 km, the max Q factor is 2.01. The achieved max Q factor for design B is 14.01 for 20 km and 10.01 for 40 km. For design C, the max Q factor is 20.01 for 20 km and 21.5 over 40 km SMF transmission length.

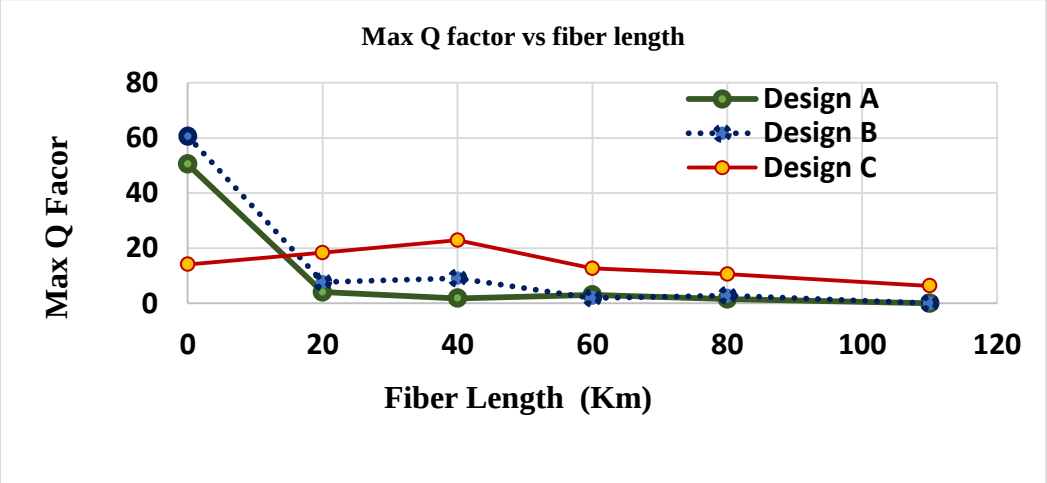

Figure 3-13: Max Q factor for different designs at different fibre length distances

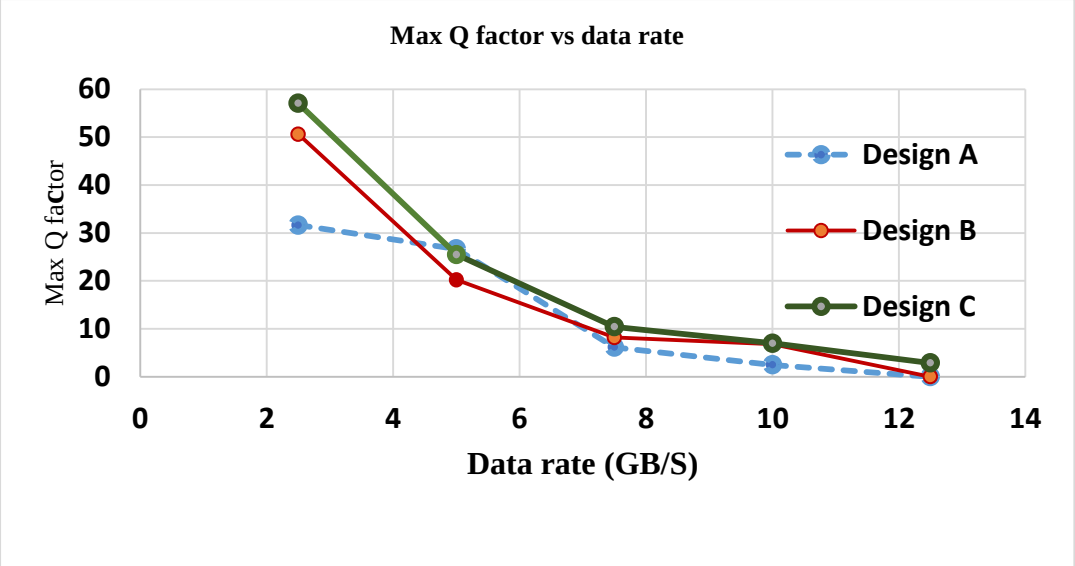

Figure 3-14: Max Q factor with different bit rates.

In addition, figure (3-14) shows that the proposed designs B and C can work effectively with different data rate like; 5 Gb/s , 7.5 Gb/s over SMF of 2 km with the same parameter setup. The max Q factor decreases when there are increases in data rates at same fibre length as it shown in figure (3-14. As illustrated in the previous figure, at 10 Gb/s, the Max Q factor for Design A is 2 while those Design B and Design C are 7.8 and 10, respectively. A key advantage of these designs is that, the optical modulator with a maximum operating frequency of 15 GHz can generate an mm-wave signal up to 60 GHz based on carrier suppression with acceptable performance.

3.5 Summary

This chapter has been approved that the mm-wave signal can be generated effectively with carrier suppression using an inverted optical filter in a simple, low-cost design.

Using an inverted optical filter adds the advantage of suppressing the carrier, balancing the received signal power of the desired obtained signal. Moreover, what is proposed reduces the number of optical components, making it easy to implement. The Optisystem simulation has demonstrated that the proposed design has good transmission performance in both scenarios of implementing the data when the data modulates while generating optical mm-wave and when the data is modulation after the optical mm-wave is generated.

However, the results show that modulating the data with the obtained mm-wave has better performance than in modulating the data directly while generation of mm-wave. For 2.5 Gb/s data transmission, the max Q factor for 40 km is 21.42 and 17.4 for 20 km. With the scenario of modulating the data directly while generating mm-wave, the max Q factors are 15.083 for 20 km and 7.45 for 40 km.

The performance of the obtained mm-wave signal is effective up to 10 Gb/s over 2 km in both scenarios of modulating the data. It is concluded that carrier suppression using the inverted optical filter can generate effective mm-wave.

Chapter 4 Downlink Of High Quality 72 GHz Millimeter Wave

4.1 Overview

In this chapter, a high clarity optical 72 GHz mm-wave signal is generated using a frequency quadrupling technique based on carrier suppression. The optical carrier suppression ratio of the generated 72 GHz signal is 71dB. Thus, highly suppression of optical carrier and harmonics lead for obtaining high purity mm-wave, which will decrease suffering from impairment due to fibre dispersion. Therefore, there is an improvement of the obtained OSSR compared with obtained OSSR in the previous chapter for about 42%. In addition, OSSR is improved from 42.3 to 71.4 compared to the reference.

Then, the performance of a modulated mm-wave in downlink data transmission is investigated using an additional optical modulator. Two different optical modulators are employed separately to compare the performance of achieved mm-wave; MZM and EAM. It is found that the signal when modulated using EAM has better performance than when this is done with MZM. The max Q factor for 80 km is nearly 20 with the EAM modulator, but just 2.3 with MZM. In addition, the performance of generated mm-wave is investigated with two different types of PD, PIN, and APD, as optical receivers to get the best result to achieve a high-quality signal. The ability of the system to carry a higher data rate is examined by varying the bit rate up to 10 Gb/s successfully over 20 Km.

4.2 Introduction

With the massive growth in the number of wireless communication users and the bandwidth required per subscriber, migrating to higher frequencies from lower radio frequency to mm-wave carriers is an essential solution. Mm-wave for RoF technologies has been a robust area of research and investigation over the past decade, which combines the benefits of mm-wave frequencies and RoF technologies [6]. There are two essential processes for mm-wave over RoF: generating mm-waves and downlink data modulation [12]. Optical generation of an mm-wave signal is one of the main stages over fibre technology to get a high-quality signal. As mentioned previously, many approaches have been reported recently to generate such waves. Optical generation of mm-waves using the external modulation technique is more accurate. Such schemes have shown the most potentiality for a high-frequency signal generation due to the sizeable tunable range, excellent stability, high spectral purity, and

lower system cost [3]. MZM, EAM and a Phase Modulator are examples of devices that can be used as external modulators in RoF [3]. Two techniques are demonstrated for generating mm-waves using external modulation, with optical frequency multiplication and without [2]. External modulation leads to higher-order harmonics since it is a source of nonlinearities in the transmission characteristic. The generation of harmonics associated with the desired signal depends on bias voltage and modulation index. Different modulation schemes using MZM have been deployed to generate mm-waves which among them, OCS is preferred because of its advantage in enhancing the receiver sensitivity [83].

Moreover, desired frequency multiplication factor can be accomplished by the proper setting of the RF LO phases, modulation index, and the biasing voltages of the MZMs. Common scenarios of optical N-tupling implementations are discussed in chapter 2. Different combinations of MZMs were utilised to generate mm-waves with desired frequency multiplication of input frequency by different settings of the modulation index and RF LO phases. In [80], the researcher used the quadrupling technique where two cascaded MZMs based on a multiplication factor of four to generate a photonic microwave frequency. A multiplication factor of six was demonstrated to create mm-waves for RoF in [82]. In [86], a sixtupling frequency scheme for high-quality optical Millimeter-wave signal generation based on carrier suppression was investigated. In [73], two cascaded dual-electrode MZMs, MI-insensitive, were utilised and a filterless frequency octupling scheme based on two parallel dual-parallel Mach Zehnder modulators. In [75], frequency decoupling techniques using two parallel DD-MZMs and an interlayer were deployed to get a 60 GHz OCS mm-wave signal. A 72 GHz mm-wave was generated using quadrupling techniques by using three different MZMs. However, these proposed systems need more than one optical filter or external modulators to remove undesired optical sidebands, significantly increasing system complexity and cost. Therefore, the frequency quadrupling technique without optical filters is of great interest. In this work, mm-waves at 72 GHz based on carrier suppression are generated using a quadrupling technique. Then, the downlink data modulation performance is investigated using two types of optical modulation, EAM and MZM, to obtain the best performance of a modulated mm-wave.

4.3 Principle Of The Proposed Design

A schematic diagram of generating mm-wave using the frequency quadrupling is shown in Figure 4-1. Starting with a continuous wave (CW) laser with finite spectral width is injected into the dual parallel configuration of upper and lower MZM, which is expressed as:

$$E(t) = E_o cos\omega_c t \quad (4\text{-}1)$$

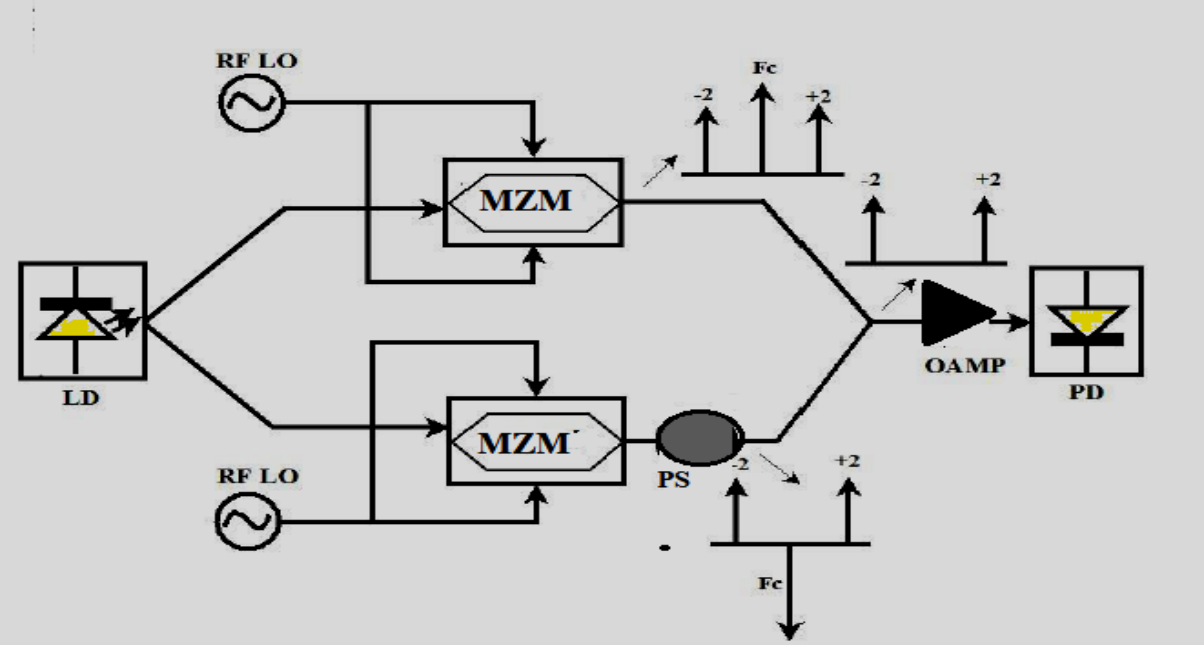

Figure 4-1: Schematic diagram of generating mm-wave using quadrupling technique

E_o is the amplitude and

ω_c is the angular frequency of emitted light

Both electrodes of upper MZM is driven by RF LO by

$$V_{rf}(t) = V_{rf} \cos \omega_m t \quad (4\text{-}2)$$

V_{rf} is the amplitude of RF signal and

ω_m The angular frequency.

RF LO drives the lower MZM.

$$V_{rf}(t) = V_{rf} \sin \omega_m t \quad (4\text{-}3)$$

Both the MZMs are biased at the Maximum Transmission Point of the MZM. Also, RF local oscillator drives upper and lower MZMs with an equal phase shift of 90 ° introduced between the RF-driving signals applied to each MZM drive electrode.

The output of upper MZM can be expressed as

$$E_{upper\ MZM}(t)=\frac{E_0}{4}\cos\omega_c t\begin{bmatrix} e^{j\frac{\pi V_{rf}}{V\pi}\cos(\omega_m t)+j^{V_{b2}}/_{V_\pi}} \\ +e^{-j\frac{\pi V_{rf}}{V\pi}\cos(\omega_m t)+j^{V_{b1}}/_{V_\pi}} \end{bmatrix} \quad (4\text{-}4)$$

V_π is switching bias voltage of MZM, $V_{b1}$and V_{b2} are biasing voltage of the MZM. if $V_{b1} = V_{b2}$ =0, the equation can be expressed as

$$E_{upper\ MZM}(t)=\frac{E_0}{4}\cos\omega_c t\ \begin{matrix} e^{j\frac{\pi V_{rf}}{V\pi}\cos(\omega_m t)+0} \\ +e^{-j\frac{\pi V_{rf}}{V\pi}\cos(\omega_m t)+0} \end{matrix} \quad (4\text{-}5)$$

$$E_{upper\ MZM}(t)=\frac{E_0}{4}\cos\omega_c t\ \begin{matrix} e^{j\frac{\pi V_{rf}}{V\pi}\cos(\omega_m t)} \\ +e^{-j\frac{\pi V_{rf}}{V\pi}\cos(\omega_m t)} \end{matrix} \quad (4\text{-}6)$$

m= $\frac{\pi V_{rf}}{V\pi}$. is the modulation index

The equation can be reduced to

$$E_{upper\ MZM}(t) = \frac{E_0}{4}\cos\omega_c * [\cos(\mathrm{m}\cos(\omega_m t)] \quad (4\text{-}7)$$

Using Bessel function of the first kind in the equation (4-7) can be expressed as

$$\frac{E_0}{4}\cos\omega_c t\ [j_0(m) + 2\sum_{n=1}^{\infty}(-1)^n J2n\cos(2n\omega_m t)] \quad (4\text{-}8)$$

Equation (4-8) shows the optical output of upper MZM. It has a major carrier and even orders terms. Similarly, the production of lower MZM can be written as follows

$$E\ of\ MZM_{lower}(t) = \frac{E_0}{4}\cos\omega_c t * [\cos(msin\omega_m t)] \quad (4\text{-}9)$$

Using Bessel function of the first kind equation can be expressed as

$$\text{E of } MZM_{lower}(t) = \frac{E_0}{4}\cos\omega_c t * j_0(m) + 2\sum_{n=1}^{\infty} J_{2n}\cos(2n\,\omega_m t)e^{j\pi} \quad (4\text{-}10)$$

This equation indicates that the output of lower MZM contains the even order sideband and carrier. By applying 180^0 phase shift to the output of lower MZM. Then the output of both MZMs are combined by the optical couple, which is expressed as follows:

$$E_0(t) = E\ of\ MZM_{lupper}(t) + \text{E} \quad \text{of} \quad MZM_{lower}(t) = \frac{E_0}{4} \cos \omega_c t * \left\{[J_0(m) + 2\ \sum_{n=1}^{\infty} J_{2n}\ (-1)^n \cos(2n\omega_m t)] + [J_0(m) + 2\ \sum_{n=1}^{\infty} J_{2n} \cos(2n\omega_m t)]e^{j\pi}\right\} \quad (4\text{-}11)$$

This equation can be reduced to

$$\frac{E_0}{4} \cos \omega_c t\ [J_0(m)\cos(2\omega_m t] \quad (4\text{-}12)$$

Using the trigonometric relationship

$$E_0 = E_0 J_2(m)[\cos(\omega_c + 2\omega_m t) + cos(\ \omega_c - 2\ \omega_m t)] \quad (4\text{-}13)$$

$$[j_0(m) + 2] + \quad j_0(m) + \frac{E_0}{4}\cos\omega_c t * j_0\ (m) + 2\sum_{n=1}^{\infty} J_{2n} \cos(2n\ \omega_m\ t) e^{j\pi} \quad (4\text{-}13)$$

The above equation clearly shows that the output of the optical coupler consists of only second-order sidebands. The photocurrent resulting from the beating of ±2 order sidebands can be written as,

$$\text{I (0.t)} = \Re\ |E_0\ (t)|^2 \quad (4\text{-}14)$$

$$\text{(0.t)} = \Re|E_0\ (t).E_0{}^*\ (t)| \quad (4\text{-}15)$$

$\Re$ is responsivity of the photodetector

$E_0{}^*\ (t)$: the complex conjugate.

The equation 4-16 can be simplified to

$$\text{I(0,t)} = E_0{}^2 J_2{}^2(\text{m})[1 + \cos 4\omega_m t\ ] \quad (4\text{-}16)$$

The above equation shows that the detected photocurrent consists only of the signal at $4\omega_m t$, which is the desired mm-wave signal.

Equation (4-16) shows that the detected photocurrent at receiver consists only of the signal at 4ω, the desired Mm-wave signal. This scheme is filterless, highly stable and tunable since no optical filtering is used.

4.4 Simulation Set-up And Results

The simulation set-up of generating mm-wave using quadrupling technique is shown in Figure 4-1. The simulation set-up of generating mm-wave using quadrupling technique is shown in Figure 4-1. A continuous-wave (CW) laser with finite spectral width is injected into the dual parallel configuration of upper and lower MZMs. The output of upper MZM contains second and fourth sidebands. Then lower MZM is driven by the same RF signal with 180° phase difference; this will cause the polarities of fourth-order sidebands at the output of lower MZM to be in opposition to those at the output of upper MZM. Then, the outputs of the MZMs are combined using an optical coupler, which has only one band output, second-order sidebands, 72 GHz. Therefore, after the output coupler, the even-order sidebands generated by lower MZM cancel out the even-order sidebands generated by upper MZM and only the optical sidebands of the order of fourth is obtained. Finally, the fourth-order sidebands are detected using a photodetector, and the detected signal is observed using an electrical spectrum analyzer.

The Optisystem software is used to generate and investigate the performance of 72 GHz in downlink transmission. The simulation experiment is divided into three parts: firstly, the mm-wave is generated at 72 GHz (The simulation is presented in appendix 5). Secondly, the performance of the obtained mm-wave is investigated when it is modulated with data using MZM as optical modulator. Then, it is repeated to examine the performance of this wave when it is modulated with data using EAM as optical modulator. Finally, the system's performance is measured through different data rates to observe the affectivity of the proposed design.

4.4.1 Generating mm-wave At 72 GHz

The simulation set-up for generating 72 GHz mm-waves is presented in Figure (4-1), with the parameter simulation set up is displayed in table.1. The light signal of the spectral width of 10 MHz is emitted and injected into the MZMs using the CW laser source. The upper and lower

MZMs are driven by 18 GHz with a phase shift of 90°. Both MZMs are biased with a switching bias voltage of 4 V. The biasing voltage for both MZMs is set to zero to overcome the chirp issues caused by MZM. Because both MZMs are biased at the peak operation point, only carrier and even order sidebands are generated. The simulation set up design is presented in appendix 8.

Table 4.1: Parameters setup for generating 72 GHz.

Device	Parameter	Value
CW-laser	Optical signal frequency	193.1THz
	Optical power signal	10 dBm
	Spectral width	10 MHz
LO	Radio frequency	18 GHz
MZM	Bias voltage	0 V
	Switching bias voltage	4 V
	RF voltage	4 V
PIN-PD	Responsivity	1 A/w

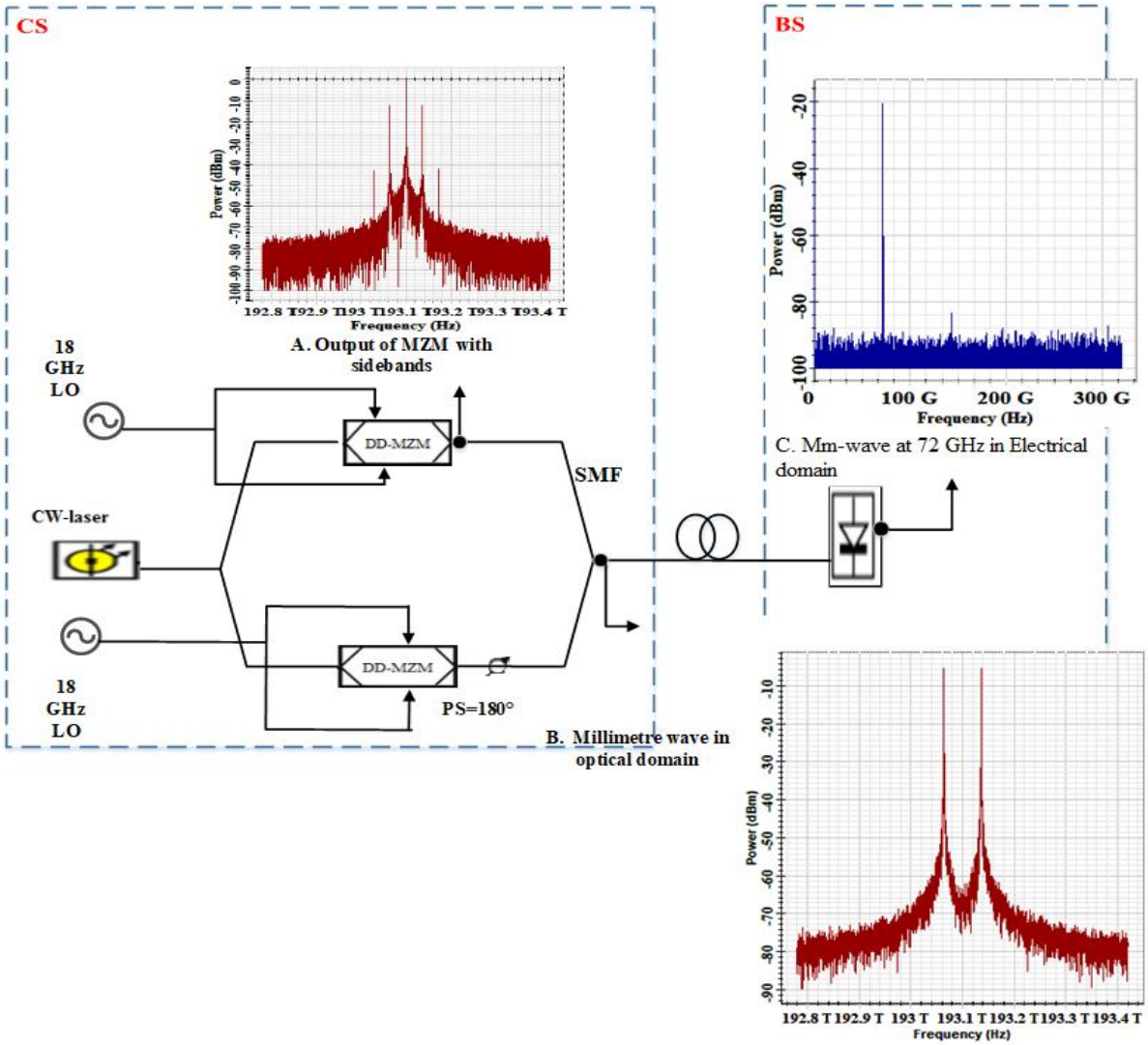

Figure 4-2: Simulation design to generate 72 GHz. (A) mm-wave without carrier suppression in the optical domain, (B) Carrier suppressed mm-wave in the optical domain, (C) mm-wave at 72 GHz in the electrical domain.

Figure (4-1) B shows that the OSSR of obtained mm-wave in the optical domain is 71.4 dB. At the same time, Figure (4-1) C shows the desired mm-wave at 72 GHz for the electrical field with an RFSSR of 60dB. Compared with obtained result in chapter 3, the OSSR in the previous chapter is 30.5dB, and RFSSR is 25dB. So, the obtained result in this work shows there is improvement in term of suppression of sideband compared to the obtained result in previous chapter.

Additionally, compared to the obtained result in reference [131] using the same technique, the obtained OSSR was 33dB in [131]. Moreover, obtained RFSSR was 32dB. Hence, generating mm-wave signal using this technique improves the obtained OSSR and RFSSR about 44 %. On the other hand, this system is tunable while we can generate different

frequencies by tunning the input frequency generated at LO. For example, 60 GHz is generating by setting the input RF to 15 GHz as it shown in following figure.

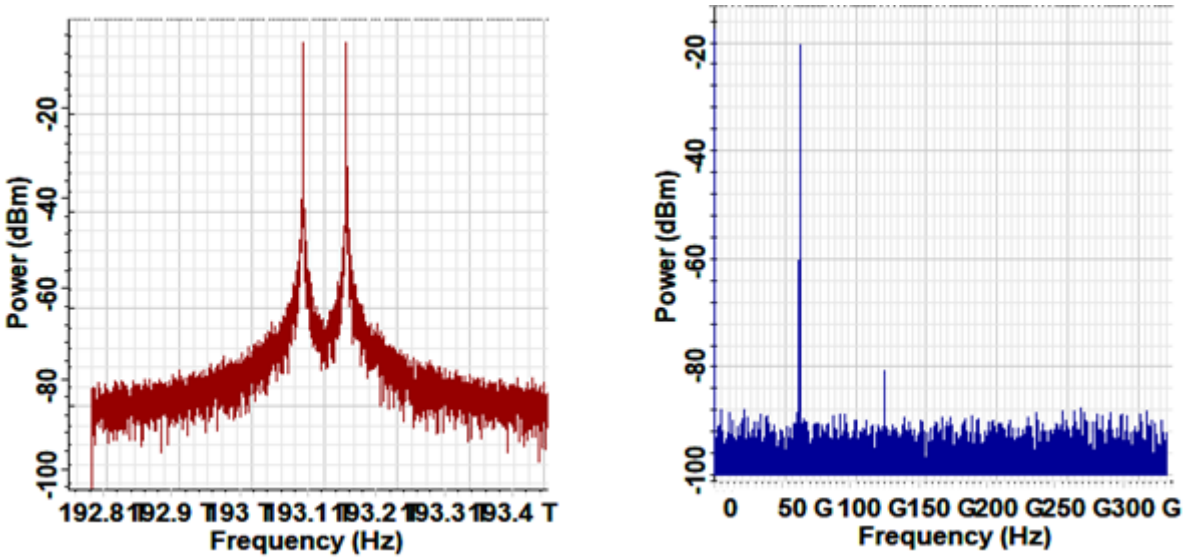

Figure 4-3:A. Optical 60 GHz related to 193.1 THz B. Obtained mm-wave at 60 GHz

High quality of the obtained signals performance leads to avoiding firmly using the electrical filter at the receiver. Thus, the obtained mm-wave has more excellent immunity to chromatic dispersion caused by fibre, which gives it the ability to be transmitted over a longer fibre distance.

4.4.2 Downlink Data Transmission

The system is simulated using Opisystem software with additional optical devices to investigate the quality of the generated optical mm-wave over SMF, as is shown in figure (4-2). The obtained mm-wave is modulated with a baseband signal with two different optical modulators to investigate the performance of obtained signal with the best quality factor (QF). Firstly, the obtained mm-wave signal is modulated using MZM optical modulator data. Then the obtained mm-wave signal is modulated with data using EAM optical modulator with the same simulation setup. The same simulation parameters set up are used in table 1, with additional parameters set up for additional added components. Additionally, two types of PD (PIN-PD and APD) are used to evaluate the validity of the optical device used to examine the performance of the obtained mm-wave in downlink transmission. Thus, the simulation setup is running first with PIN-PD, and then it will be replacing the PIN PD by APD to see how the performance of the signal could be improved (the simulation set up design is presented in appendix 9 and appendix 10).

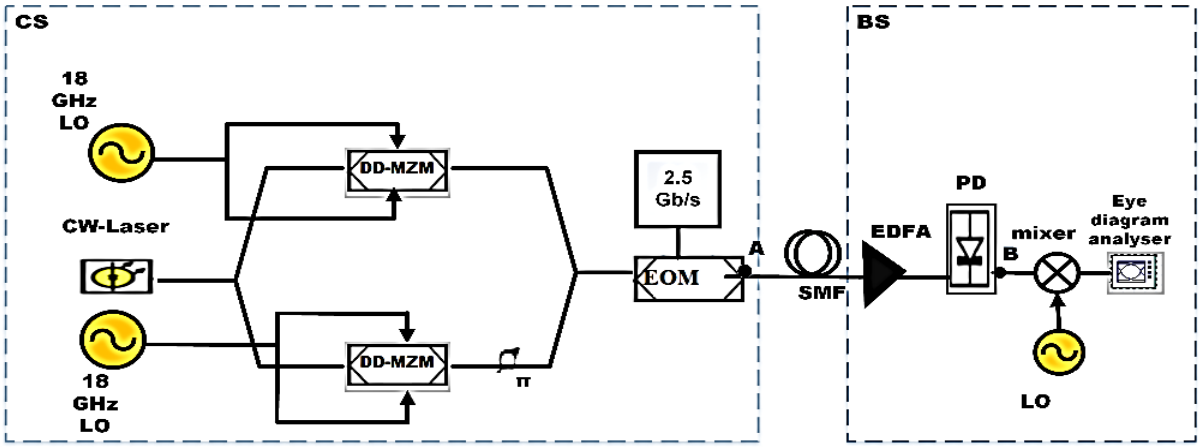

Figure 4-4: Simulation design using additional optical devices for data modulation, LO: Local oscillator, CW laser: continuous wave, EOM: Electro-optical Modulator. SMF Single-mode fibre, EDFA: (Erbium-doped fibre amplifier, PD: Photodetector.

4.4.3 PIN - PD

After the mm-wave is generated, it will be modulated with 2.5 Gb/s data using MZM. Then it will be transmitted through SMF to PIN-PD to extract the mm-wave in the electrical domain. The same steps are repeated when the mm-wave is modulated with 2.5 Gb/s by using EAM optical modulator as presented in figure (4 -4). Both systems are simulated to observe the performance of modulated mm-wave to investigate the performance of modulated mm-wave signals by MZM and EAM sent over different SMF distances. As it shown in figure (4-5), the max Q factor and received signal power reduce as the fibre length increases and that is obviously due to fibre characteristics like; attenuation and dispersion. As shown in figure (4-5.A), the achieved max Q factor when mm-wave is modulated using EAM is 40.1 over 20 km, and the max Q factor when the mm-wave is modulated using MZM is 28 the same fibre length.

For 40 km, the achieved max Q factor is 51 when EAM is used for optical data modulation and 17.2 when MZM is used as optical data modulation. For 80 km, the max Q factor for a design using EAM is 38.2, while using MZM, the max Q factor is 10.

The received signal power for obtained 72 GHz mm-wave over different SMF length is shown in Figure (4-5. B). it shows that the electrical received power of 72GHz is -18 dBm when the EAM is used over 20 km fibre length, and for 80 km almost the mm-wave power reached -48 dBm. On the other hand, the received signal power reached -38 dBm when

system used MZM for optical data modulation over 20 km and -58 over 80 km. Table (4-2) illustrated the obtained result.

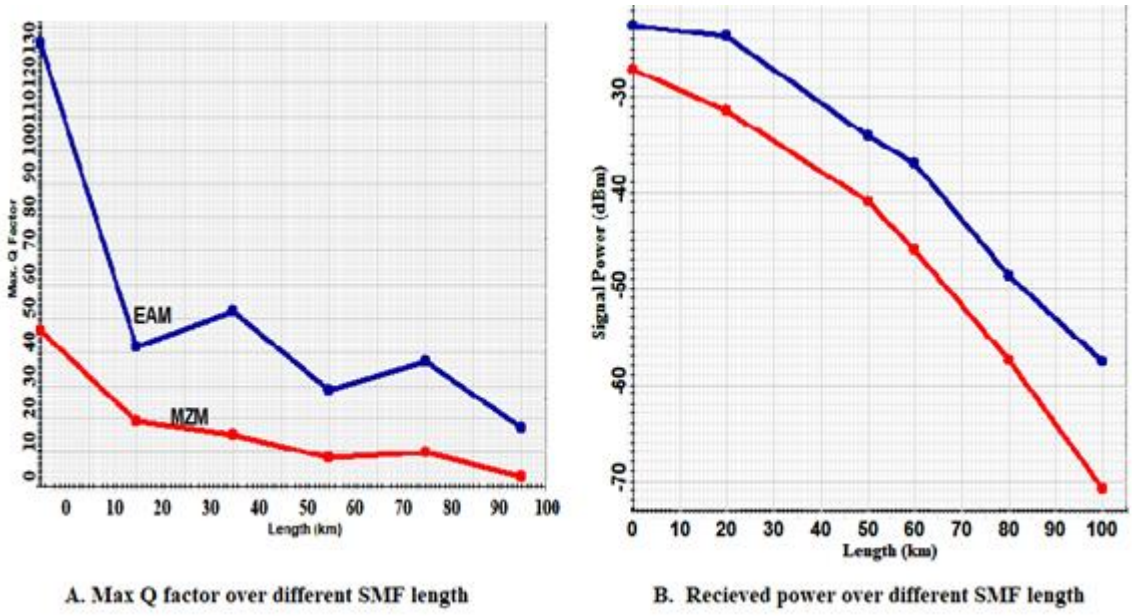

A. Max Q factor over different SMF length

B. Recieved power over different SMF length

Figure 4-5: Performance of 72 GHz mm-wave when PD is PIN-PD.

When employing PIN-PD, the mm-wave power using EAM is slightly higher than the received modulated mm-wave power by using the MZM modulator. However, the received signal power for modulated mm-wave has the same power decreasing as long as fibre length increases.

4.4.4 APD

Then, the performance of modulated mm-wave is investigated, but this time with APD -PD. The modulated mm-wave in two scenarios is sent to be received by APD to extract 72 GHz mm-wave signal in different SMF ranges. Figure (4-6) shows the performance result of simulating systems. It is found that the received signal power is better than the first system where PIN-PD is used. The max Q factor and received signal power in both curves in figure (4-6) decrease in increasing fibre length, but that, as maintained previously, is expected because of the characteristics of the fibre. Figure (4-6.A) shows the max Q factor for obtained signal in different fibre lengths; at 20 km, the max Q factor is 40 when EAM is used as data modulator, at the same fibre length, the max Q factor is 21. At 80 km, the max Q factor is 38 when the system uses EAM, while in another scenario; the max Q factor is 18.1. Figure (4-6) B shows the received signal power of modulated mm-wave through different fibre lengths. It is found that the received signal power at 20 km is 28 dBm when the system is using EAM

and 25 when the system is using MZM. At 80 km, the received signal power is 8 dBm when the system uses EAM and -6 dBm when the system uses MZM. At 100 km, the received signal power decreases to -11 dBm when using EAM and -20 for another scenario. Thus, the received electrical power of modulated mm-wave in the first scenario (MZM) is slightly less than achieved in the second (EAM) scenario based on the shown curve in figure (4- 6. B).However, when employing APD as photodetection at the receiver, the proposed system works well even over 100 km based on the obtained result.

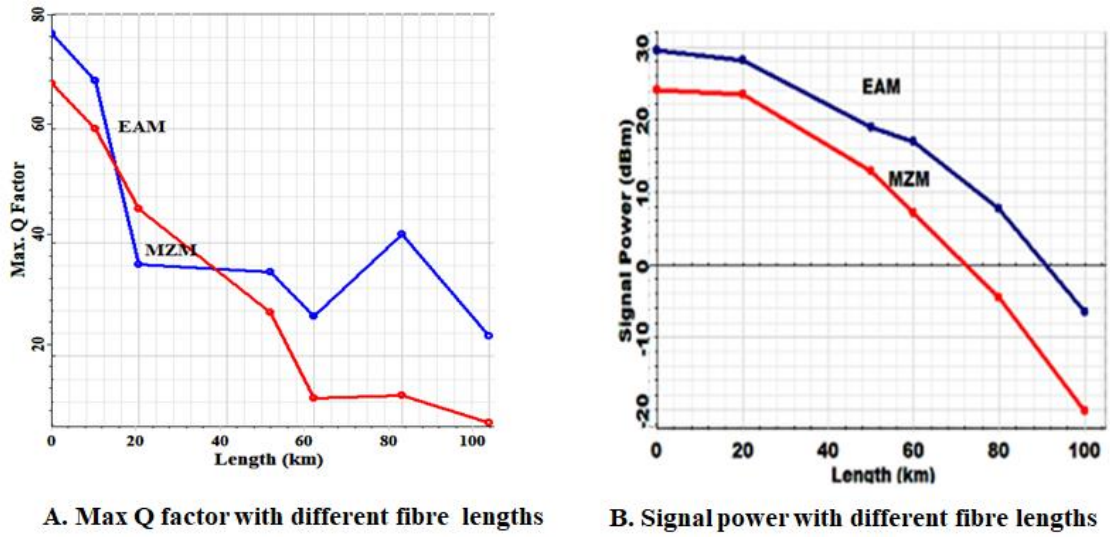

A. Max Q factor with different fibre lengths

B. Signal power with different fibre lengths

Figure 4-6: Performance of 72 GHz mm-wave when PD is APD.

Thus, the performance of the mm-wave using EAM has better performance than the mm-wave than is obtained by using MZM according to the obtained result. Regarding the PD, the proposed system is working well with both types of PD that are implemented to extract the mm-wave signal for RoF technology. The main limitation of PIN PD is that the receiver performance becomes very limited by the thermal noise compared to APD, which is preferred for long-distance links; APD is used, which provide a current gain due to its process of impact ionization [133][134]. However, the effect of APD appears clearly in received electrical powers, as it is presented in Figure (4-6. B). Table 4-2 summarised the obtained result for different photo detectors with different electro optical modulations (EOM)s.

Table 4-2: Obtained results of proposed design with PIN PD and APD in different EOM

PD	PD-PIN				APD			
EOM	EAM		MZM		EAM		MZM	
Obtained result	Max Q factor	Received signal power	Max Q factor	Received signal power	Max Q factor	Received signal power	Max Q factor	Received signal power
20 km	40	-22	20	-32	40	28	21	25
40 km	51	-32	16.1	-42	30	18	28	12
80 km	38	-48	10	-58	38	8	18	-6

4.4.5 Investigate The Performance Of 72 GHz With Different Bit Rates

The generated 72 GHz mm-wave performance using this design is also measured by varying the bit rate at the input data of EAM and MZM. The simulation was set up using the proposed design over 20 km SMF lengths. Figure (4-5) shows the obtained max Q factor with different bit rates (2.5, 5, 7.5,10 and 12.5) using PIN-PD and APD, respectively. For 20 km, the Max Q factor of received 10 Gb/s is 10 when the system uses EAM and 9 when the system uses MZM. The simulation result shows that the proposed system can successfully work up to 10 Gb/s.

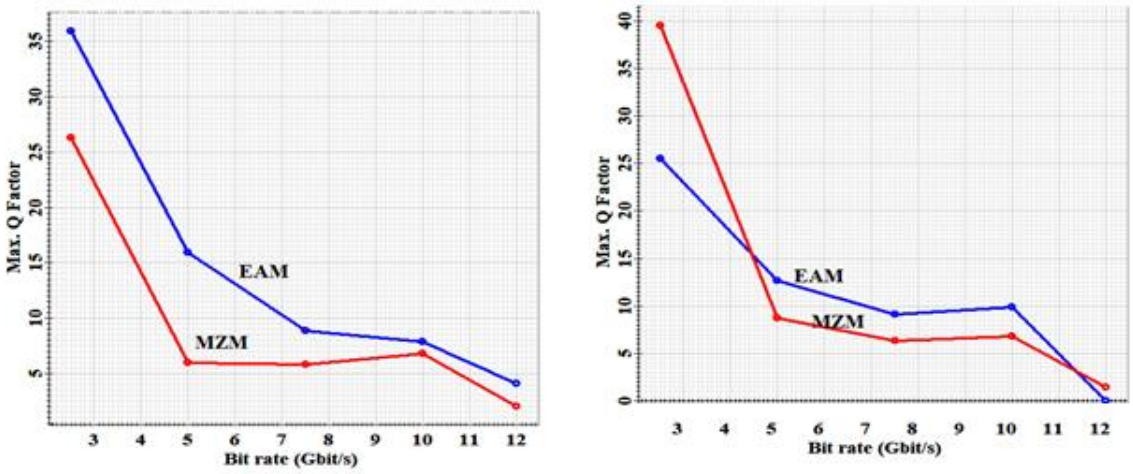

Figure 4-7: The performance of 72 GHz with different Bit rates. A. PD is PIN-PD B. PD is APD

4.5 Summary

The work in this chapter shows that 72 GHz can be generated with high-quality performance using quadrupling techniques. The optical carrier suppression ratio (OSSR) of 72 GHz mm-wave signals generated by 18 GHz driving signal can exceed 71dB. High optical carrier suppression and harmonics leads to decreased impairment due to fibre chromatic dispersion. Among Modulating mm-wave in downlink transmission, this work demonstrated that modulation mm-wave with data using EAM optical modulator has achieved high quality modulated mm-wave compared with MZM optical modulator by about 20 %. Additionally, APD as PD enhances the obtained 72 GHz signal performance compared to PIN-PD by about 35%. This technique's performance of generated signal can work effectively up to BER of 10 Gb/s successfully over 20 km.

Chapter 5 Investigating The Performance Of The Generated Lower Band Of Terahertz Frequencies Using A 12 Tupling Technique Over Fiber

5.1 Overview

In this chapter, for first-time upper band of mm-wave signals generated by just using dual Parallel Mach-Zehnder modulators (DP-MZMs). 216 GHz, 240 GHz, 264 GHz, 288 GHz, and 300 GHz are generated by tuning the input of Radio frequency a local oscillator (RFLO) to 18 GHz, 20 GHz, 22 GHz, 24 GHz, and 25 GHz, respectively. The impact of the extinction ratio of both MZMs on the optical sideband suppression ratio (OSSR) and Radio frequency spurious suppression ratio (RFSSR) has been considered. By properly setting the MZM parameters, biasing point voltages, RF LO frequencies, and phase shift of input signals, sixth-order optical sidebands are generated. The achieved OSSR and RFSSR are 36.7dB and 30.01dB, respectively. A power penalty of 2.2dB is achieved over 20 km single-mode fibre. Further, the performance of the generated terahertz frequencies is studied by modulating the generated signals with baseband signals of 10 Gb/s and 20 Gb/s using an electro-absorption modulator. The max Q factor for the obtained frequencies over different transmission distances is measured and analysed. The achieved max Q factor is 8.22 for 300 GHz with 10 Gb/s over 10 km transmission link distance.

5.2 Introduction

The upper band of mm-wave frequencies (0.200 – 0.300) THz in wireless communications can be an attractive candidate for providing capacity improvements for future communication systems. These have garnered interest because of the enormous bandwidth offered in wireless communication, which has not been allocated for any application yet in wireless communication systems [32]. Accordingly, massive throughput per user device could reach up to several Terabits per second (T) b/s at this band. Besides that, the attenuation of this band is less than 60 GHz, as is shown in figure (5-1).

The optical generation of mm-waves is the main factor in hiring this band. A frequency-tuples technique with a frequency multiplication aspect could be a proper solution to generate mm-wave by using a local oscillator (LO) with low frequency. Many research has been undertaken in generating mm-waves using external modulation based on carrier suppression

with optical N-tupling implementations, including frequency doubling, frequency quadrupling, frequency tripling, frequency six-tupling and frequency 12-tupling. In [146], [169], the researchers used two parallel MZMs based on a multiplication factor of four local oscillator frequencies to generate the mm-wave frequency. Specifically, a 36 GHz mm-wave was generated with an OSSR of 30dB and an RFSSR of 24.6dB.

In [136], the researcher used two Parallel MZMs based on a multiplication factor of four to generate a photonic microwave frequency with an OSSR of 38.2dB. A multiplication factor of six was demonstrated to create mm-waves at 60 GHz for RoF with an OSSR of 23dB in [137]. A tunable system was implemented to generate mm-waves at 20 GHz to 100 GHz by employing a uniform fibre Bragg grating-based acousto-optic tunable filter (UFBG-AOTF) [138]. Moreover, a 240 GHz mm-wave signal was generated using SiGe: CBiCMOS technology in [118], where 30 GHz was used as the input frequency to generate 216 – 256 GHz. In [139], 120 GHz was generated using a 12-tupling mm-wave generation system with two cascaded dual-parallel Mach–Zehnder modulators, including four MZMs.

The previous system was a tunable system of up to 216 GHz with an OSSR of 25.1dB and an RFSSR of 19.1dB. An optical mm-wave signal with 26.4dB OSSR and 20.3dB RFSSR was achieved using a 12-tupling mm-wave generation system based on two cascaded dual-parallel Mach-Zehnder modulators in [140]. Recently, in [141], a filterless approach of 16 frequency tupling was used to generate 160 GHz. This research used only two MZMs with two optical attenuators (OATT). The achieved OSSR and RFSSR are 30.34dB and 23.79dB, respectively.

In this chapter, 12-tupling frequencies are generated using Dual Parallel MZMs (DP-MZMs) only. A higher band of mm-wave frequencies can be generated by a low-cost and straightforward design with better OSSR and RFSSR than previous results in the same research area. The work's idea is to generate a higher mm-wave band with fewer components and less input frequency. Then, the performance of transmitted data of 10 Gb/s and 20 Gb/s through this generated signal is investigated to see the performance of the obtained signal.

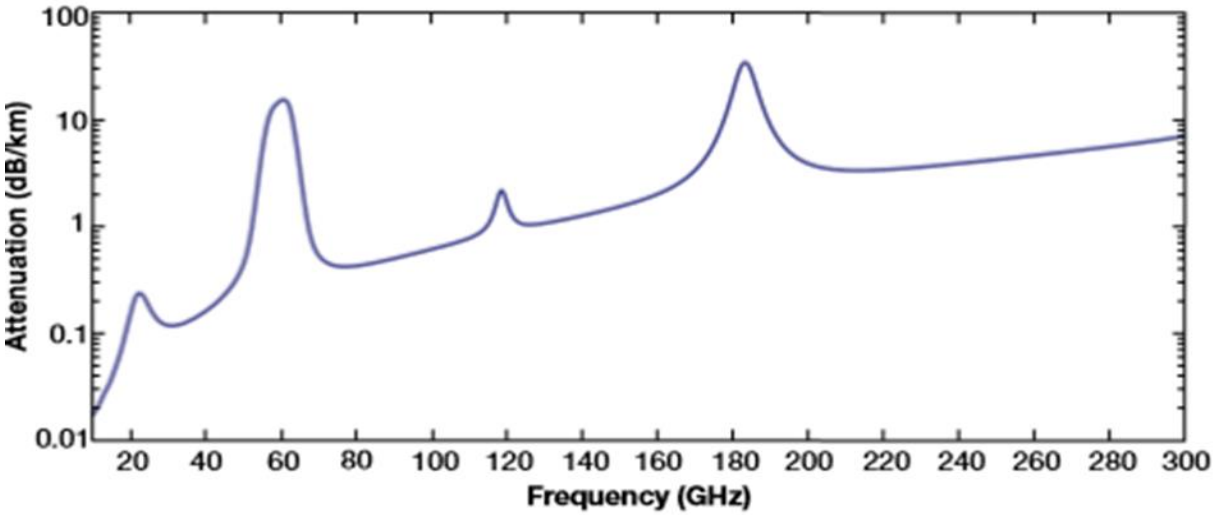

Figure 5-1: Atmospheric attenuation at sea level as a function of frequency [20]

However, the data signal can be switched to an M-PSK signal or M-QAM signal to increase the spectral efficiency of the transmitted data to achieve 40 Gb/s and more. Simulations were completed in this work by using Optisystem software [142], with 216, 240, 264, 288 and 300 GHz mm-waves being achieved by tuning the local input oscillator to 18, 20, 22, 24 and 25 GHz, respectively.

5.3 Principle Of The Proposed Design

İn proposed design as shown in Figure (4-3), the optical field is emitted to both of Dual Drive- MZMs (DD-MZM), which are indicated Dual Parallel - MZMs (DP-MZM) using a continuous wave (CW) laser:

$E_n(t) = E_0 cos(\omega_0 t)$ (1)

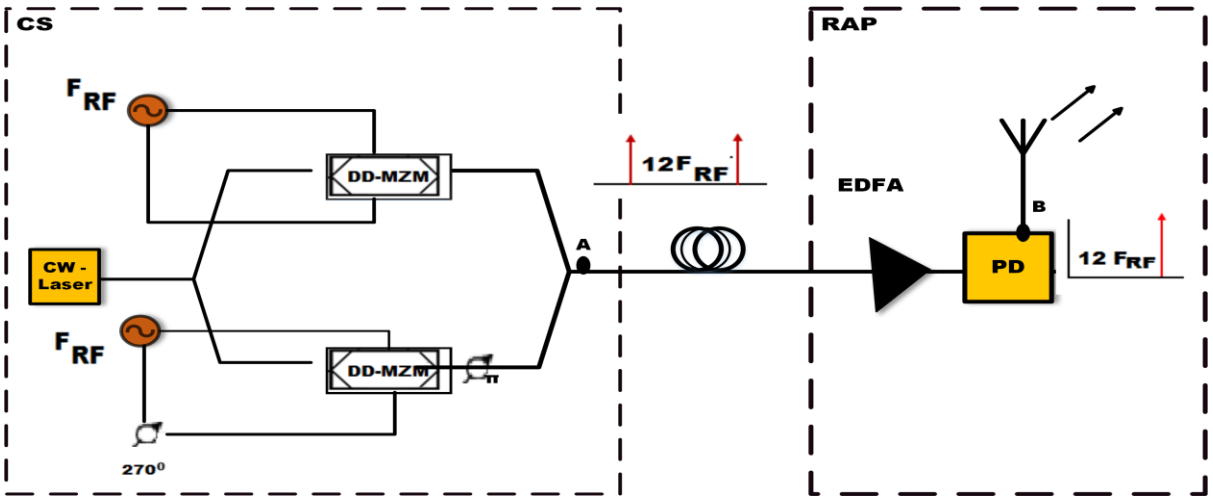

Figure 5-2: Block diagram of the mm-wave frequency with 12-tupling techniques. CW: continuous-wave laser, DD-MZM: /Dual-Drive Mach–Zehnder modulator, EDFA: erbium-doped optical fibre amplifier; single-mode fibre; PD, photodetector.

$$E_n(t) = E_0 cos(\omega_0 t) \tag{5-1}$$

where, E_0 represents the amplitude of the optical field and ω_0 indicates the angular frequency of the optical carrier. Both DD-MZMs are biased at the peak transmission point. Then, electrical voltage driving signals are sent to the upper and lower MZMs, which are denoted by:

$V_{01} = V_m \cos \omega t$ and

$V_{02} = V_m \cos(\omega t + 3\frac{\pi}{2})$, respectively (5-2)

Then, the phase shift is applied at the output of the lower DD-MZM. Thus, the output of the Parallel DD-MZMs as in [143][144]:

$$E_{out}(t) = E_0\{co\,s(\omega_0 t)\, cos[mcos\,(\omega t)] - cos(\omega_0 t)\, cos[mcos(\omega t + 3\,\frac{\pi}{2})]\} \tag{5-3}$$

where,

m indicates that the phase modulation index

m of DD-MZM is $\frac{\pi V_m}{2V_\pi}$,

where Vm is the amplitude of RF signal

and V_π is the switching RF voltage.

Expanding $cosmcos\ (\omega t)\ and\ cos(m\omega t + \mathbf{3}\frac{\boldsymbol{\pi}}{\mathbf{2}})$ in equation 3 using the Bessel function, the optical output field can be written as [31]as:

$$E_{out}(t) = -E_0 \sum_{n=1}^{\infty} J_{4n-2}(m)(\cos\{[\omega_0 + (4n-2)\omega]t\} + \cos\{[\omega_0 - (4n-2)\omega]t\}) \quad (6\text{-}4)$$

where Jn denotes the Bessel function of the first kind of order n. The output optical signal can be simplified to:

$$E_{out}(t) = -E_0 J_6(m)(\cos\{[\omega_0 + 6\omega]t\} + \cos\{[\omega_0 - 6\omega]t\}) \quad (5\text{-}5)$$

After square law detection using a photodiode (PD) with responsivity, then:

$$i_{12} = R|E_0 J_6(m)|^2 \cos(12\ \omega t) \quad (5\text{-}6)$$

5.4 Simulation and discussion

Optisystemsoftware is used to generate and investigate the performance of 240 GHz over SMF in downlink transmission (see appendix 12).

5.4.1 Generating 240 GHz

Figures (5-3) shows that the CW laser source with a central frequency of 193.1 THz is launched into both MZMs. Upper MZM is driven by a 20 GHz and shifted phase shift of 0°. The lower MZM is driven by 20 GHz, and the phase is shifted by 270°. The switching RF voltage for both MZMs is set to 3 V. The biasing voltages of both MZMs are set to zero to ensure that they are operated at their peak transmission point. The Extinction ratios (ER) of both MZMs are set to 60 dB to obtain the best OSSR based on the results obtained in part 3.1. Both biasing voltages for the upper and lower DD-MZMs are set to zero to eliminate the chirp issues caused by the MZMs. Because both DD-MZMs are biased at the peak operation point, the output optical spectrum contains carrier and even order sidebands only, as shown in figure (5-3.A) and figure (5-3.B). Most second-order terms cancel out at the optical adder's output, as shown in figure (5-3.C). At this figure, the optical spectrum is obtained, which has the upper sidebands of (ωc + 2ωm), (ω+6ωm) and (ωc + 10ωm), which occur at 193.13 THz, 193.24 THz and 193.3 THz, respectively, whilst the lower sidebands are (ωc − 4ωm), (ωc − 6ωm) and (ωc − 10ωm), appearing at 193.1 THz, 193.02 THz and 192.9 THz, respectively. The achieved OSSR in this study between the strongest obtained sideband is 37.69dB, as shown in figure (5-3.C). Then, these obtained optical mm-wave frequencies are transmitted

over SMF for a 20 km transmission length. At the receiver, EDFA is used to compensate for the power loss of the received generated optical harmonics. Then, the strongest obtained order sidebands are allowed to beat at PD. At the PD, the other sidebands with less power are eliminated.

A high quality and stable electrical signal 12 times the input RF LO is generated. The generation was done during the 4th order optical sideband powers are more than 30dB below the 12th order optical sidebands. As shown in figure (5-3. D), the undesired harmonic electrical signals are effectively suppressed.

The extinction ratio is a significant parameter in the specifications of fibre optics transmitters and receivers. It is assumed that the ON-OFF optical extinction ratio of the MZM modulator. The ER is set to 60 dB to achieve a higher suppression ratio in this work. The impact of the ER on the undesired optical and RF sidebands suppression ratio is shown in figure (5-4). It shows that even if the ER is set to a practical limit of 30 dB, the achieved OSSR and RFSSR are 35.1dB and 25.1dB, respectively, which are acceptable values.

Moreover, for the best obtained OSSR, the ER must be not less than 40 dB to suppress unwanted harmonics by reducing their power level. Thus, it has been proven that 240 GHz can be generated using the proposed system without a filter to remove an unwanted harmonics signal. Additionally, the proposed approach is tunable, which means frequencies can be generated at the upper bands of mm-waves of 216 GHz, 240 GHz, 276 GHz, 288 GHz, and 300 GHz. The generation is done by tuning the input LO signals with 18 GHz, 20 GHz, 22 GHz, 24 GHz and 25 GHz, respectively, as illustrated in figure (5-5). The quality of the obtained five optical spectra is high because each of the generated mm-waves has an OSSR of more than 36dB.

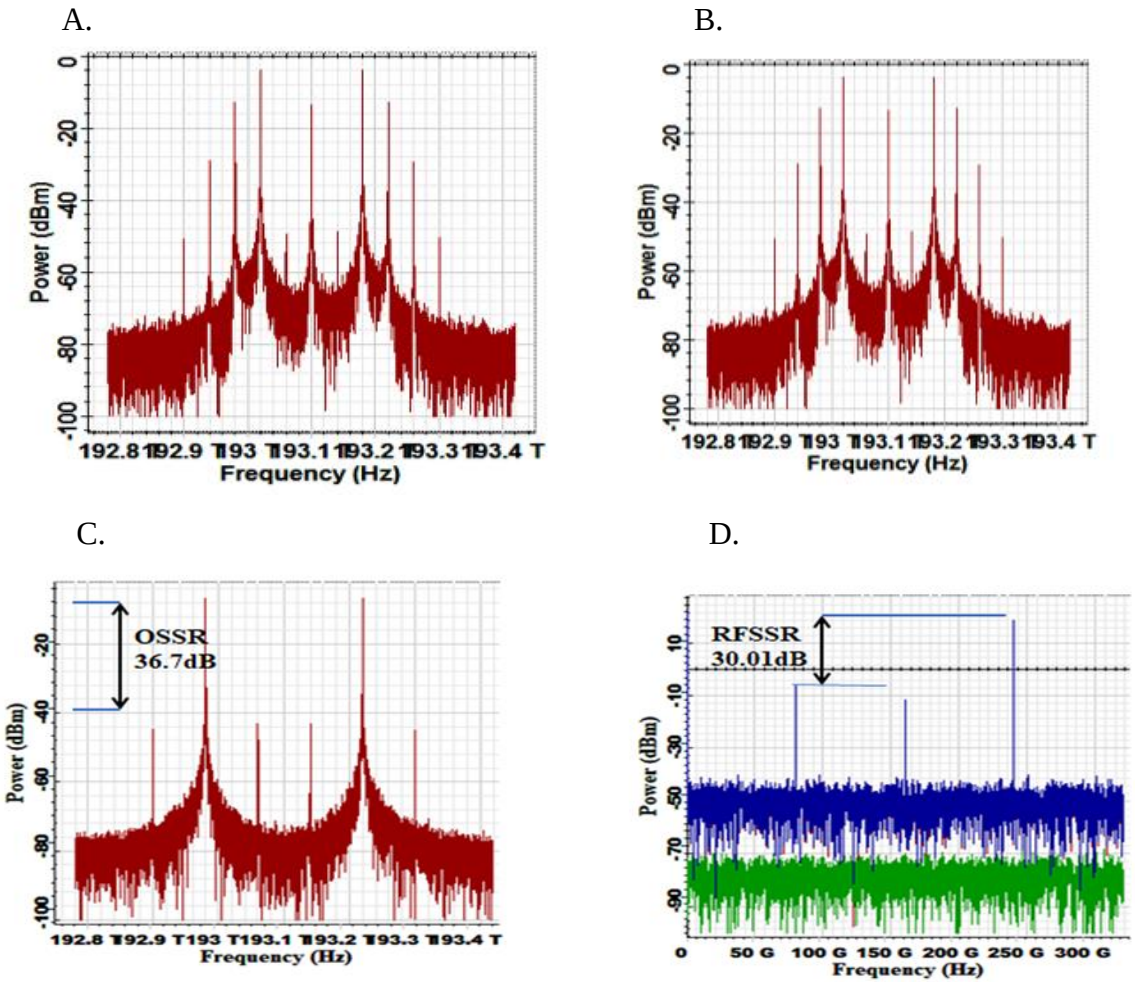

Figure 5-3: Optical mm-wave related to 193.1 THz. (A) Optical mm-wave related to 193.1 THz at the upper MZM; (B) Optical mm-wave related to 193.1 THz at the lower MZM. (C) Obtained optical spectrum at output of DP-MZM. (D) Obtained 240 GHz at the output of PD.

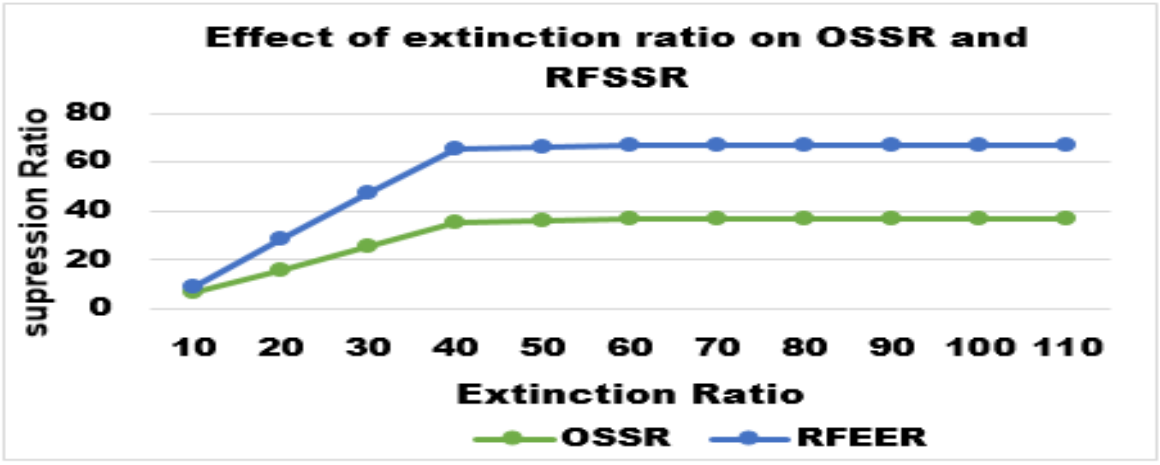

Figure 5-4: The effect of the extinction ratio on OSSR and RFSSR.

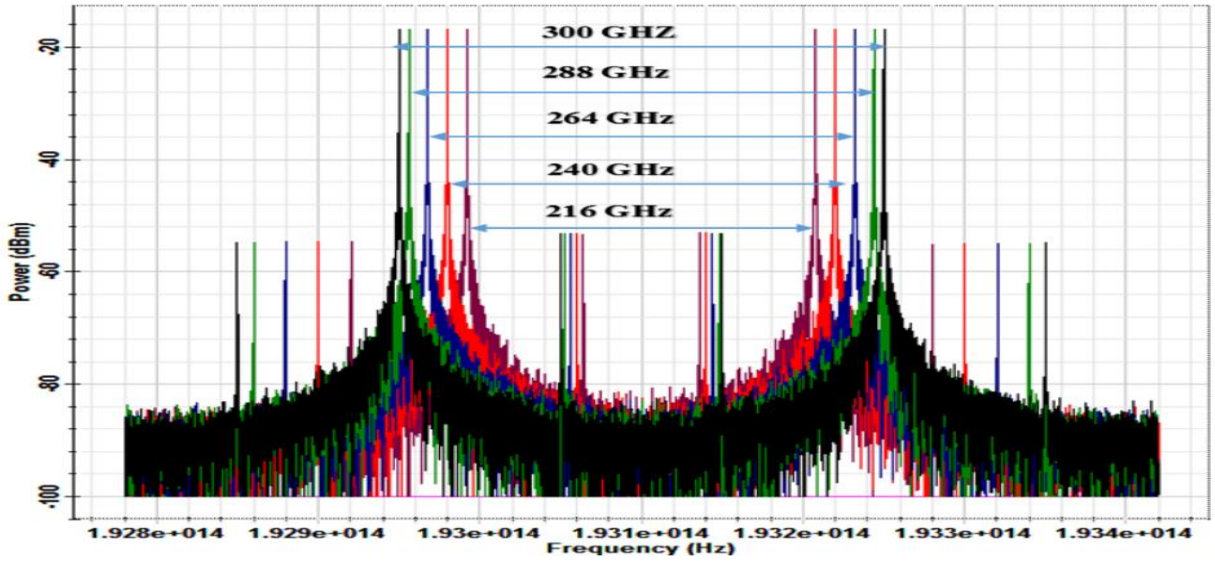

Figure 5-5: Generated optical mm-wave frequencies using the proposed scheme

5.4.2 Downlink Data Transmission At 240 GHz

To investigate the performance of the generated higher bands of mm-wave frequencies over single-mode fibre (SMF), the system is simulated using the Optisystem software with an additional external modulator to modulate 10 Gb/s with an optical signal. Hence, the generated optical sidebands are separated by 240 GHz (0.24 THz). Then, the obtained optical mm-wave is modulated with a 10 Gb/s baseband signal using an electro-absorption modulator (EAM). The data is modulated on both the optical sidebands, as shown in Figure (5-6). Then, modulated optical mm-waves are sent over different lengths of SMF, with 16.75 ps/nm/km dispersion and fibre attenuation of 0.2 dB/km. EDFA is used to amplify the received modulated optical mm-waves. A PIN- PD with 1 A/W responsivity is used to extract the modulated electrical mm-wave signal at the base station.

The detected signal comprises a 240 GHz mm-wave. After this, an electrical band pass filter with a bandwidth of 1.5 times the bitrate separates the data modulated over the 240 GHz mm-wave. The demodulated data are low pass filtered with a cut off frequency of 0.75 times the bitrate and sent to an eye diagram analyser to assess the performance of the received mm-wave signal. The max Q factor for the different transmission distances is measured using the eye diagram spectrum analyser, as shown in figure (5-7). It shows the max Q factor of the obtained 240 GHz signal when modulated with two different data rates: 10 Gb/s and 20 Gb/s. The max Q factor at 240 GHz with a 10 Gb/s data rate is 27.11, and with 20 Gb/s is 11.26 over a 5 km transmission distance, as shown in figure (5-7. B). The max Q factor over 10 km for 10 Gb/s is 16.7, while for 20 Gb/s, it is 2.1.

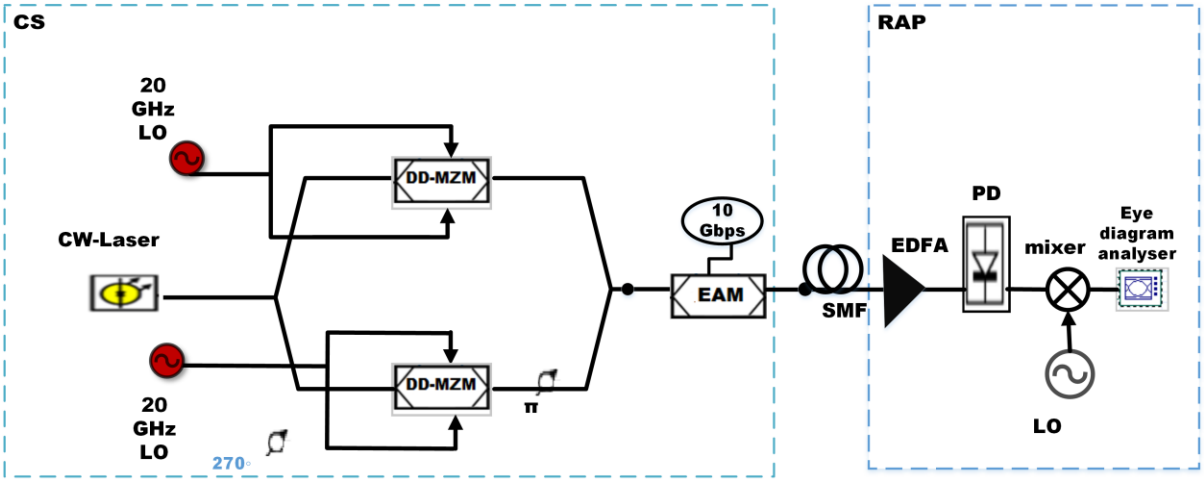

Figure 5-6: Simulation scheme of modulating the optical mm-wave with 10 Gb/s using EAM

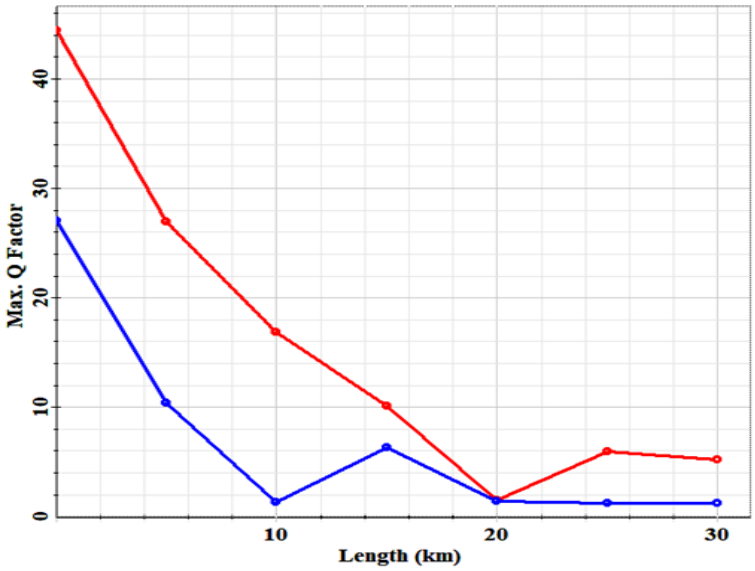

Figure 5-7: Max Q factor of 240 GHz for different SMF length.

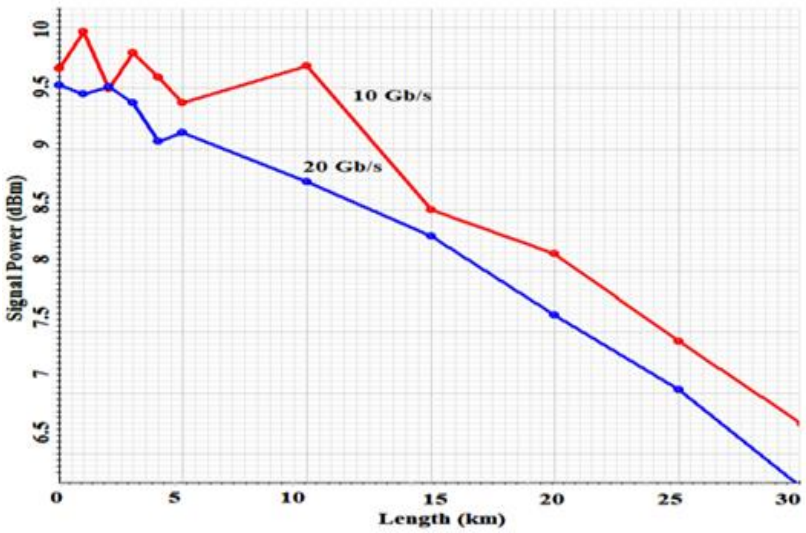

Figure 5-8: Received signal power over different transmission lengths.

The reasons behind the decrease in the value of max Q factor when extending the fibre length are the chromatic dispersion and attenuation that affect the fibre itself, as seen in figure (5-7). Because of the dispersion effect of the fibre, the time slot and profile of an optical pulse are changed in the course of propagation into the fibre, causing inter-symbol interference, which results in bit errors at the receiver. Another source of decrease in the performance of the obtained signals is birefringence, which occurs because of the polarization mode of dispersion in SMF. SMF can tolerate only one transverse mode, and it carries this with two different polarizations, which cause slight imperfections or distortions. Hence, the propagation velocities are changed for the two polarizations.

Figure (5-8) illustrates the received signal power of 240 GHz with a different transmission distance of SMF. The curve in Figure (5-8) shows that there is decreasing slightly in receiving signal power in different transmission lengths with both data rates. However, it shows that a well-received signal power is achieved while transmitting the modulated 240 GHz over different transmission distances. For example, at 15 km, the received signal power is around 8.5 dBm when the data rate is 10 Gb/s. For 20 Gb/s at the same transmission distance, the achieved received signal power is 8.3 dBm. At 25 km, the achieved received signal power is 7.4 dBm for 10 Gb/s and 7 dBm for 20 Gb/s

5.5 Downlink Data Transmission At 220 GHz, 264 GHz, 288 GHz And 300 GHz

The simulation is repeated to measure the performance of generated 220 GHz, 264 GHz, 288 GHz and 300 GHz, as realized in figure (5-9), illustrating the achieved max Q factors for these frequencies ate different SMF transmission distances. The achieved max Q factors for all the generated frequencies are satisfied. The max Q factors for 216 GHz with 10 Gb/s and 20 Gb/s data rates are 24 and 10 at a 5 km transmission distance. At 10 km, the max Q factors for 216 GHz, 288 GHz, 264 GHz, and 300 GHz with 10 Gb/s are 14.2, 14.88, 15.9 13.22, respectively. At the same transmission distance, the max Q factors for 216 GHz, 264 GHz and 288 GHz and 300 GHz with the data rate of 20 Gb/s are 13.6, 10.3, 6.1and 8.22, respectively. At 20 km, with generated frequencies of 216 GHz, 264 GHz, 288 GHz, and 300 GHz with 10 Gb/s, the achieved max Q factors are 15, 8, 10 and 8.2, respectively. At the same transmission distance for 20 Gb/s, the max Q factors are 4.1, 2.1, 1.3 and 2.26 for 216, 264, 288, and 300 GHz, respectively. Thus, the max factors that have been achieved have confirmed that the generated frequencies by proposed techniques can obtain high-quality signals that are modulated with 10 Gb/s and 20 Gb/s up to 20 km.

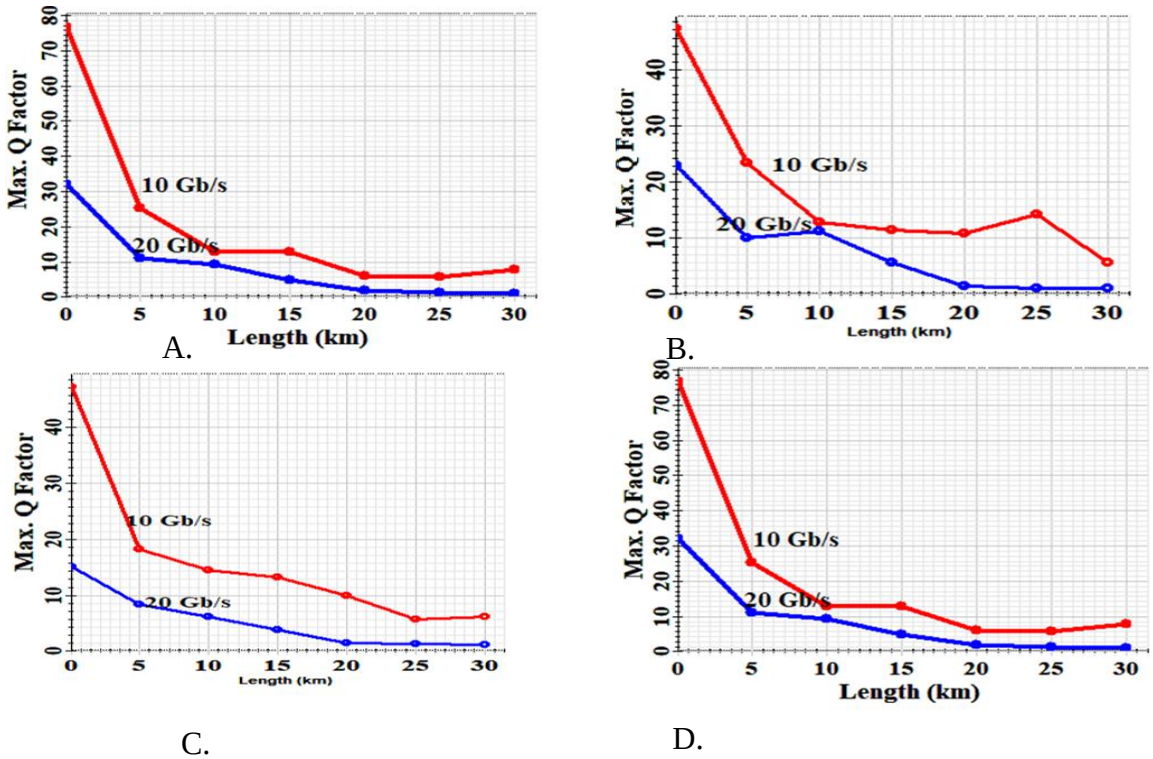

Figure 5-9: Max Q factor for different SMF transmission distances: (a) 216 GHz; b) 264 GHz; (c) 288 GHz; (d); 300 GHz.

5.6 Summary

Using the higher bands mm-waves frequency (lower band of terahertz frequencies) solves the congestion issues in future mobile channels. The upper band of mm-wave can be effectively generated using this proposed scheme of 12 frequency tupling techniques. Therefore, higher frequencies can be achieved using a low input Radio frequency and with two DD-MZMs only, which reduces the design cost for terahertz frequencies transmitted over fibre. A lower Terahertz frequency band has been obtained with an OSSR of 36.7dB and the RFSSR of 30.01dB. As one influencing factor for the OSSR and RFSSR, the extinction ratio has been examined to achieve acceptable OSSR and RFSSR in the communication system.

Furthermore, the performance of generated frequencies 214 GHz, 240 GHz, 264 GHz, 288 GHz, and 300 GHz with a data rate of 10 Gb/s and 20 Gb/s over different SMF lengths is investigated. Based on the max Q factor that has been obtained through different distances, the obtained signal performance is high quality. Thus, the upper band of mm-wave frequencies can handle a high data rate over a long distance, achieving a satisfactory max Q factor at these frequencies.

Chapter 6 Investigating Photonic Generation Of 300 GHz Over An FSO Link

6.1 Overview

In this chapter, the obtained optical 300 GHz signal performance examined over the Free Space Optics (FSO) link in different ranges using two other Free Space Optics channel models: Gamma-Gamma and lognormal under clear weather conditions. The achieved Max Q factor of the obtained 300 GHz in these two-channels models for 3 km are 5.6 and 6.7, respectively. The 300 GHz performance was examined under different attenuation values from 10 dBm/km to 120 dBm/km over 2 Km FSO link; the examination resulted in the max Q factor of 7.6 lognormal 6.2 Gamma Gamma, respectively. Furthermore, the signal performance improved by 70.1% only by reducing the divergence angle from 2 mrad to 0.5 mrad. The signal examined in different weather conditions up to 3 Km as the signal is not affected over the 3 Km range. Therefore, the generated 300 GHz using the proposed methodology can be implemented in 6G technology for future indoor and outdoor communication networks.

6.2 Introduction

Nowadays, most of the backhaul of cellular networks offers optical fibre as transmission links, where the mm-wave is transmitted between base stations and the core network [145][146][147]. The cellular system's capacity is projected to handle 1,000 times the current cellular system capacity, with ten times the data rate and 25 times the current average cell throughput [148]. An essential requirement for networks is transferring vast traffic quantities to and from many users' devices in the core network. As the advantages of fibre in handling more capacity and data rates up to 15.5 Tbit/s over a single 7,000 km fibre [149][150], although, there are some limitations, especially for the backhaul in areas with high-density urban and licensed spectrum.

FSO systems are considered an appropriate alternative or assisting systems for cellular networks, particularly in areas where the deployment of optical fibre is not achievable. FSO pertains to fiberless optical wireless networks that transmit optical signal carriers that carry the data signal at high bit rates over a free space transmission link between two fixed points over distances of up to several kilometres. An FSO link is similar to fibre technology as they share the feature of having massive bandwidth for data transmission.

FSO is all-optical, which allows it to reach the speed of light without additional costs of digging up sidewalks. FSO technology has an unregulated spectrum such that it does not require government licensing for installation. It can be deployed less if the line-of-sight (LOS) link is established between the transmitter and the receiver sites. The FSO system features allow easy deployment in urban areas where fibre optics are unsuitable. Moreover, FSO delivers high transmission security, high bit rates in an unlicensed spectrum, and full-duplex transmission. Combining the advantages of FSO and fibre optics as backhaul for a cellular system means achieving effective services for 5G and beyond. It can increase the capacity and handle a higher data rate to meet future needs. Figure (1-1) shows the proposal network connectivity beyond 5G [14][25].

Furthermore, compared to radio-frequency (RF) links, FSO has a much higher optical bandwidth available, which allows for the aforementioned higher data rates. Hence, transmitting 300 GHz over an FSO link will add the benefits of increasing the capacity and bandwidth beyond 6G networks, thereby meeting the huge application demand for future wireless communication systems. Many methods have been reported lately for generating such waves, including direct modulation, optical heterodyning, and external modulation [6], [151]–[153].

Transmission of mm-waves over an FSO system can enable high data rates to be transmitted and received to meet future users' needs [154]. However, as the air is the transmission media through which the optical mm-wave signal is sent for such a system, atmospheric conditions will affect this link, including rain, fog, and snow [155][156]. The rain is considered a dominant attenuation source in the mm-wave link, while the fog is such for an FSO system, as shown in Figure (6-2). The performance of the model under the rain will be better if the mm-wave is sent optically than transmitted as a microwave signal. The rain attenuation has a different impact for both technologies, whereby a rate of 150 mm/h can cause attenuation up to 25 dB/Km for an FSO system, while the effect at the same rate for mm-wave can reach up to 50 dB/km [160].

Moreover, in foggy weather, attenuations can harm the FSO link. Attenuations caused by fog were up to 100 dB/km over the FSO link in the climate around Graz, Austria, while for mm-wave frequencies, this can be up to 5dB/km [16]. There has been much research in designing hybrid backhaul networks [25][158][159][160]. [25] introduced hybrid free-space optics mm-wave architecture for 5G cellular backhaul networks. In [161], the researcher proposed a high-capacity wireless backhaul network using seamless convergence of radio-over-fibre (RoF) with 90 GHz mm-wave. In [161], a seamlessly converged RoF and mm-wave system at

90 GHz for high-speed wireless signal transmission in a mobile backhaul network was experimentally demonstrated. In [160], Li *et al*. presented cost-effective solutions involving FSO links upgrading the cellular backhaul with optical fibres in 5G networks. However, the distance limitation was because no amplification was provided by the mirror used in the proposed design. In [159], radio integration- over-PON was studied for implementing wireless backhaul over optical access networks. Additionally, in [25], Pham and his group proposed a cellular system backhaul for a 60-GHz mm-wave and FSO links beyond 5G networks.

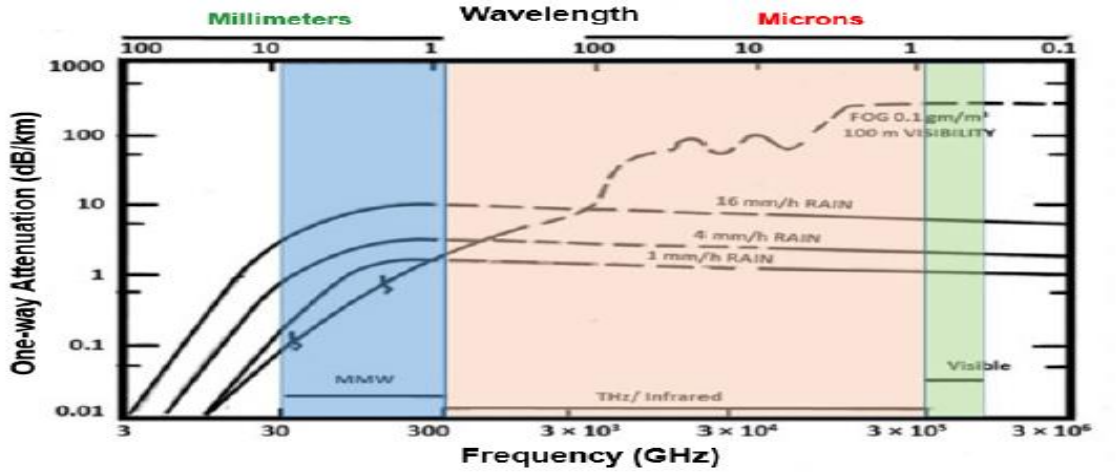

Figure 6-1: Attenuation effect for mm-wave communication [160]

There has been substantial research on the Legacy FSO systems to exhibit high total transmission capacity involving the FSO system. In [162], 40 Gb/s was transmitted over FSO and achieved up to 420 m. In [163], hybrid 60GHz with/10 Gb/s over 500 m FSO link was successfully achieved, and a POLMUX technique was proposed and demonstrated. In [164], 10 Gb/s 32-QAM data with 40 GHz optical carrier suppression were generated at MZM without any optical filter, with an RF power level higher than −40 dBm. Whereby, signals distribution demonstrated over a hybrid network composed of 10 km SMF and 70 cm FSO links. The achieved signal was successfully transmitted along with the hybrid link with a minimum EVM of 8 %.

Also, in [16] experimentally proved that a combination of FSO systems and mm-wave frequency in Graz in Austria has the advantage of wirelessly transmitted signals, which offers high bandwidth under varying weather conditions. In reference [165], 100 Gbit/s for 200GHz over the FSO system using higher-order modulation (Quadrature phase-shift keying and quadrature amplitude modulation) schemes over a short distance backhaul were achieved.

The measured Bit Error rate was below a single THz carrier's forward error correction limit. In [166], performance analysis of a chaotic FSO communication system under different weather conditions was undertaken. Under heavy rains, the max Q factor was 19. Moreover, a max Q factor of 23.1 and 13.4 for moderate fog and heavy rainfall, respectively, achieved over 1 km.

Various statistical models, e.g. the lognormal, gamma-gamma (G−G), I-K, K, the negative exponential, and the Rician lognormal distribution implemented to describe the optical channel characteristics when considering atmospheric turbulence strength [167][168][169][170][171][172][173][174][175][176]. In [177], Sajid provided a statistical channel model for fog conditions affected by the signal in the FSO link. He concluded that lognormal and Gamma Gamma channel models provide the two closest fits for continental fog at Graz. Al-Habash recently proposed G-G distribution [171], which was found to deliver a good fit with the simulation data in nearly all cases tested.

For the first time, an optical 300 GHz (0.3 THz) is generated based on a 12 frequency tupling technique, as there is a strong interest in utilising the frequencies between 0.1 THz to 3 THz, which have not yet been allocated to any active services among wireless scientists and engineers [178]. Then, the obtained optical 300 GHz is transmitted over an FSO link to investigate its performance. Two-channel models for the FSO link were implemented to ascertain the received signal's best performance.

6.3 Proposed Design

Firstly, the 300 GHz is generated based on 12 tupling techniques explained in chapter 5. Then, the obtained signal the transmitted through an FSO channel. FSO channel is a subsystem of two telescopes with the free space channel. It is best suited for modelling the line of sight free space terrestrial links. The FSO link in the current design is a subsystem of a transmitter telescope, free space and a receiver telescope. [179][180]. The attenuation of the input laser power depends on two main parameters: attenuation and geometrical loss. Attenuation is defined as the attenuation of the laser power in the atmosphere. The geometrical loss results from spreading the transmitted beam between the transmitter and the receiver.

The FSO link is presented by the equation (6-1):

$$P_r = P_t \frac{d^2_R}{(d_T+\theta R)^2} 10^{-\alpha^R_{10}} \quad (6\text{-}1)$$

where,

P_r: Received signal power

P_t: Transmitted signal power

d_R: Receiver aperture diameter (m)

d_T: Transmitter aperture diameter (m)

θ: Beam divergence angle (mrad)

R: Range (km)

α: Atmospheric attenuation (dB/km)

Additional losses can be integrated into the received signal due to scintillation and integrated into the transmitted signal. Scintillation is a further loss caused by slight temperature variations in the free space medium, thus resulting in index-of-refraction fluctuations. It can be calculated by either a gamma-gamma or lognormal distribution [181]–[183].

6.4 Simulation setup and result discussion

This chapter shows the mm-wave performance at 300 GHz over the FSO transmitting link is investigated over different FSO links under different possible attenuations using the Optisystem software. The simulation process is divided into three parts.

1) 300 GHz (0.3 THz) is generated using the 12 frequency tupling technique. The performance of the generated 300 GHz at a rate of 10 Gb/s over the FSO link is examined by considering two types of FSO channel models, gamma-gamma and lognormal channel models. The system shows simulation; the parameters are presented in Table 6-1.

2) The obtained signal's performance is studied by varying the beam divergence angle.

3) The transmitted 300 GHz performance is evaluated under different attenuation types.

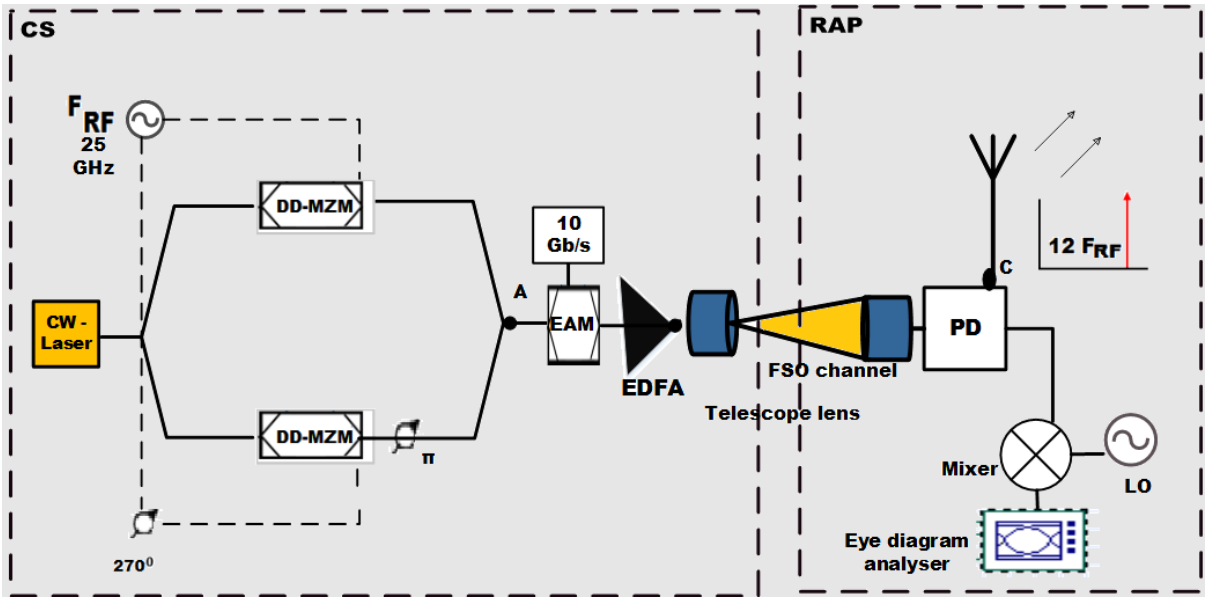

Figure 6-2: The simulation setup for transmitting 300 GHz over the FSO channel. CW is a continuous-wave laser; DD-MZM is the dual-drive Mach–Zehnder modulator; EDFA is the erbium-doped optical fibre amplifier; FSO, Free space optics, PD, photodetector.

As shown in Figures (6-3), the CW laser source with a central frequency of 193.1 THz is launched into the upper MZM and lower MZMs. Upper MZM is driven by a 25 GHz Local Oscillator (LO) with a phase shift of 360°, while the lower MZM is driven by 25 GHz and is shifted by 270°. The switching RF voltage for both MZMs is set at 3 V, whilst the biasing voltages are set to zero to ensure that they are operated at their peak transmission point. The ER ratios of both MZMs are set to 60 dB to obtain the best undesired harmonic elimination. Both biasing voltages for the upper and lower DD-MZMs are set to zero to eliminate the chirp issues caused by them. Then, the obtained optical mm-wave frequencies are transmitted over the FSO link. At the receiver, an erbium-doped optical fibre amplifier (EDFA) is used to compensate for the power loss of the received generated optical harmonics. The strongest obtained order sidebands are achieved at a photodetector (PD), while the other sidebands with less power are eliminated. The simulation setup design is presented in appendix 13.

Table 6.1: Parameters setup for transmission 300 GHz over FSO link:

Device	Parameter	Value
CW-laser	Optical signal frequency	193.1THz
	Optical power signal	10 dBm
	Spectral width	10 MHz
LO	Radio frequency	25 GHz
MZM	Bias voltage	0 V
	Switching bias voltage	3 V
	RF voltage	3 V
PIN-PD	Responsivity	1 A/w
FSO link	Range	(100-1000) m
	Attenuation (clear weather)	14 dB/km
	Transmitter aperture diameter	5 cm
	Beam divergence	2 mrad
	Transmitter aperture diameter	20 cm

6.5 Results And Discussion

Firstly, the obtained optical spectrum is shown in figure (6-4. A). The optical spectrum obtained at the optical adder's output has upper sidebands at 193.13 THz, 193.22 THz, and 193.3 THz, whilst the lower sidebands appear at 193.1, 193.02, and 192.9 THz. The optical sideband suppression ratio (OSSR) between the strongest obtained sideband is 37.69 dB, which means the received signal is good. The obtained optical mm-wave modulated with a 10 G/s data rate using an electro-absorption modulator (EAM). The data modulated on both the optical sidebands are shown in figure (6-3). At the receiver, the obtained optical signal is high quality and stable, with a frequency of 12 times that of the input RF LO generated.

Moreover, the 4th order optical sideband powers are more than 30 dB below the 12th order optical sidebands, and the undesired harmonic electrical signals are effectively suppressed, as shown in figure (6 – 4. B). The achieved OSSR and RFSSR are 37.69dB and 30.1dB, respectively; the resulting values allow the receivers to work without filters. Hence, 300 GHz

is generated using the proposed system without a filter to remove an unwanted harmonics signal.

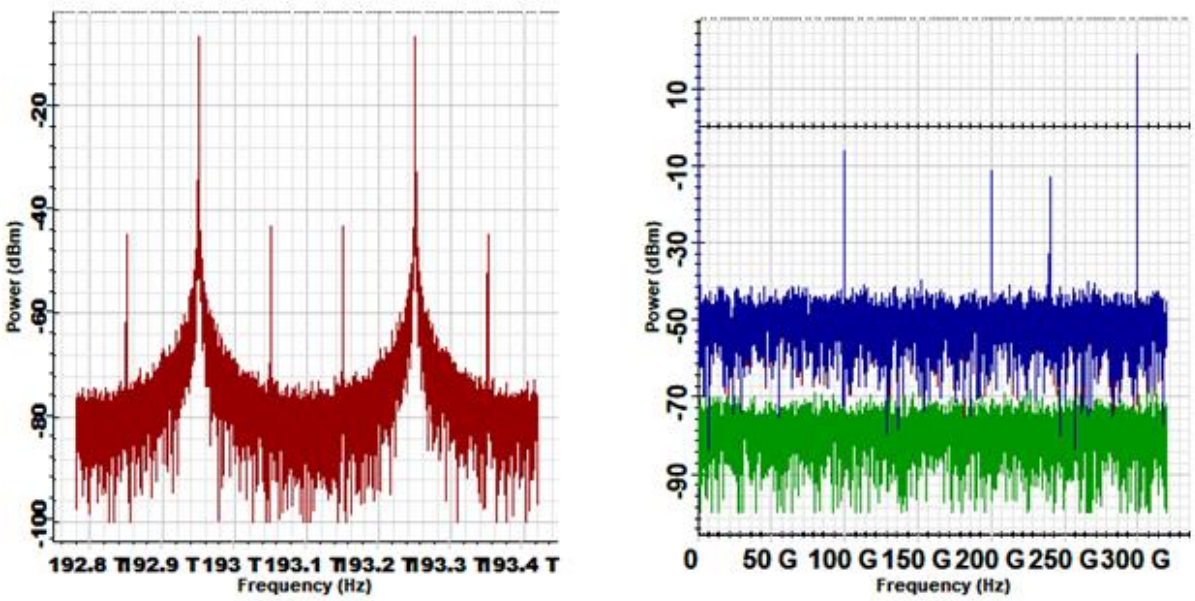

Figure 6-3: The optical and electrical spectrum at 300 GHz.

Secondly, the obtained 300 GHz performance was investigated using different FSO channel model distributions, gamma-gamma and lognormal, to choose the best signal performance.

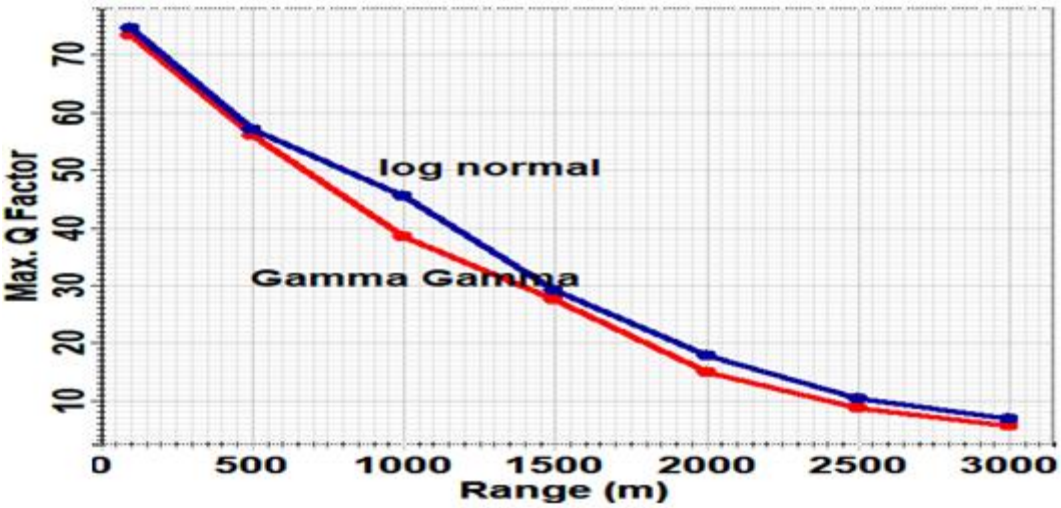

Figure 6-4: Max Q factor through FSO link ranges using two FSO channel models

The max Q factors decrease with an increase in transmission distances, which is clearly because of reducing the power signal of 300 GHz in both models for longer distances. However, the signal's performance in the lognormal channel model is slightly better than

Gamma Gamma. At 2500 m, the max Q factor is 10.34 for lognormal, while it is 8.6 over the same FSO link range for Gamma Gamma. At 2500 m, the max Q factor is 10.34 for lognormal, while it is 8.6 over the same FSO link range for Gamma Gamma. Then, the performance of the obtained signal compared over FSO link channels models for gamma-gamma and lognormal, under different attenuation values owing to various weather conditions (light rain, heavy rain, haze, and moderate fog) at 1 km range through measuring the Q factor, illustrated in Figure (6-6).

The performance of the signal degrades gradually with increasing atmospheric turbulence. However, the lognormal channel model has better tolerance to attenuation up to 80 dB/ km than the Gamma Gamma channel model. At an attenuation of 30 dB/km, which pertains to a moderate fog, the max Q value is around 20 in the lognormal channel model, while the max Q factor is 9.2 for the other channel model. At 80 dB/km, the max Q factor is 7.6 in the lognormal channel model, whereas it is 6.2 with Gamma Gamma. However, both channel models share the same max Q factor at an attenuation value of 120 dBm/ km, 3. Hence, FSO link performance is poor in terrible weather conditions regardless of the channel models. The performance of the received 300 GHz mm-wave signal with different beam divergence angles in various FSO links was investigated, with the results provided in figure (6-5). Figure (6-5) shows that the obtained signal's received power if the beam divergence angle is 0.5 mrad is better than one mrad, two mrad, or five mrad. For example, as shown in Figure(6-6), when the signal was sent through a 3 km distance with beam divergence angles of 0.5 mrad, one mrad, two mrad and five mrad, the received signals power obtained are -15,-28, -50 and -75 dBm, respectively.

These results demonstrate that the transmitted signal power through the FSO channel will be more substantial when a slight beam divergence angle. Hence, reducing the beam divergence angle positively impacts improving the received signal's performance. With a divergence beam angle of 2 mrad, the achieved signal power is nearly -86 dBm for both Gamma Gamma and the lognormal channel model. While at the same attenuation value, the received signal power when θ is 0.5 mrad for lognormal and gamma-gamma channel models is -25, -30 dBm, respectively, as shown in figure (6-6).

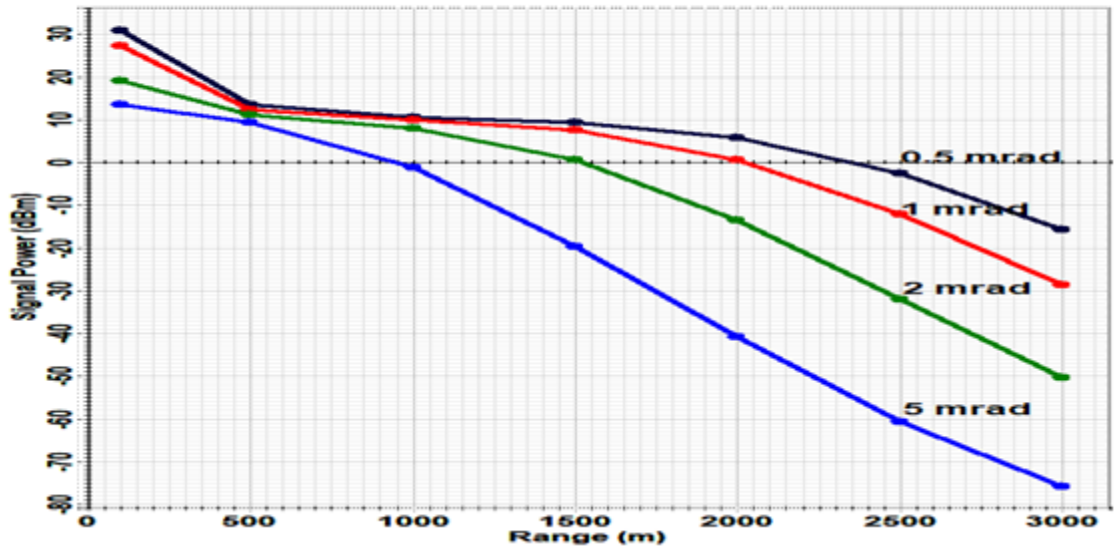

Figure 6-5: The received signal powers through different FSO link distances with different beam divergence angles.

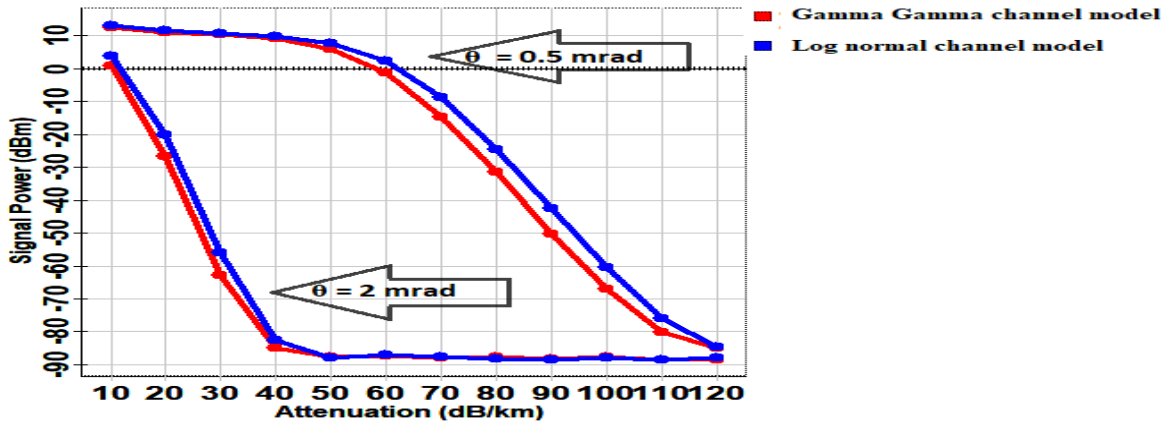

Figure 6-6: Received signal power vs different attenuation levels.

Then, the design was re-stimulated using the lognormal channel model for an FSO link with a beam divergence angle of 0.5 mrad. The max Q factor is measured under different weather conditions to assess the transmitted signal's performance over the FSO link.

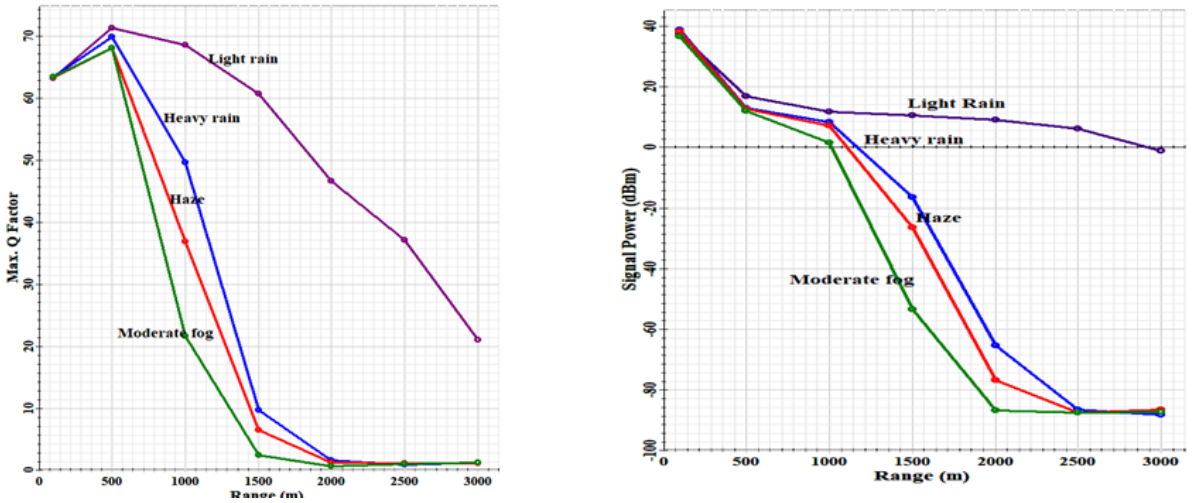

A. The received signal power vs FSO link ranges. **B. Max Q factor vs FSO link ranges.**

Figure 6-7: The obtained performance of 300 GHz over an FSO link for different weather conditions.

The performance of obtained optical 300 GHz propagated in the FSO link is evaluated under different weather conditions (fog, haze and rain) in terms of the attenuation levels. The simulation of the design is presented in appendix 14. Figure (6-1) shows less rain attenuation when the signal frequencies increase. The attenuation of light rain (when the rain rate is 25 mm/1hr) is 7dB/km, while the attenuation is 14 dB/km at a rain rate of 50 mm/h. Moreover, when the rain rate is 100 mm / hr, the attenuation is around 23.8 dB, whilst it is 25 dB/km under heavy rain (rain rate of 150 mm/1 hr) [157]. Haze also affects the optical signal. When there is a low visibility of 0.2 Km, the attenuation is 42 dB/km, whilst when the haze has a moderate level (0.6 km), it stands at 23 dB/km [184], similar to that for moderate rain. For the stand-alone FSO system, fog can cause attenuations of up to 100 dB/km in the climate around Graz, Austria. Additionally, the moderate fog has an attenuation of 30 dB [157]. However, rainfall does not strongly affect the FSO link, relating to THz frequency features, as shown in figure (6-1).

Moreover, water is not absorbing the 1550 nm laser wavelength easily. Thus, it explains why the FSO link is not heavily impacted by rain and snow, as seen in the obtained result in Figure (6-7). The received signal power of 300 GHz at 3 km is -20 dBm, and the max Q factor is 25. The FSO link is slightly affected by haze, i.e. when the visibility is low, as

shown in Figure (6-7.A), with the received signal power going from -38 dBm at 2 km to -67 dBm at 2.5 km from the link.

Similarly, the effect of fog attenuation on the FSO link's received signal power goes down from -42 dBm at 2 km to -70 dBm at 2.5 km. Therefore, the performance of the obtained signal is very poor, with low visibility caused by haze in the atmosphere, as shown in Figure (6-7). However, the performance of 300 GHz when it is raining is good at different distances, according to the obtained max Q factor shown in Figure (6-7.B). Additionally, at 1 km, the max Q factors for moderate fog, heavy rain and haze are 55, 55, and 66, respectively.

6.6 Summary

A high quality 300 GHz mm-wave signal is obtained using the 12 tupling frequency technique. The received signal's performance is investigated over an FSO link using two FSO channel models: lognormal and gamma-gamma. The performance of the obtained signal was compared for the two-channel models. The 300 GHz has a high performance of up to 3 km in clear weather conditions for both FSO link models with max Q factors of 8.6 and 5.6, respectively. The obtained optical 300 GHz was evaluated at different attenuation values for a 1 km FSO link range and provided good performance up to 80 dBm/km for both channel models. Furthermore, the FSO link performance improved by reducing the beam divergence angle. Subsequently, the proposed system performance was good over different FSO link ranges under various atmospheric conditions (rain, haze, fog) up to 3 Km.

Chapter 7 Conclusion and Future Work

7.1 Conclusion

Given the importance of mm-wave frequencies for future wireless communication systems in terms of increasing system capacity and bandwidth, mm-wave communication still has many issues that need to be addressed. In particular, mm-wave signal generation and transmission over fibre and wireless will bring significant challenges, including the system design and the application to wireless communication systems. Approaches delivering less complexity and cost-effective mm-wave generation and transmission are essential for developing efficient future communication systems. In this thesis, different methods for mm-wave generation for various bands and transmission systems have been proposed. Four main contributions have been presented in four chapters to address these perspectives, summarized in this chapter.

Photonics generation of a 60 GHz mm-wave could be achieved using a single DD-MZM. The advantage of this method is that it is a simple and cost-effective design for generating mm-wave frequency by using a single DD-MZM and an inverted optical filter. Carrier suppression in optical signal adds benefits to improve the transmitted signal. An inverted optical filter adds the advantage of suppressing the carrier of the obtained optical mm-wave, which enhances the strength of the received signal. The performance of the obtained signal based on carrier suppression using an inverted optical filter has been verified.

Additionally, modulating the signal with obtained optical mm-wave has better performance than modulating while generating mm-wave, as shown in the simulation result obtained in chapter 3. Moreover, the performance of the accomplished mm-wave signal is successfully performed up to 10 Gb/s. It is thus concluded that carrier suppression using an inverted optical filter can generate an effective mm-wave.

A high-quality 72 GHz has been generated using quadrupling techniques based on carrier suppression for the first contribution. The simulation results show that the impairment due to fibre chromatic dispersion and attenuation could be decreased by achieving high optical carrier suppression and harmonics. Additionally, a filter can be avoided at the receiver, giving the cost-effectiveness of the proposed design. The simulation results have demonstrated that a modulation mm-wave with data using an EAM optical modulator provides advantages in transmitting the obtained mm-wave over 80 km, with a max Q factor of around 20 with

satisfactory received electrical power. Additionally, the simulation result shows that APD improved the performance of the received power signal by 35% compared with PIN-PD.

Given the importance of mm-wave frequencies for future wireless communication systems in terms of increasing system capacity and bandwidth, mm-wave communication still has many issues that need to be addressed. In particular, mm-wave signal generation and transmission over fibre and wireless will bring significant challenges, including the system design and the application to wireless communication systems. Approaches delivering less complexity and cost-effective mm-wave generation and transmission are essential for developing efficient future communication systems. In this thesis, different methods for mm-wave generation for various bands and transmission systems have been proposed.

There is a study in this thesis about photonics generation of a 60 GHz mm-wave could be achieved using a single DD-MZM. The advantage of this method is that it is a simple and cost-effective design for generating mm-wave frequency by using a single DD-MZM and an inverted optical filter. Carrier suppression in optical signal adds benefits to improve the transmitted signal. An inverted optical filter adds the advantage of suppressing the carrier of the obtained optical mm-wave, which enhances the strength of the received signal.

Additionally, modulating the signal with obtained optical mm-wave has better performance than modulating the signal while generating mm-wave, as shown in the simulation result obtained in chapter 3. Moreover, the performance of the accomplished mm-wave signal is successfully performed up to 10 Gb/s. It is thus concluded that carrier suppression using an inverted optical filter can generate an effective mm-wave.

A high-quality 72 GHz has been generated using quadrupling techniques based on carrier suppression . The simulation results show that the impairment due to fibre chromatic dispersion and attenuation could be decreased by achieving high optical carrier suppression and harmonics. Additionally, a filter can be avoided at the receiver, giving the cost-effectiveness of the proposed design. The simulation results have demonstrated that a modulation mm-wave with data using an EAM optical modulator provides advantages in transmitting the obtained mm-wave over 80 km, with a max Q factor of around 20 with satisfactory received electrical power. Additionally, the simulation result shows that APD improved the performance of the received power signal by 35% compared with PIN-PD.

A tunable approach is proposed to generate higher mm-wave frequencies (lower band of terahertz frequencies) for a third contribution. 216 GHz, 240 GHz, 264 GHz, 288 GHz, and

300 GHz can be generated effectively using 12-tupling techniques by the proposed design. The novelty of this contribution generation can be achieved by using a low input frequency and fewer optical components, which minimizes the cost of the design for terahertz frequencies for an optical communication system. The quality of the obtained five optical spectra is high, with each of the generated mm-waves having an OSSR of more than 36.7dB. And RFSSR of 30.01dB. The simulation results show that the extinction ratio is one of the influencing factors regarding the obtained OSSR and RFSSR. Further, downlink data transmission with a data rate of10 Gb/s and 20 Gb/s of generated frequencies 214 GHz, 240 GHz, 264 GHz, 288 GHz, and 300 GHz over SMF is investigated using the Optisystem simulation software. The max Q factor for 300 GHz is 8.2 over 30 km, while 30 GHz with 20 Gb/s is 6.2 over 15 Km.

A 300 GHz mm-wave signal is investigated over an FSO link as a third contribution. The performance of the obtained signal is compared in two-channel models (lognormal and gamma-gamma). The Optisystem software demonstrated that the signal could be transmitted with good performance up to 3 km in clear weather for both FSO link models, with max Q factors of 8.6 and 5.6, respectively. Simulation results show that when the obtained optical 300 GHz is evaluated under different attenuation values for a 1 km FSO link range, good performance is delivered under 80 dBm/km for both channel models.

Additionally, it has emerged that the transmitted signal's performance is improved by reducing the value of beam divergence angles. Moreover, according to the obtained results, rain hardly affects the obtained optical signal up to 2.5 km, while fog and haze impact the signal after 2.5 km. Thus, the proposed system works well for optical 300 GHz with an FSO link up to 3 km. Accordingly, FSO is considered a promising solution for backhaul applications in future wireless indoor and outdoor networks.

This finding will assist in ascertaining the best way to generate mm-wave at different bands, which is considered one factor that will enhance future wireless communication systems. The applications of mm-waves for 5G cellular and B5G technologies will be supported by manufacturing low-cost mm-wave chips of a small size.

7.2 Future Work

Recently, there has been substantial research on the application of mm-wave frequencies, responding to increasing demand on the services considered the biggest challenges for next-generation networks. The mm-wave spectrum has an available wide bandwidth higher than all the current cellular wireless commination systems. The new mm-wave bands for indoor and outdoor wireless propagation will improve the capacity beyond 5G. In particular, we specifically consider a network where vehicles are served by mm-wave base stations (BSs) deployed alongside the road. We propose that future work should consider the following.

1. Investigate the performance of obtained frequencies in this work in wireless links. It is proposed that the focus is on the performance of 60 GHz, 72 GHz, 240 GHz and 300 GHz between the BSs and the users in local area networks, both indoors and outdoors.
2. Investigate the performance of 60 GHz and 300 GHz for vehicular communication systems for a highway communication network, considering the following points; Fundamental link budget metrics, with fixed BSs and the user moving in a car at high speed, Antenna height, Penetration losses and diffraction losses (affect the user inside the car).
3. Additionally, the terahertz frequency band could play an essential role for frequency bands that could be utilised for future wireless communication networks beyond 6G.. Future work aims to investigate the performance of terahertz (THz) frequency such as 600 GHz and 1 THz over the fibre transmission link.

7.3 Research Impact

Mm-wave communication has been considered a solution to spectrum congestion for future communication systems. Despite the advantages of mm-wave frequencies in delivering high capacity communication systems, designing an efficient generation and transmission system with simple infrastructure, low cost is an issue that still needs to be addressed. The contributions provided in this thesis can deal with three main issues, namely: photonic generation, optical transmission over fibre and FSO. The proposed photonic mm-wave generation methods could benefit RoF transmission systems and applications beyond 5G optical networks. The proposed RoF technique has simplified the mm-wave generation and transmission design.

Additionally, the proposed hybrid Fibre/FSO system where the FSO link cab be considered as back up for fibre link is is the breakdown or for increasing the speed of such network. All these contributions advance overall mm-wave communication system performance. In summary, this research work contributes beyond 5G communications by offering cost-effective and straightforward design in mm-wave communication.

References

[1] International Telecommunications Union, "ITU towards 'IMT for 2020 and beyond,'" *www.itu.int*, 2016. https://www.itu.int/en/ITU-R/study-groups/rsg5/rwp5d/imt-2020/Pages/default.aspx (accessed Apr. 24, 2020).

[2] "Ericsson Mobility Visualizer: mobility data app - Ericsson." https://www.ericsson.com/en/mobility-report/mobility visualizer?f=1&ft=1&r=2,3,4,5,6,7,8,9&t=8&s=1,2,3&u=1&y=2019,2025&c=1 (accessed Apr. 10, 2020).

[3] "The Truth About Terahertz - IEEE Spectrum." https://spectrum.ieee.org/aerospace/military/the-truth-about-terahertz (accessed Jan. 09, 2021).

[4] A. J. Seeds, H. Shams, M. J. Fice, and C. C. Renaud, "TeraHertz Photonics for Wireless Communications," *JOURNAL OF LIGHTWAVE TECHNOLOGY*, vol. 33, no. 3, p. 579, 2015, doi: 10.1109/JLT.2014.2355137.

[5] V. Petrov, A. Pyattaev, D. Moltchanov, and Y. Koucheryavy, "Terahertz band communications: Applications, research challenges, and standardization activities," in *International Congress on Ultra Modern Telecommunications and Control Systems and Workshops*, Oct. 2016, vol. 2016-Decem, pp. 183–190. doi: 10.1109/ICUMT.2016.7765354.

[6] J. Beas, G. Castanon, I. Aldaya, A. Aragon-Zavala, and G. Campuzano, "Millimeter-wave frequency radio over fiber systems: A survey," *IEEE Communications Surveys and Tutorials*, vol. 15, no. 4, pp. 1593–1619, 2013, doi: 10.1109/SURV.2013.013013.00135.

[7] T. KIMURA, “Optical Transmission,” *The Review of Laser Engineering*, vol. 3, no. 3, pp. 154–159, 1975, doi: 10.2184/lsj.3.154.

[8] Qualcomm Technologies, “Spectrum for 4G and 5G,” *Qualcomm Technologies, Inc.*, no. 4155039, pp. 1–15, 2017, Accessed: Oct. 31, 2019. [Online]. Available: https://www.qualcomm.com/media/documents/files/spectrum-for-4g-and-5g.pdf%0Ahttps://www.qualcomm.com/media/documents/spectrum-4g-and-5g

[9] H. A. Mohammed, “Performance Evaluation of DWDM for Radio over Fiber System with Dispersion Compensation and EDFA,” 2013. Accessed: Apr. 29, 2019. [Online]. Available: https://pdfs.semanticscholar.org/21f0/cddaab8edbcfaf30873ed2dba13438d36e9b.pdf

[10] P. T. Dat, A. Kanno, T. Umezawa, N. Yamamoto, and T. Kawanishi, “Millimeter- and terahertz-wave radio-over-fiber for 5G and beyond,” *Summer Topicals Meeting Series, SUM 2017*, pp. 165–166, 2017, doi: 10.1109/PHOSST.2017.8012702.

[11] H. Shams and A. Seeds, “Photonics, Fiber and THz Wireless Communication,” *Optics and Photonics News*, vol. 28, no. 3, p. 24, Mar. 2017, doi: 10.1364/opn.28.3.000024.

[12] A. Ghosh *et al.*, “Millimeter-wave enhanced local area systems: A high-data-rate approach for future wireless networks,” *IEEE Journal on Selected Areas in Communications*, vol. 32, no. 6, pp. 1152–1163, 2014, doi: 10.1109/JSAC.2014.2328111.

[13] O. Omomukuyo, M. P. Thakur, and J. E. Mitchell, “Simple 60-GHz MB-OFDM ultrawideband RoF system based on remote heterodyning,” *IEEE Photonics Technology Letters*, vol. 25, no. 3, pp. 268–271, 2013, doi: 10.1109/LPT.2012.2234735.

[14] M. Z. Chowdhury, M. J. Rahman, G. M. Muntean, P. v. Trinh, and J. C. Cano, "Convergence of heterogeneous wireless networks for 5G-and-beyond communications: Applications, architecture, and resource management," *Wireless Communications and Mobile Computing*, vol. 2019. Hindawi Limited, 2019. doi: 10.1155/2019/2578784.

[15] T. S. Rappaport *et al.*, "Wireless communications and applications above 100 GHz: Opportunities and challenges for 6g and beyond," *IEEE Access*, vol. 7, pp. 78729–78757, 2019, doi: 10.1109/ACCESS.2019.2921522.

[16] E. Leitgeb, M. Gebhart, U. Birnbacher, W. Kogler, and P. Schrotter, "High availability of hybrid wireless networks," Sep. 2004, vol. 5465, p. 238. doi: 10.1117/12.545456.

[17] A. Douik, H. Dahrouj, T. Y. Al-Naffouri, and M. S. Alouini, "Hybrid Radio/Free-Space Optical Design for Next Generation Backhaul Systems," in *IEEE Transactions on Communications*, 2016, vol. 64, no. 6, pp. 2563–2577. doi: 10.1109/TCOMM.2016.2557789.

[18] E. Zedini, "Free Space Optics for Next Generation Cellular Backhaul," 2016, Accessed: Apr. 25, 2020. [Online]. Available: https://repository.kaust.edu.sa/handle/10754/621942

[19] A. T. Pham, P. v. Trinh, V. v. Mai, N. T. Dang, and C. T. Truong, "Hybrid free-space optics/millimeter-wave architecture for 5G cellular backhaul networks," 2015. doi: 10.1109/OECC.2015.7340269.

[20] E. A. Kadir, R. Shubair, S. K. Abdul Rahim, M. Himdi, M. R. Kamarudin, and S. L. Rosa, "B5G and 6G: Next Generation Wireless Communications Technologies, Demand and Challenges," *2021 International Congress of Advanced Technology and Engineering, ICOTEN 2021*, Jul. 2021, doi: 10.1109/ICOTEN52080.2021.9493470.

[21] BR, “IMT traffic estimates,” 2015, Accessed: Nov. 02, 2021. [Online]. Available: http://www.itu.int/ITU-R/go/patents/en

[22] Qualcomm Technologies, “Spectrum for 4G and 5G,” *Qualcomm Technologies, Inc.*, no. 4155039, pp. 1–15, 2017, [Online]. Available: https://www.qualcomm.com/media/documents/files/spectrum-for-4g-and-5g.pdf%0Ahttps://www.qualcomm.com/media/documents/spectrum-4g-and-5g

[23] H. Chen, T. Ning, J. Li, L. Pei, C. Zhang, and J. Yuan, “Study on filterless frequency-tupling millimeter-wave generator with tunable optical carrier to sideband ratio,” *Optics Communications*, vol. 350, pp. 128–134, 2015, doi: 10.1016/j.optcom.2015.04.003.

[24] ericsson, “Ericsson Mobility Visualizer: Interactive mobility data app,” *mobility-report*, 2013. https://www.ericsson.com/en/mobility-report/mobility-visualizer?f=1&ft=1&r=2,3,4,5,6,7,8,9&t=8&s=1,2,3&u=1&y=2018,2024&c=1 (accessed May 03, 2019).

[25] T. S. Rappaport *et al.*, “Wireless communications and applications above 100 GHz: Opportunities and challenges for 6g and beyond,” *IEEE Access*, vol. 7, pp. 78729–78757, 2019, doi: 10.1109/ACCESS.2019.2921522.

[26] M. Alzenad, M. Z. Shakir, H. Yanikomeroglu, and M. S. Alouini, “FSO-Based Vertical Backhaul/Fronthaul Framework for 5G+ Wireless Networks,” *IEEE Communications Magazine*, vol. 56, no. 1, pp. 218–224, 2018, doi: 10.1109/MCOM.2017.1600735.

[27] Rep. ITU-R F.2323-0, “R-REP-F.2323-2014-PDF-E.pdf | Video | Internet Access,” *Electronic Publication Geneva*, 2015.

https://www.scribd.com/document/329672093/R-REP-F-2323-2014-PDF-E-pdf (accessed Sep. 25, 2019).

[28] V. A. Thomas, M. El-Hajjar, and L. Hanzo, "Millimeter-wave radio over fiber optical upconversion techniques relying on link nonlinearity," *IEEE Communications Surveys and Tutorials*, vol. 18, no. 1, pp. 29–53, 2016, doi: 10.1109/COMST.2015.2409154.

[29] A. J. Seeds, H. Shams, M. J. Fice, and C. C. Renaud, "TeraHertz photonics for wireless communications," *Journal of Lightwave Technology*, vol. 33, no. 3, pp. 579–587, 2015, doi: 10.1109/JLT.2014.2355137.

[30] S. Mumtaz, J. M. Jornet, J. Aulin, W. H. Gerstacker, X. Dong, and B. Ai, "Terahertz Communication for Vehicular Networks," *IEEE Transactions on Vehicular Technology*, vol. 66, no. 7, pp. 5617–5625, Jul. 2017, doi: 10.1109/TVT.2017.2712878.

[31] Y. Niu, Y. Li, D. Jin, L. Su, and A. v Vasilakos, "A Survey of Millimeter Wave (mmWave) Communications for 5G: Opportunities and Challenges," 2015. Accessed: May 03, 2019. [Online]. Available: https://arxiv.org/pdf/1502.07228.pdf

[32] H. Shams *et al.*, "100 Gb/s multicarrier THz wireless transmission system with high frequency stability based on a gain-switched laser comb source," *IEEE Photonics Journal*, vol. 7, no. 3, Jun. 2015, doi: 10.1109/JPHOT.2015.2438437.

[33] H. J. Song and T. Nagatsuma, "Present and future of terahertz communications," *IEEE Transactions on Terahertz Science and Technology*, vol. 1, no. 1, pp. 256–263, 2011, doi: 10.1109/TTHZ.2011.2159552.

[34] K. Martin, "Terahertz Communications: A 2020 vision," *springer*, vol. 35, pp. 325–338, 2007, doi: https://doi.org/10.1007/978-1-4020-6503-3_18.

[35] A. A. A. Boulogeorgos, E. N. Papasotiriou, J. Kokkoniemi, J. Lehtomaeki, A. Alexiou, and M. Juntti, “Performance evaluation of THz wireless systems operating in 275-400 GHz band,” *IEEE Vehicular Technology Conference*, vol. 2018-June, pp. 1–5, 2018, doi: 10.1109/VTCSpring.2018.8417891.

[36] J. Federici and L. Moeller, “Review of terahertz and subterahertz wireless communications,” *Journal of Applied Physics*, vol. 107, no. 11, p. 111101, Jun. 2010, doi: 10.1063/1.3386413.

[37] S. Koenig *et al.*, “Wireless sub-THz communication system with high data rate,” *Nature Photonics*, vol. 7, no. 12, pp. 977–981, Dec. 2013, doi: 10.1038/nphoton.2013.275.

[38] “5G mmWAVE Technology Design Challenges and Development Trends | IEEE Conference Publication | IEEE Xplore.” https://ieeexplore.ieee.org/document/9196316 (accessed Jan. 07, 2022).

[39] F. Al-Ogaili and R. M. Shubair, “Millimeter-wave mobile communications for 5G: Challenges and opportunities,” *2016 IEEE Antennas and Propagation Society International Symposium, APSURSI 2016 - Proceedings*, pp. 1003–1004, Oct. 2016, doi: 10.1109/APS.2016.7696210.

[40] A. M. J. Koonen and M. G. Larrodé, “Radio-over-MMF techniques - Part II: Microwave to millimeter-wave systems,” *Journal of Lightwave Technology*, vol. 26, no. 15, pp. 2396–2408, 2008, doi: 10.1109/JLT.2008.927182.

[41] Y. Qi *et al.*, “5G Over-the-Air Measurement Challenges: Overview,” *IEEE Transactions on Electromagnetic Compatibility*, vol. 59, no. 6, pp. 1661–1670, Dec. 2017, doi: 10.1109/TEMC.2017.2707471.

[42] R. I. Ansari *et al.*, "5G D2D Networks: Techniques, Challenges, and Future Prospects," *IEEE Systems Journal*, vol. 12, no. 4, pp. 3970–3984, Dec. 2018, doi: 10.1109/JSYST.2017.2773633.

[43] C. Zhang, W. Zhang, W. Wang, L. Yang, and W. Zhang, "Research challenges and opportunities of UAV millimeter-wave communications," *IEEE Wireless Communications*, vol. 26, no. 1, pp. 58–62, Feb. 2019, doi: 10.1109/MWC.2018.1800214.

[44] M. Polese *et al.*, "Integrated Access and Backhaul in 5G mmWave Networks: Potential and Challenges," *IEEE Communications Magazine*, vol. 58, no. 3, pp. 62–68, Mar. 2020, doi: 10.1109/MCOM.001.1900346.

[45] M. N. Sokolskii, J. E. Midwinter, P. Bayvel, and F. N. Timofeev, "High-performance, free-space ruled concave grating demultiplexer," *Electronics Letters*, vol. 31, no. 17, pp. 1466–1467, Aug. 1995, doi: 10.1049/el:19950968.

[46] M. Polese *et al.*, "Integrated Access and Backhaul in 5G mmWave Networks: Potential and Challenges," *IEEE Communications Magazine*, vol. 58, no. 3, pp. 62–68, Mar. 2020, doi: 10.1109/MCOM.001.1900346.

[47] T. Kürner and S. Priebe, "Towards THz communications - Status in research, standardization and regulation," *Journal of Infrared, Millimeter, and Terahertz Waves*, vol. 35, no. 1, pp. 53–62, 2014, doi: 10.1007/s10762-013-0014-3.

[48] T. Zugno, M. Drago, M. Giordani, M. Polese, and M. Zorzi, "Toward Standardization of Millimeter-Wave Vehicle-to-Vehicle Networks: Open Challenges and Performance Evaluation," *IEEE Communications Magazine*, vol. 58, no. 9, pp. 79–85, Sep. 2020, doi: 10.1109/MCOM.001.2000041.

[49] X. Yang, M. Matthaiou, J. Yang, C. K. Wen, F. Gao, and S. Jin, "Hardware-Constrained Millimeter-Wave Systems for 5G: Challenges, Opportunities, and Solutions," *IEEE Communications Magazine*, vol. 57, no. 1, pp. 44–50, Jan. 2019, doi: 10.1109/MCOM.2018.1701050.

[50] S. A. Busari, S. Mumtaz, S. Al-Rubaye, and J. Rodriguez, "5G Millimeter-Wave Mobile Broadband: Performance and Challenges," *IEEE Communications Magazine*, vol. 56, no. 6, pp. 137–143, Jun. 2018, doi: 10.1109/MCOM.2018.1700878.

[51] Y. Huo, X. Dong, and W. Xu, "5G cellular user equipment: From theory to practical hardware design," *IEEE Access*, vol. 5, pp. 13992–14010, Jul. 2017, doi: 10.1109/ACCESS.2017.2727550.

[52] J. Zhang, X. Ge, Q. Li, M. Guizani, and Y. Zhang, "5G Millimeter-Wave Antenna Array: Design and Challenges," *IEEE Wireless Communications*, vol. 24, no. 2, pp. 106–112, Apr. 2017, doi: 10.1109/MWC.2016.1400374RP.

[53] X. Yin, A. Wen, Y. Chen, and T. Wang, "Studies in an optical millimeter-wave generation scheme via two parallel dual-parallel Mach-Zehnder modulators," *Journal of Modern Optics*, vol. 58, no. 8, pp. 665–673, May 2011, doi: 10.1080/09500340.2011.565375.

[54] H. Chen *et al.*, "D-band millimeter-wave generator based on a frequency 16-tupling feed-forward modulation technique," *Optical Engineering*, vol. 52, no. 7, p. 076104, Jul. 2013, doi: 10.1117/1.oe.52.7.076104.

[55] X. Li *et al.*, "An optical millimeter-wave generation scheme based on two parallel dual-parallel Mach-Zehnder modulators and polarization multiplexing," *Journal of Modern Optics*, vol. 62, no. 18, pp. 1502–1509, Oct. 2015, doi: 10.1080/09500340.2015.1045948.

[56] Z. Zhu, S. Zhao, X. Chu, and Y. Dong, “Optical generation of millimeter-wave signals via frequency 16-tupling without an optical filter,” *Optics Communications*, vol. 354, pp. 40–47, Jun. 2015, doi: 10.1016/j.optcom.2015.05.035.

[57] L. Chen, H. Wen, and S. Wen, “A radio-over-fiber system with a novel scheme for millimeter-wave generation and wavelength reuse for up-link connection,” *IEEE Photonics Technology Letters*, vol. 18, no. 19, pp. 2056–2058, Oct. 2006, doi: 10.1109/LPT.2006.883293.

[58] Z. Jia *et al.*, “Multiband signal generation and dispersion-tolerant transmission based on photonic frequency tripling technology for 60-GHz radio-over-fiber systems,” *IEEE Photonics Technology Letters*, vol. 20, no. 17, pp. 1470–1472, Sep. 2008, doi: 10.1109/LPT.2008.927901.

[59] H. Chi and J. Yao, “Frequency quadrupling and upconversion in a radio over fiber link,” *Journal of Lightwave Technology*, vol. 26, no. 15, pp. 2706–2711, 2008, doi: 10.1109/JLT.2008.927613.

[60] “A Photonic Microwave Frequency Quadrupler Using Two Cascaded Intensity Modulators With Repetitious Optical Carrier Suppression - IEEE Journals & Magazine.” https://ieeexplore.ieee.org/document/4252151 (accessed Aug. 25, 2020).

[61] A. Yang, W. Gu, S. Yu, C. Wang, and T. Jiang, “A Frequency Quadrupling Optical mm-Wave Generation for Hybrid Fiber-Wireless Systems,” *IEEE Journal on Selected Areas in Communications*, vol. 31, no. 12, pp. 797–803, 2014, doi: 10.1109/jsac.2013.sup2.12130012.

[62] N. A. Al-Shareefi, S. I. S. Hassan, F. Malek, R. Ngah, S. A. Abbas, and S. A. Aljunid, “A cost-effective method for high-quality 60GHZ optical millimeter wave signal

generation based on frequency quadrupling," *Progress in Electromagnetics Research*, vol. 137, pp. 255–274, 2013, doi: 10.2528/PIER13011307.

[63] H. Li, T. Huang, C. Ke, S. Fu, P. P. Shum, and D. Liu, "Photonic generation of frequency-quadrupled microwave signal with tunable phase shift," *IEEE Photonics Technology Letters*, vol. 26, no. 3, pp. 220–223, 2014, doi: 10.1109/LPT.2013.2290691.

[64] P. Shi *et al.*, "A novel frequency sixtupling scheme for optical mm-wave generation utilizing an integrated dual-parallel Mach-Zehnder modulator," *Optics Communications*, vol. 283, no. 19, pp. 3667–3672, 2010, doi: 10.1016/j.optcom.2010.05.021.

[65] Shilong Pan and Jianping Yao, "Tunable Subterahertz Wave Generation Based on Photonic Frequency Sixtupling Using a Polarization Modulator and a Wavelength-Fixed Notch Filter," *IEEE Transactions on Microwave Theory and Techniques*, vol. 58, no. 7, pp. 1967–1975, 2010, doi: 10.1109/tmtt.2010.2050182.

[66] Y. Qiao *et al.*, "A frequency sixtupling scheme for high-quality optical millimeter-wave signal generation without optical filter," *Optical Fiber Technology*, vol. 17, no. 3, pp. 236–241, 2011, doi: 10.1016/j.yofte.2011.02.007.

[67] J. Liu, A. Wen, H. Zhang, X. Hu, Q. Yu, and Z. Wu, "A novel MI-insensitive and filterless frequency octupling scheme based on two parallel dual-parallel Mach-Zehnder modulators," *Optik*, vol. 125, no. 23, pp. 6887–6890, 2014, doi: 10.1016/j.ijleo.2014.08.122.

[68] K. Esakki Muthu and A. Sivanantha Raja, "Millimeter wave generation through frequency 12-tupling using DP-polarization modulators," *Optical and Quantum Electronics*, vol. 50, no. 5, p. 227, May 2018, doi: 10.1007/s11082-018-1488-y.

[69] X. Chen, L. Xia, and D. Huang, “A filterless 24-tupling optical millimeter-wave generation and RoF distribution,” *Optik*, vol. 147, no. 16, pp. 22–26, 2017, doi: 10.1016/j.ijleo.2017.08.065.

[70] W. Technologies, “A 216 – 256 GHz fully differential frequency multiplier-by-8 chain with 0 dBm output,” *International Journal of Microwave and Wireless*, vol. 10, no. special issue 5-6, pp. 562–569.

[71] X. Chen, L. Xia, and D. Huang, “Optical generation of 12-tupling millimeter-wave signal without optical filtering,” *Journal of Optical Communications*, vol. 2015, no. 3, pp. 295–299, Sep. 2016, doi: 10.1515/joc-2015-0073.

[72] J. Webster and R. T. Watson, “Analyzing the Past to Prepare for the Future: Writing a Literature Review.,” *MIS Quarterly*, vol. 26, no. 2, pp. xiii–xxiii, 2002, doi: 10.1.1.104.6570.

[73] J. Webster and R. T. Watson, “Analyzing the Past to Prepare for the Future: Writing a Literature Review.,” *MIS Quarterly*, vol. 26, no. 2, pp. xiii–xxiii, 2002, doi: 10.1.1.104.6570.

[74] H. M. Cooper, “Organizing knowledge syntheses: A taxonomy of literature reviews,” *Knowledge in Society*, vol. 1, no. 1, pp. 104–126, Mar. 1988, doi: 10.1007/BF03177550.

[75] R. C. Nickerson, U. Varshney, and J. Muntermann, “A method for taxonomy development and its application in information systems,” *European Journal of Information Systems*, vol. 22, no. 3, pp. 336–359, 2013, doi: 10.1057/ejis.2012.26.

[76] G. P. Agrawal, *Fiber-Optic Communications Systems, Third Edition.*, vol. 6. 2002.

[77] J. Carroll, J. Whiteaway, and D. Plumb, “Distributed feedback semiconductor lasers.”

[78] Y. Matsui, H. Murai, S. Arahira, S. Kutsuzawa, and Y. Ogawa, “30-GHz bandwidth 1.55-μm strain-compensated InGaAlAs-InGaAsP MQW laser,” *IEEE Photonics Technology Letters*, vol. 9, no. 1, pp. 25–27, Jan. 1997, doi: 10.1109/68.554159.

[79] “Enhanced direct-modulated bandwidth of 37 GHz by a multi-section laser with a coupled-cavity-injection-grating design - IET Journals & Magazine.” https://ieeexplore.ieee.org/document/1244112 (accessed Jan. 27, 2020).

[80] “A single light-source configuration for full-duplex 60-GHz-band radio-on-fiber system.” https://pdfslide.net/documents/a-single-light-source-configuration-for-full-duplex-60-ghz-band-radio-on-fiber.html (accessed Jan. 28, 2020).

[81] S. T. Choi *et al.*, “A 60-GHz Point-to-Multipoint Millimeter-Wave Fiber-Radio Communication System,” vol. 54, no. 5, pp. 1953–1960, 2006.

[82] M. F. Huang, J. Yu, Z. Jia, and G. K. Chang, “Simultaneous generation of centralized lightwaves and double/single sideband optical millimeter-wave requiring only low-frequency local oscillator signals for radio-over-fiber systems,” *Journal of Lightwave Technology*, vol. 26, no. 15, pp. 2653–2662, 2008, doi: 10.1109/JLT.2008.925653.

[83] A. Wiberg, P. Pérez-Millán, M. v. Andrés, P. A. Andrekson, and P. O. Hedekvist, “Fiber-optic 40-GHz mm-wave link with 2.5-Gb/s data transmission,” *IEEE Photonics Technology Letters*, vol. 17, no. 9, pp. 1938–1940, Sep. 2005, doi: 10.1109/LPT.2005.853035.

[84] P. Shen, N. J. Gomes, P. A. Davies, W. P. Shillue, P. G. Huggard, and B. N. Ellison, “High-purity millimetre-wave photonic local oscillator generation and delivery,” *MWP 2003 - Proceedings, International Topical Meeting on Microwave Photonics*, pp. 189–192, 2003, doi: 10.1109/MWP.2003.1422862.

[85] J. O'Reilly and P. Lane, "Remote Delivery of Video Services Using mm-Waves and Optics," *Journal of Lightwave Technology*, vol. 12, no. 2, pp. 369–375, 1994, doi: 10.1109/50.350584.

[86] S. Ghafoor and L. Hanzo, "Sub-carrier-multiplexed duplex 64-QAM radio-over-fiber transmission for distributed antennas," *IEEE Communications Letters*, vol. 15, no. 12, pp. 1368–1371, 2011, doi: 10.1109/LCOMM.2011.101711.111794.

[87] F. van Dijk, A. Enard, X. Buet, F. Lelarge, and G. H. Duan, "Phase noise reduction of a quantum dash mode-locked laser in a millimeter-wave coupled opto-electronic oscillator," *Journal of Lightwave Technology*, vol. 26, no. 15, pp. 2789–2794, 2008, doi: 10.1109/JLT.2008.927608.

[88] D. Novak, Z. Ahmed, R. S. Tucker, and R. B. Waterhouse, "Signal Generation Using Pulsed Semiconductor Lasers for Application in Millimeter-Wave Wireless Links," *IEEE Transactions on Microwave Theory and Techniques*, vol. 43, no. 9, pp. 2257–2262, 1995, doi: 10.1109/22.414573.

[89] M. Huchard *et al.*, "60 GHz radio signal up-conversion and transport using a directly modulated mode-locked laser," in *2008 IEEE International Meeting on Microwave Photonics jointly held with the 2008 Asia-Pacific Microwave Photonics Conference, MWP2008/APMP2008*, 2008, pp. 333–335. doi: 10.1109/MWP.2008.4666705.

[90] K. Mori, K. Sato, H. Takara, and T. Ohara, "Supercontinuum lightwave source generating 50 GHz spaced optical ITU grid seamlessly over S-, C- and L-bands," *Electronics Letters*, vol. 39, no. 6, pp. 544–546, Mar. 2003, doi: 10.1049/el:20030344.

[91] T. Nakasyotani, H. Toda, T. Kuri, and K. I. Kitayama, "Wavelength-division-multiplexed millimeter-waveband radio-on-fiber system using a supercontinuum light

source," *Journal of Lightwave Technology*, vol. 24, no. 1, pp. 404–410, Jan. 2006, doi: 10.1109/JLT.2005.859854.

[92] T. Kuri, T. Nakasyotani, H. Toda, and K. I. Kitayama, "Characterizations of supercontinuum light source for WDM millimeter-wave-band radio-on-fiber systems," *IEEE Photonics Technology Letters*, vol. 17, no. 6, pp. 1274–1276, Jun. 2005, doi: 10.1109/LPT.2005.846497.

[93] I. G. Insua and C. G. Schäffer, "Heterodyne radio over fiber system with 10 Gbps data rates," in *Optics InfoBase Conference Papers*, Mar. 2009, p. JWA52. doi: 10.1364/nfoec.2009.jwa52.

[94] A. Mohan and A. A. P, "Performance Comparison of Radio over Fiber System Using WDM and OADM with Various Digital Modulation Formats," 2013. Accessed: Jun. 29, 2021. [Online]. Available: www.ijsr.net

[95] L. Vallejo, B. Ortega, J. Bohata, S. Zvanovec, and V. Almenar, "Photonic multiple millimeter wave signal generation and distribution over reconfigurable hybrid SSMF/FSO links," *Optical Fiber Technology*, vol. 54, p. 102085, Jan. 2020, doi: 10.1016/j.yofte.2019.102085.

[96] H. Brahimi, P. Lacroix, O. Llopis, and P. Lacroix, "Optimization of a microwave frequency discriminator based on an optical delay line Optimization of a microwave frequency discriminator based on an optical delay line Optimization of a microwave frequency discriminator based on an optical delay line," 2009. Accessed: Jun. 29, 2021. [Online]. Available: https://hal.archives-ouvertes.fr/hal-00410793

[97] K. C. M. Varnum, "Calhoun: The NPS Institutional Archive Noncoherent detection of coherent optical heterodyne signals corrupted by laser phase noise," 1991. Accessed: Jun. 29, 2021. [Online]. Available: http://hdl.handle.net/10945/28398

[98] A. H. M. R. Islam, M. Bakaul, A. Nirmalathas, and G. E. Town, “Simplification of millimeter-wave radio-over-fiber system employing heterodyning of uncorrelated optical carriers and self-homodyning of RF signal at the receiver,” *Optics Express*, vol. 20, no. 5, p. 5707, Feb. 2012, doi: 10.1364/oe.20.005707.

[99] H. M. Cooper, “Organizing knowledge syntheses: A taxonomy of literature reviews,” *Knowledge in Society*, vol. 1, no. 1, pp. 104–126, Mar. 1988, doi: 10.1007/BF03177550.

[100] J. vom Brocke *et al.*, “RECONSTRUCTING THE GIANT: ON THE IMPORTANCE OF RIGOUR IN DOCUMENTING THE LITERATURE SEARCH PROCESS.”

[101] A. R. J Marshall, J. P. R David, S. Member, and C. Hing Tan, “Impact ionization in InAs electron avalanche photodiodes,” *IEEE Transactions on Electron Devices*, vol. 57, no. 10, pp. 2631–2638, 2010, doi: 10.1109/TED.2010.2058330.

[102] M. A. Khalighi and M. Uysal, “Survey on free space optical communication: A communication theory perspective,” *IEEE Communications Surveys and Tutorials*, vol. 16, no. 4, pp. 2231–2258, 2014, doi: 10.1109/COMST.2014.2329501.

[103] “OptiSystem Getting Started Optical Communication System Design Software,” 2014.

[104] R. H. de Souza *et al.*, “An Analytical Solution for Fiber Optic Links with Photonic-Assisted Millimeter Wave Upconversion Due to MZM Nonlinearities,” *Journal of Microwaves, Optoelectronics and Electromagnetic Applications*, vol. 16, no. 1, pp. 237–258, 2017, doi: 10.1590/2179-10742017V16I1885.

[105] Y. S. Wu, N. W. Chen, and J. W. Shi, “A W-band photonic transmitter/mixer based on high-power near-ballistic uni-traveling-carrier photodiode (NBUTC-PD),” *IEEE*

Photonics Technology Letters, vol. 20, no. 21, pp. 1799–1801, 2008, doi: 10.1109/LPT.2008.2004689.

[106] Y. Zhang, "Development of Millimeter-Wave Radio-over-Fiber Technology," vol. 9, no. 1, pp. 58–66, 2011.

[107] C.-X. Wang *et al.*, "Cellular architecture and key technologies for 5G wireless communication networks," *IEEE Communications Magazine*, vol. 52, no. 2, pp. 122–130, Feb. 2014, doi: 10.1109/MCOM.2014.6736752.

[108] M. Xiao *et al.*, "Millimeter Wave Communications for Future Mobile Networks." Accessed: Oct. 25, 2019. [Online]. Available: http://www.miweba.eu/,

[109] T. Wang, B. Li, M. Li, Y. Chen, A. Wen, and L. Shang, "A filterless optical millimeter-wave generation based on frequency octupling," *Optik*, vol. 123, no. 13, pp. 1183–1186, 2011, doi: 10.1016/j.ijleo.2011.07.047.

[110] "Fiber Optics: Understanding the Basics | Fiber Optics & Communications | Photonics Handbook | Photonics Buyers' Guide." https://www.photonics.com/Articles/Fiber_Optics_Understanding_the_Basics/a25151 (accessed Jan. 07, 2020).

[111] G. Rittenhouse and D. Phase-, "Bell Labs breaks optical transmission record , 100 Petabit per second kilometer barrier More news stories," pp. 18–20, 2019.

[112] L. Zhao, J. Yu, L. Chen, P. Min, J. Li, and R. Wang, "16QAM Vector Millimeter-Wave Signal Generation Based on Phase Modulator with Photonic Frequency Doubling and Precoding," *IEEE Photonics Journal*, vol. 8, no. 2, 2016, doi: 10.1109/JPHOT.2016.2520821.

[113] “Up to 40 Gb/s wireless signal generation and demodulation in 75–110 GHz band using photonic techniques - IEEE Conference Publication.” https://ieeexplore.ieee.org/document/5664135 (accessed Jan. 28, 2020).

[114] C. T. Tsai, C. H. Lin, C. T. Lin, Y. C. Chi, and G. R. Lin, “60-GHz millimeter-wave over fiber with directly modulated dual-mode laser diode,” *Scientific Reports*, vol. 6, Jun. 2016, doi: 10.1038/srep27919.

[115] K. Mallick, P. Mandal, G. C. Mandal, R. Mukherjee, B. Das, and A. S. Patra, “Hybrid MMW-over fiber/OFDM- transmission system based on doublet lens scheme and POLMUX technique,” *Optical Fiber Technology*, vol. 52, p. 101942, Nov. 2019, doi: 10.1016/j.yofte.2019.101942.

[116] M. A. Khalighi and M. Uysal, “Survey on free space optical communication: A communication theory perspective,” *IEEE Communications Surveys and Tutorials*, vol. 16, no. 4, pp. 2231–2258, 2014, doi: 10.1109/COMST.2014.2329501.

[117] S. Patnaik, S. Srujanika, A. Panda, and C. Jaiswal, “Free space optical communication,” *LIA Today*, vol. 10, no. 1. p. 1, 2002. doi: 10.1007/1-4020-0613-6_7587.

[118] T. Ismail, E. Leitgeb, and T. Plank, “Free space optic and mmwave communications: Technologies, challenges and applications,” *IEICE Transactions on Communications*, vol. E99B, no. 6, pp. 1243–1254, 2016, doi: 10.1587/transcom.2015EUI0002.

[119] P. T. Dat, A. Kanno, K. Inagaki, and T. Kawanishi, “High-capacity wireless backhaul network using seamless convergence of radio-over-fiber and 90-GHz millimeter-wave,” *Journal of Lightwave Technology*, vol. 32, no. 20, pp. 3910–3923, 2014, doi: 10.1109/JLT.2014.2315800.

[120] Y. Li, N. Pappas, V. Angelakis, M. Pioro, and D. Yuan, “Resilient topology design for free space optical cellular backhaul networking,” in *2014 IEEE Globecom Workshops, GC Wkshps 2014*, 2014, pp. 487–492. doi: 10.1109/GLOCOMW.2014.7063479.

[121] Y. Li, M. Pióro, and V. Angelakisi, “Design of cellular backhaul topology using the FSO technology,” in *Proceedings of the 2013 2nd International Workshop on Optical Wireless Communications, IWOW 2013*, 2013, pp. 6–10. doi: 10.1109/IWOW.2013.6777766.

[122] C. Liu, J. Wang, L. Cheng, M. Zhu, and G. K. Chang, “Key microwave-photonics technologies for next-generation cloud-based radio access networks,” *Journal of Lightwave Technology*, vol. 32, no. 20, pp. 3452–3460, 2014, doi: 10.1109/JLT.2014.2338854.

[123] C. Liberale *et al.*, “Micro-optics fabrication on top of optical fibers using two-photon lithography,” *IEEE Photonics Technology Letters*, vol. 22, no. 7, pp. 474–476, 2010, doi: 10.1109/LPT.2010.2040986.

[124] K. Mallick, P. Mandal, G. C. Mandal, R. Mukherjee, B. Das, and A. S. Patra, “Hybrid MMW-over fiber/OFDM-FSO transmission system based on doublet lens scheme and POLMUX technique,” *Optical Fiber Technology*, vol. 52, p. 101942, Nov. 2019, doi: 10.1016/j.yofte.2019.101942.

[125] L. Vallejo, B. Ortega, J. Bohata, S. Zvanovec, and V. Almenar, “Experimental photonic 40 - 90 GHz millimetre-wave signal generation and 10 Gb/s 32-QAM signal transmission over hybrid fiber/FSO 5G networks,” in *International Conference on Transparent Optical Networks*, 2019, vol. 2019-July. doi: 10.1109/ICTON.2019.8840435.

[126] A. J. Seeds, H. Shams, M. J. Fice, and C. C. Renaud, “TeraHertz Photonics for Wireless Communications,” *JOURNAL OF LIGHTWAVE TECHNOLOGY*, vol. 33, no. 3, p. 579, Feb. 2015, doi: 10.1109/JLT.2014.2355137.

[127] A. Niaz, F. Qamar, M. Ali, R. Farhan, and M. K. Islam, “Performance analysis of chaotic FSO communication system under different weather conditions,” *Transactions on Emerging Telecommunications Technologies*, vol. 30, no. 2, p. e3486, Feb. 2019, doi: 10.1002/ett.3486.

[128] L. C. Andrews and R. L. Phillips, “I–K distribution as a universal propagation model of laser beams in atmospheric turbulence,” *JOSA A, Vol. 2, Issue 2, pp. 160-163*, vol. 2, no. 2, pp. 160–163, Feb. 1985, doi: 10.1364/JOSAA.2.000160.

[129] N. D. Chatzidiamantis and G. K. Karagiannidis, “On the Distribution of the Sum of Gamma-Gamma Variates and Applications in RF and Optical Wireless Communications,” 2009.

[130] L. C. Andrews and R. L. Phillips, “Mathematical genesis of the I–K distribution for random optical fields,” *JOSA A, Vol. 3, Issue 11, pp. 1912-1919*, vol. 3, no. 11, pp. 1912–1919, Nov. 1986, doi: 10.1364/JOSAA.3.001912.

[131] J. H. Churnside and S. F. Clifford, “Log-normal Rician probability-density function of optical scintillations in the turbulent atmosphere,” *JOSA A, Vol. 4, Issue 10, pp. 1923-1930*, vol. 4, no. 10, pp. 1923–1930, Oct. 1987, doi: 10.1364/JOSAA.4.001923.

[132] A. S. Madhuri, G. Immadi, and M. V. Narayana, “Estimation of Effect of Fog on Terrestrial Free Space Optical Communication Link,” *Wireless Personal Communications 2020 112:2*, vol. 112, no. 2, pp. 1229–1241, Mar. 2020, doi: 10.1007/S11277-020-07098-4.

[133] “Bayesian and frequentist estimation of the performance of free space optical channels under weak turbulence conditions,” *Journal of the Franklin Institute*, vol. 346, no. 4, pp. 315–327, May 2009, doi: 10.1016/J.JFRANKLIN.2008.11.001.

[134] A. Laourine, A. Stéphenne, and S. Affes, “Estimating the ergodic capacity of log-normal channels,” *IEEE Communications Letters*, vol. 11, no. 7, pp. 568–570, 2007, doi: 10.1109/LCOMM.2007.070302.

[135] A. N. Stassinakis, G. K. Topalis, G. S. Tombras, H. E. Nistazakis, and K. P. Peppas, “Average Capacity of Optical Wireless Communication Systems Over I-K Atmospheric Turbulence Channels,” *Journal of Optical Communications and Networking, Vol. 4, Issue 12, pp. 1026-1032*, vol. 4, no. 12, pp. 1026–1032, Dec. 2012, doi: 10.1364/JOCN.4.001026.

[136] K. P. Peppas, A. N. Stassinakis, G. K. Topalis, H. E. Nistazakis, and G. S. Tombras, “Average capacity of optical wireless communication systems over I-K atmospheric turbulence channels,” *Journal of Optical Communications and Networking*, vol. 4, no. 12, pp. 1026–1032, Apr. 2012, doi: 10.1364/JOCN.4.001026.

[137] G. T. Djordjevic, M. I. Petkovic, M. Spasic, and D. S. Antic, “Outage capacity of FSO link with pointing errors and link blockage,” 2013, doi: 10.1364/OE.24.000219.

[138] M. S. Khan *et al.*, “Probabilistic model for free-space optical links under continental fog conditions,” *Radioengineering*, vol. 19, no. 3, pp. 460–465, 2010.

[139] S. Mumtaz, J. M. Jornet, J. Aulin, W. H. Gerstacker, X. Dong, and B. Ai, “Terahertz Communication for Vehicular Networks,” *IEEE Transactions on Vehicular Technology*, vol. 66, no. 7, pp. 5617–5625, 2017, doi: 10.1109/TVT.2017.2712878.

[140] S. Bloom, E. Korevaar, J. Schuster, and H. Willebrand, “Understanding the performance of free-space optics [Invited],” 2003.

[141] V. Takhi and S. Singh, “Free Space Optical Communication System under all weather conditions using DWDM.” Accessed: Mar. 06, 2020. [Online]. Available: www.ijraset.com

[142] L. C. Andrews and R. L. Phillips, *Laser beam propagation through random media: Second edition*. 2005. doi: 10.1117/3.626196.

[143] H. Moradi, H. H. Refai, and P. G. LoPresti, “Thresholding-Based Optimal Detection of Wireless Optical Signals,” *Journal of Optical Communications and Networking, Vol. 2, Issue 9, pp. 689-700*, vol. 2, no. 9, pp. 689–700, Sep. 2010, doi: 10.1364/JOCN.2.000689.

[144] L. C. Andrews and R. L. Phillips, *Laser beam propagation through random media: Second edition*. 2005. doi: 10.1117/3.626196.

[145] M. M. Shumani, M. F. L. Abdullah, and A. Z. Suriza, “The Effect of Haze Attenuation on Free Space Optics Communication (FSO) at Two Wavelengths under Malaysia Weather,” in *Proceedings - 6th International Conference on Computer and Communication Engineering: Innovative Technologies to Serve Humanity, ICCCE 2016*, 2016, pp. 459–464. doi: 10.1109/ICCCE.2016.102.

[146] D. H. L. T. G. O. Graham A. Jones, “National Association of Broadcasters Engineering Handbook: NAB Engineering ... - y - Google Books,” *Google book*. https://books.google.co.uk/books?id=K9N1TVhf82YC&pg=PA7&redir_esc=y#v=onepage&q&f=false (accessed Jan. 11, 2021).

Appendices

Appendix 1: Generation of 60 GHz using inverted optical filter

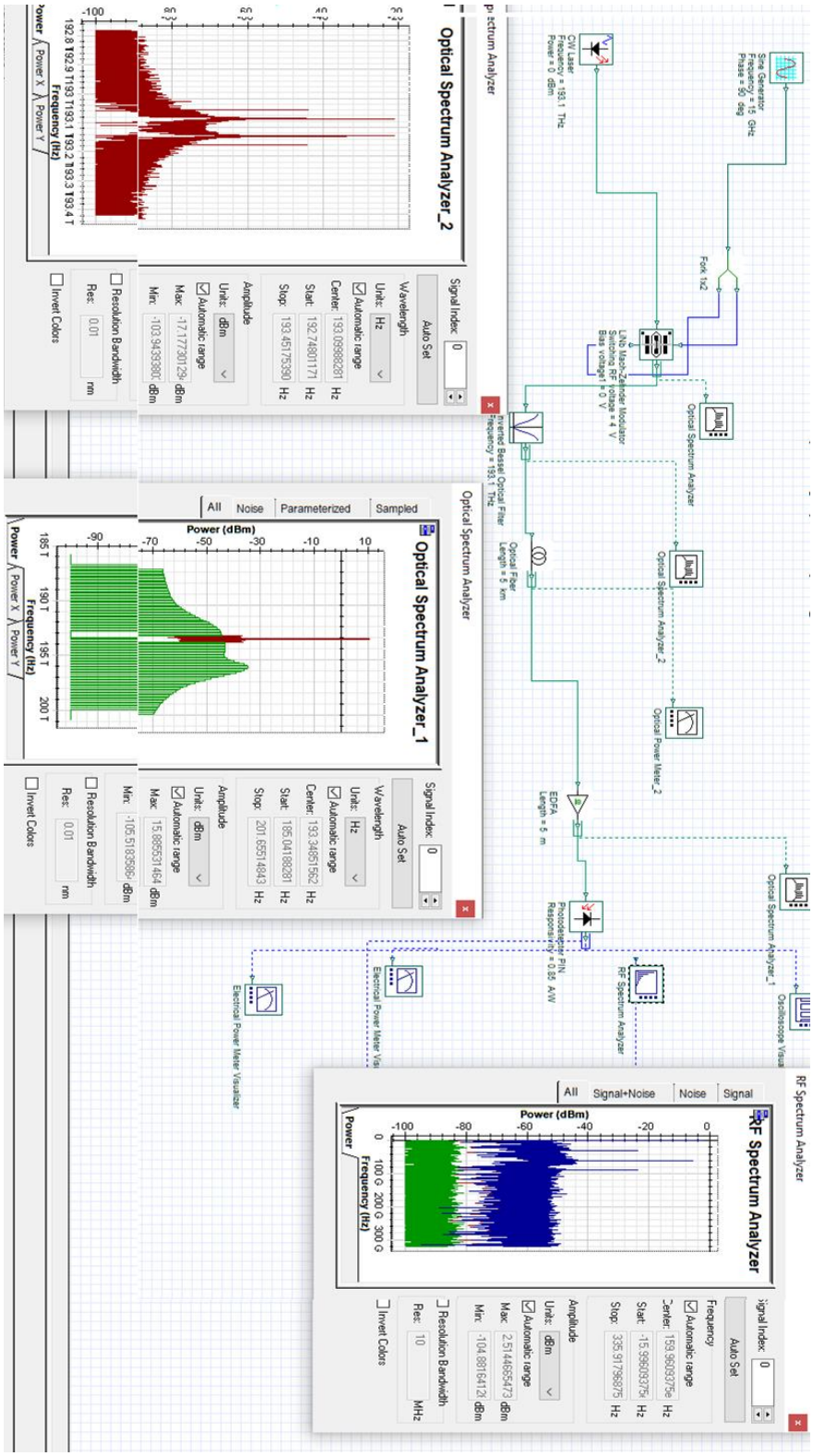

Appendix 2: Downlink data of 60 GHz with direct modulation using inverted optical filter

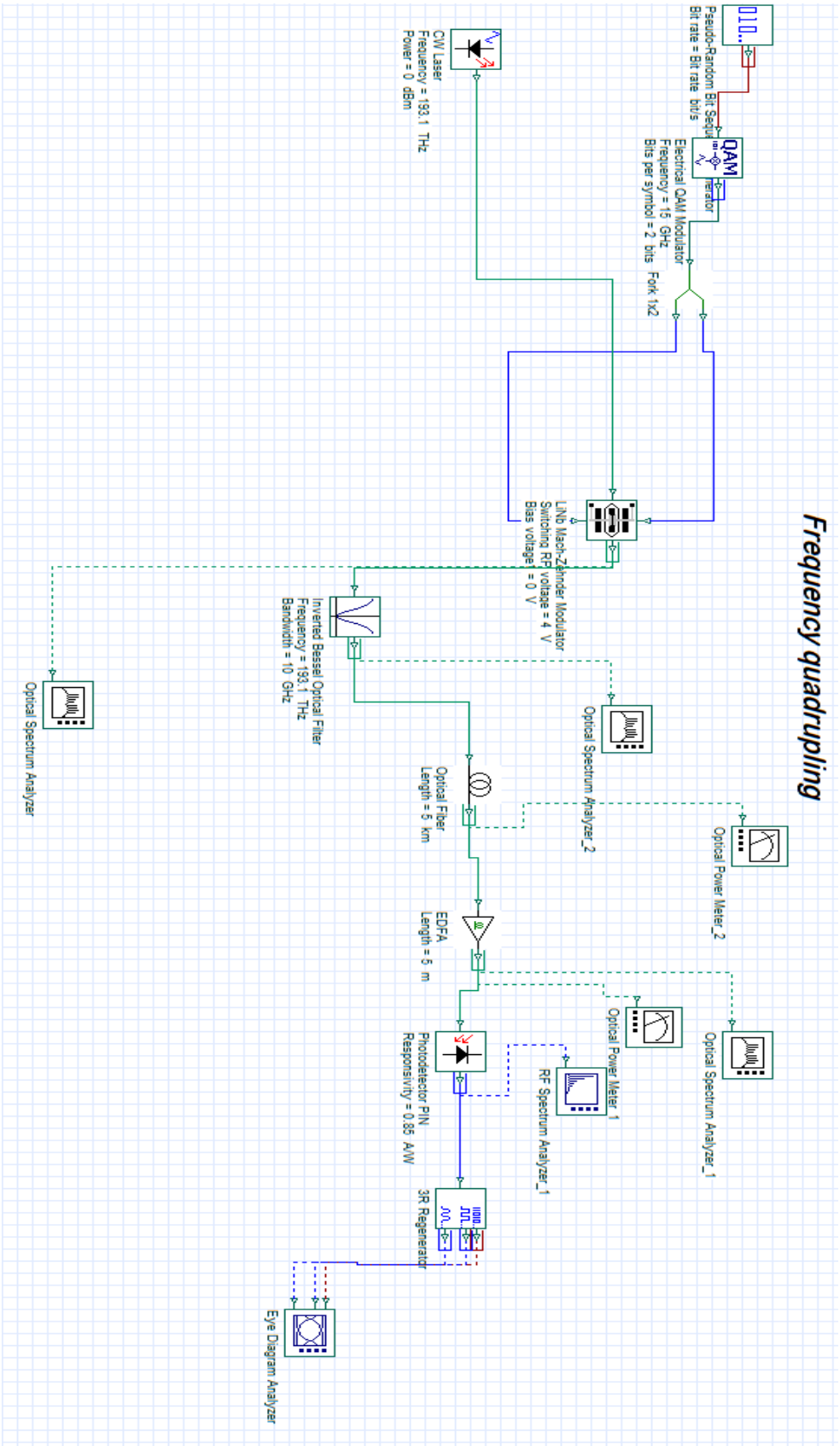

Appendix 3: Downlink data transmission using inverted optical filter after generating 60 GHz

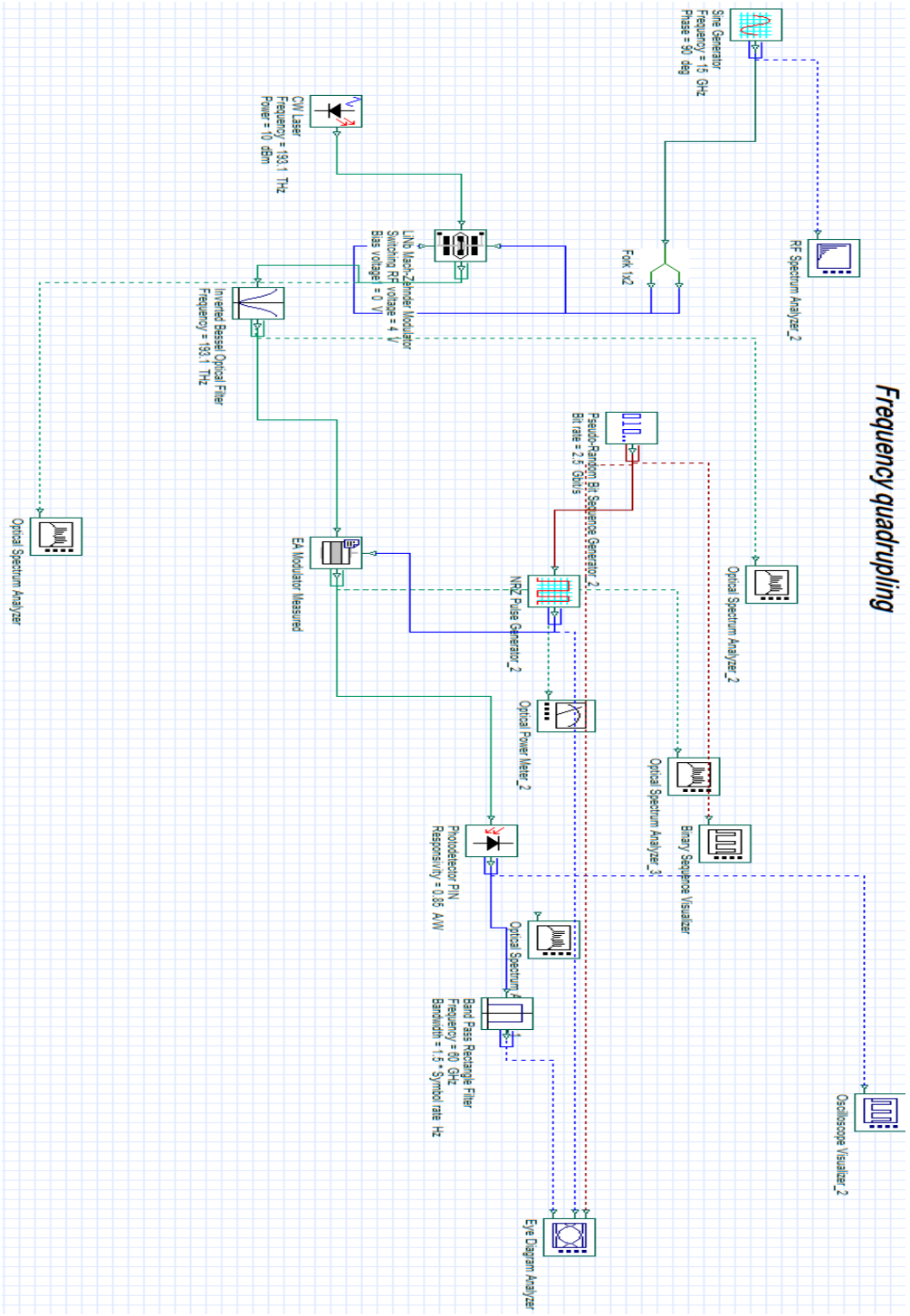

Appendix 4: Comparison of the performance of obtained 60 GHz between PIN-PD optical receiver and APD optical receiver

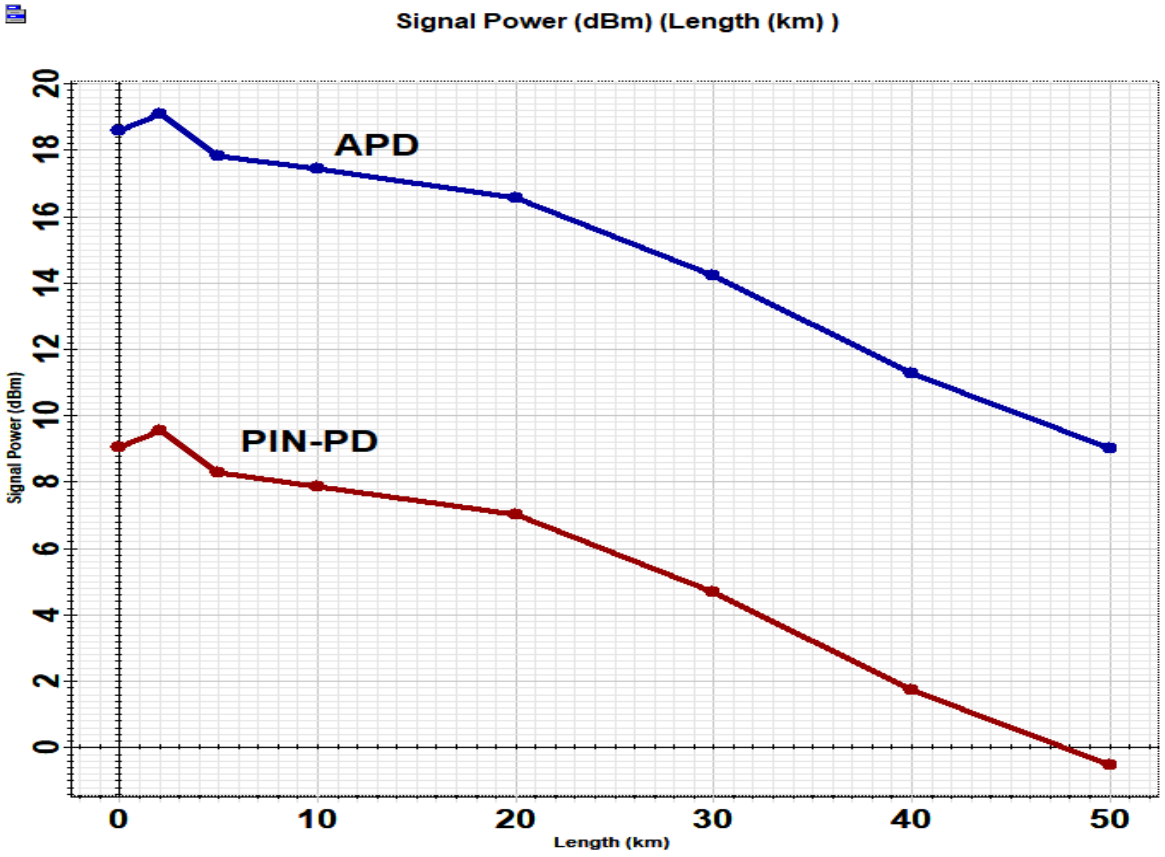

Appendix 5: Full duplex of contribution

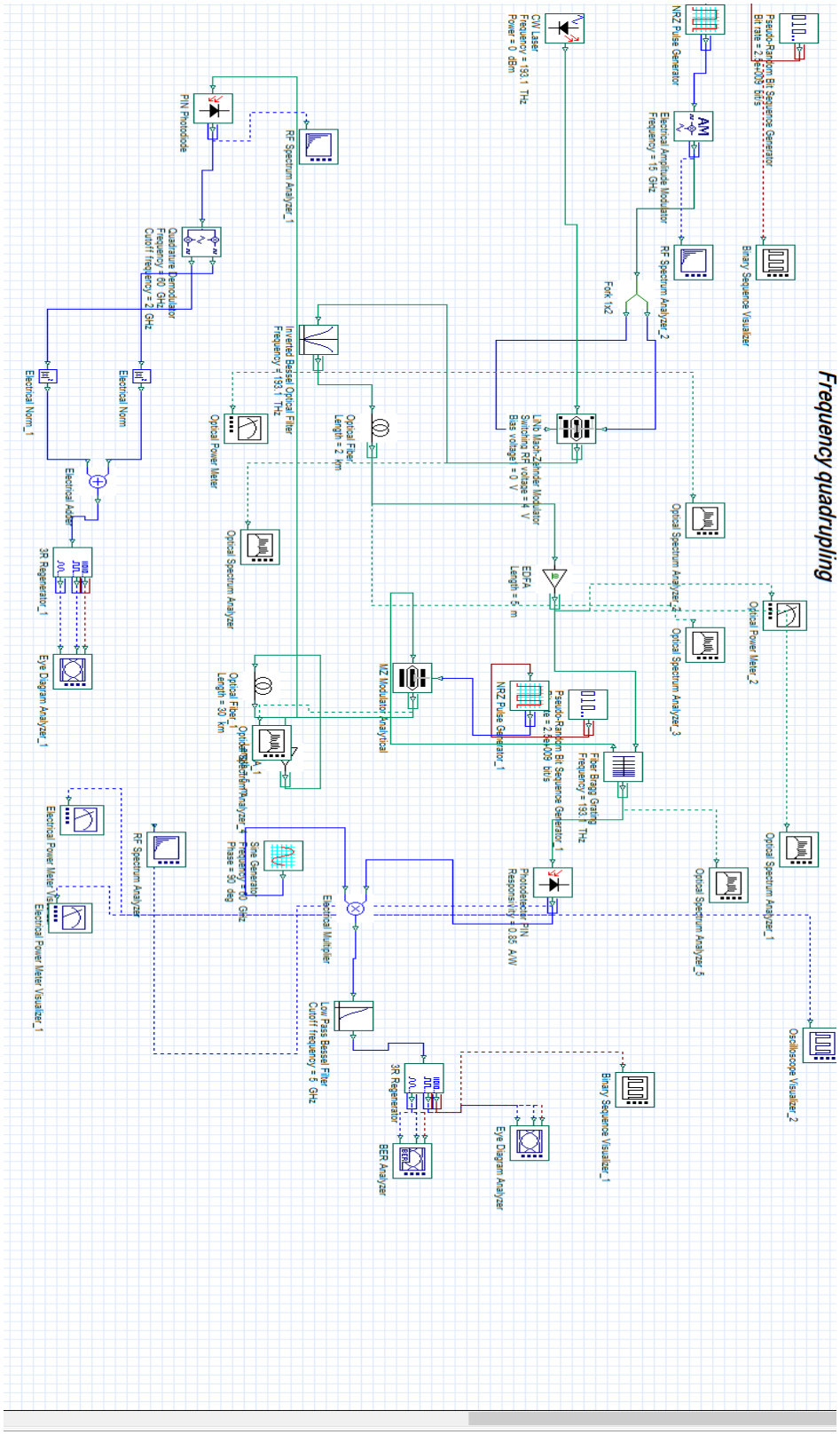

Appendix 6: Generation of 60 GHZ using quadrupling techniques

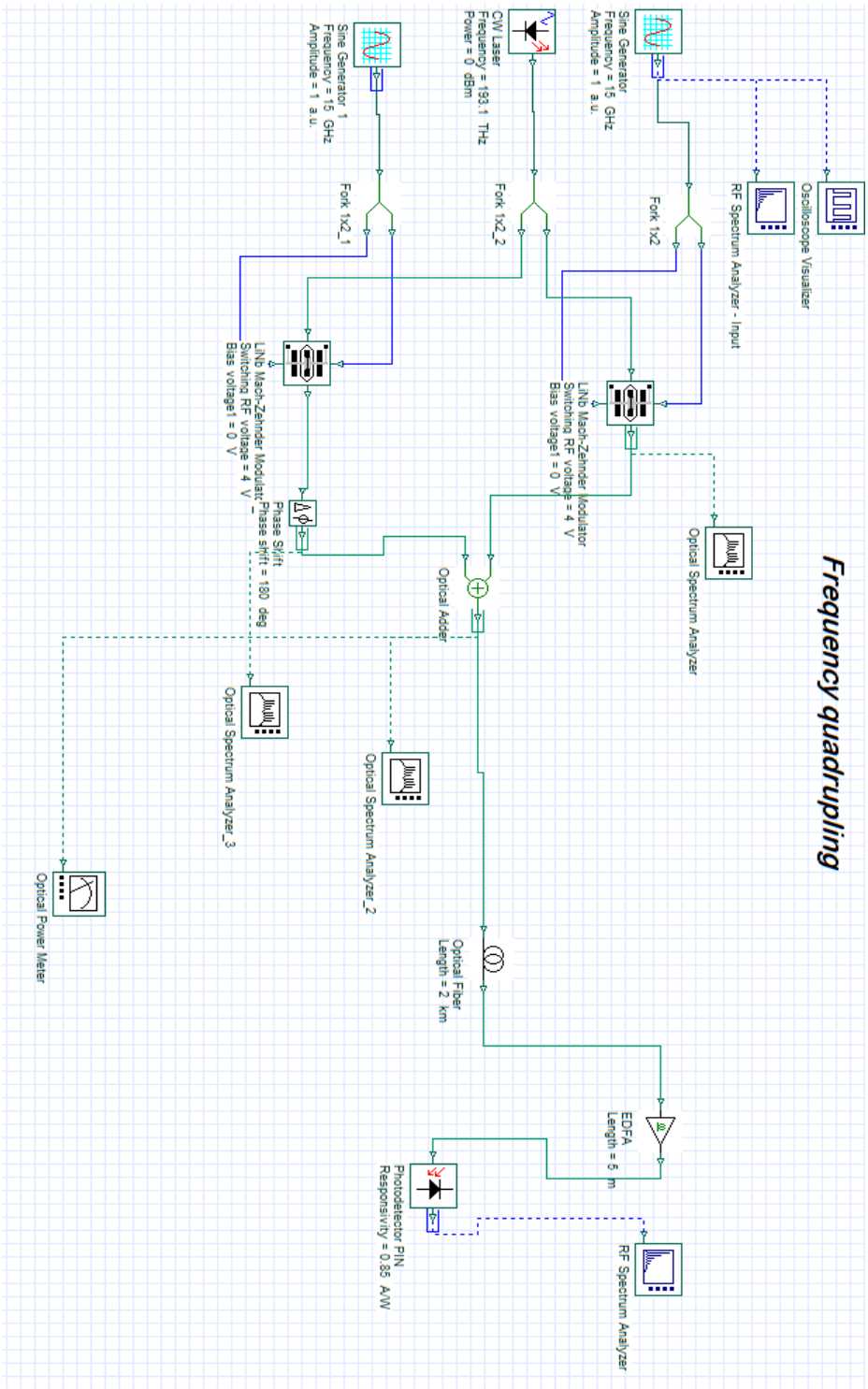

Appendix 7: Downlink data of 60 GHz transmission with PIN-PD receiver

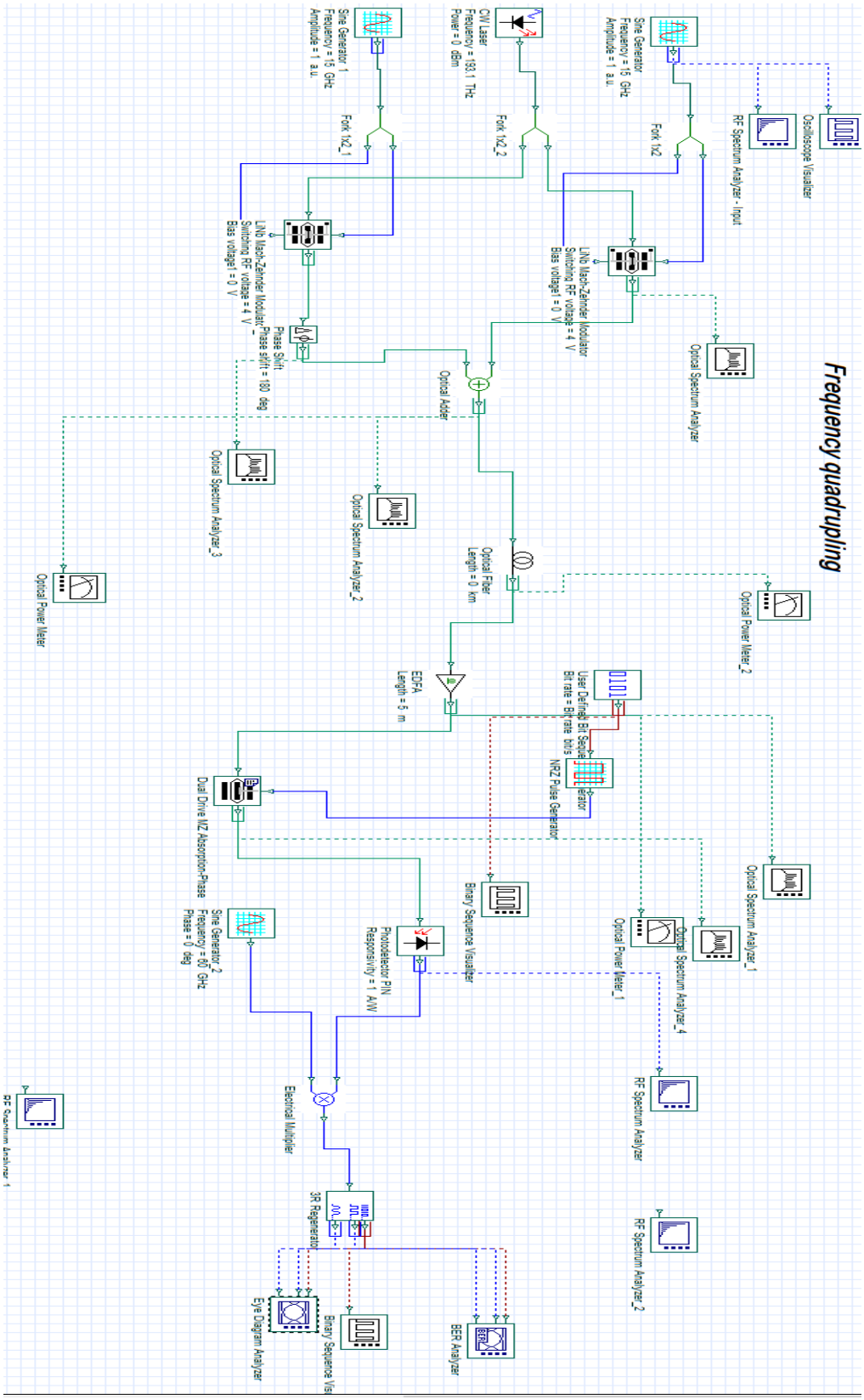

Appendix 8: Generation of 72 GHz using quadrupling technique.

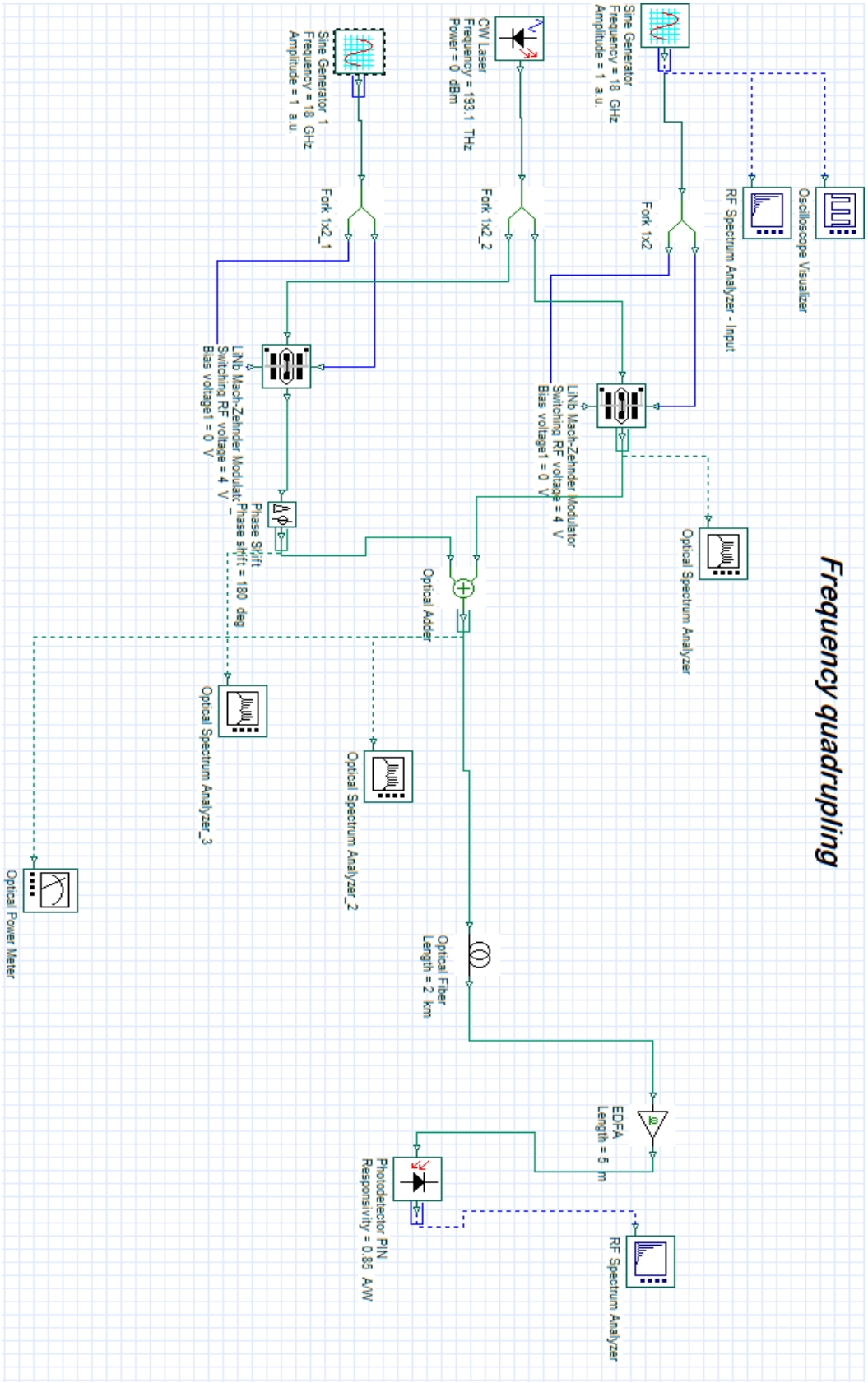

Appendix 9: Downlink of 72 GHz data transmission with PIN-PD optical receiver

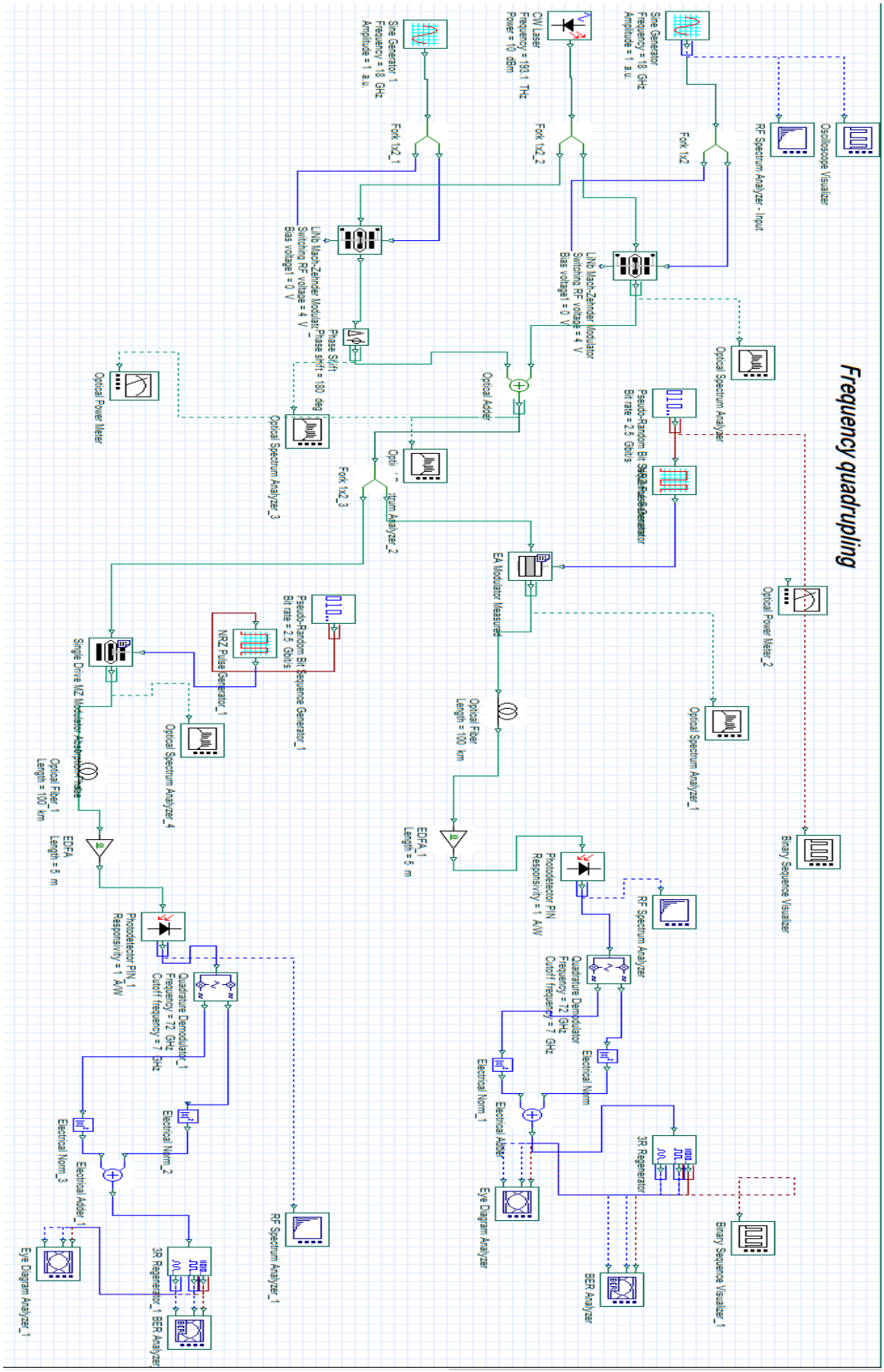

Appendix 10 72 GHz downlink data transmission with APD optical receiver

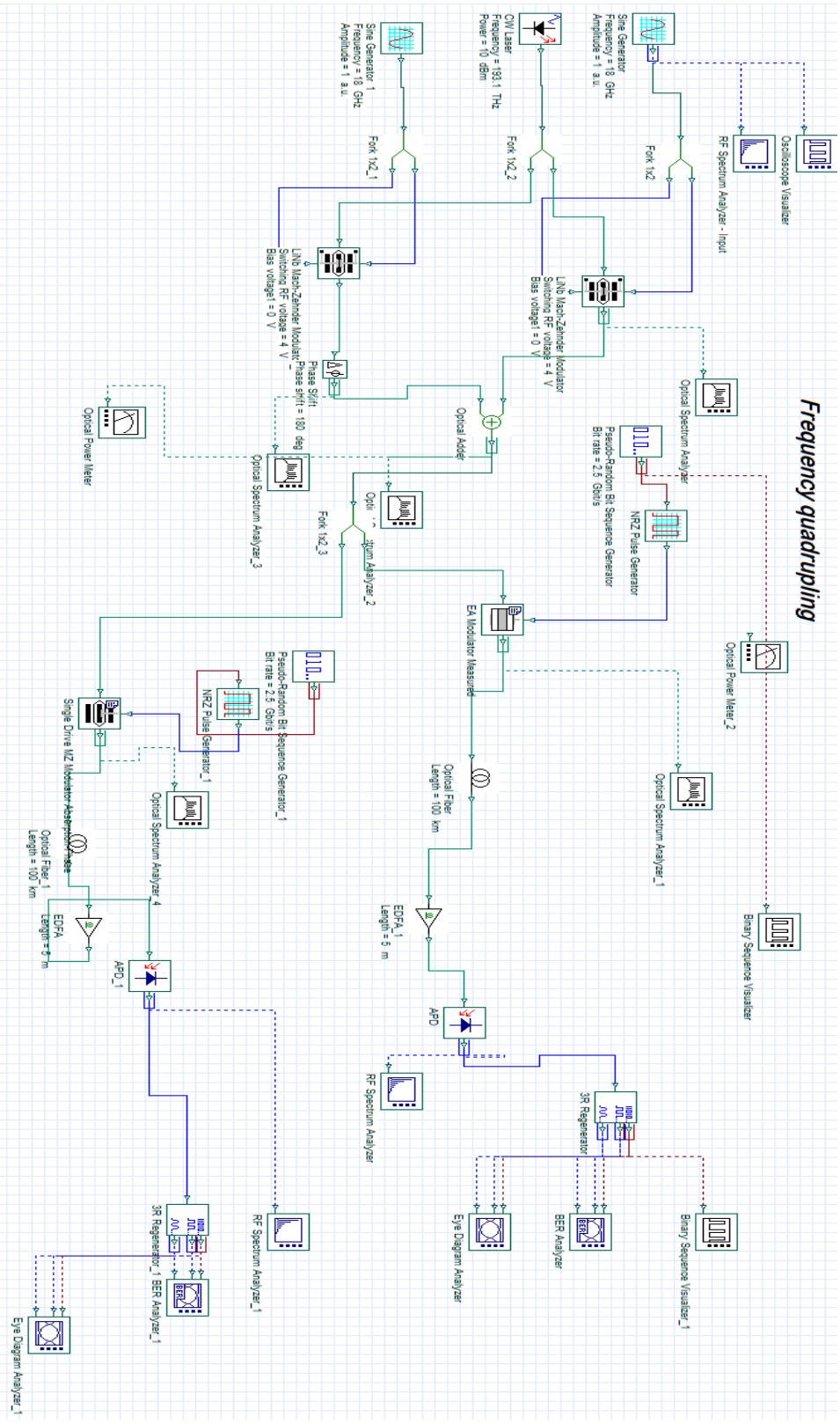

Appendix 11: Generation of 240 GHz using 12 frequency tupling technique

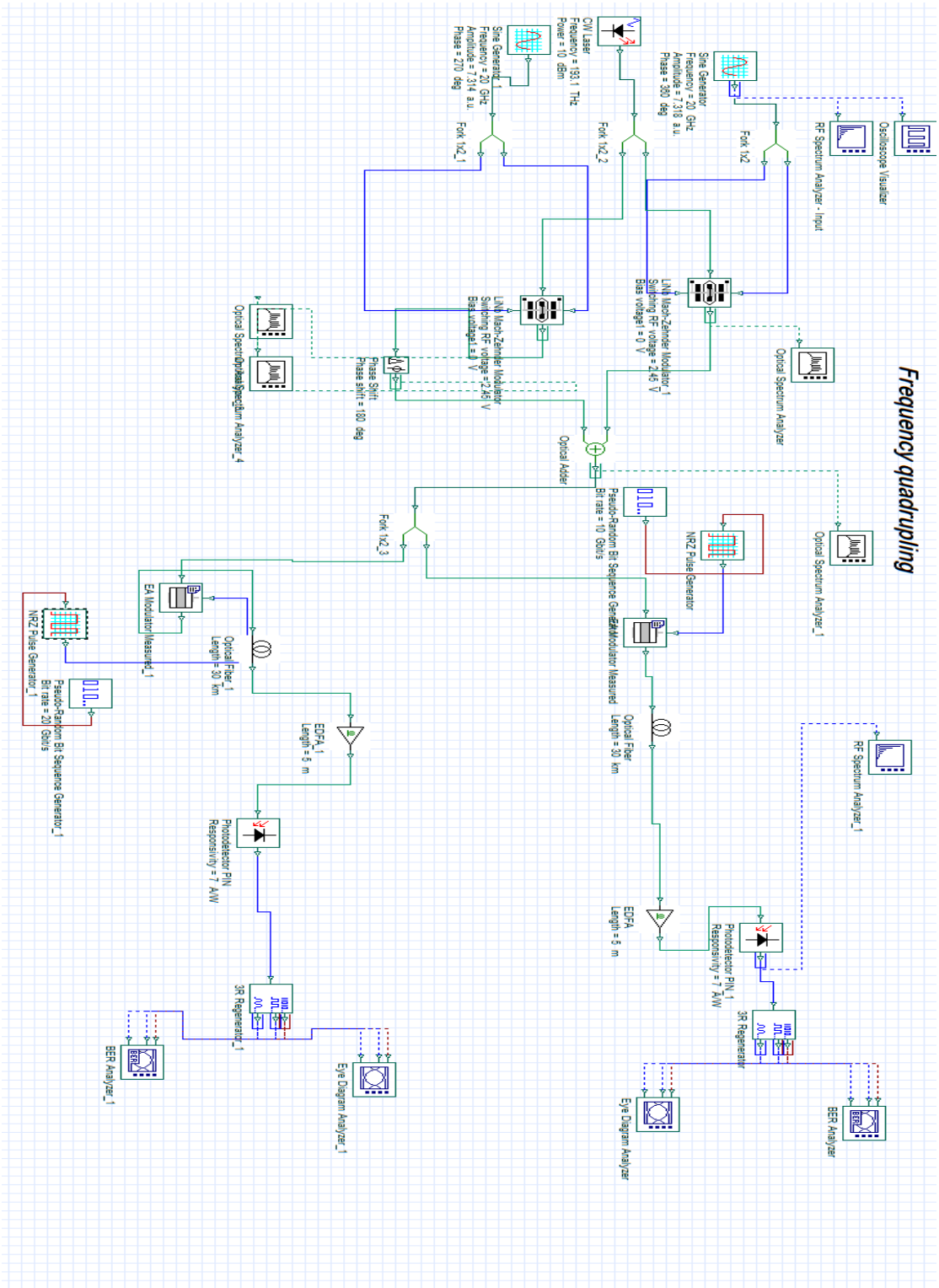

Appendix 12: The performance of 300 GHz over FSO channel.

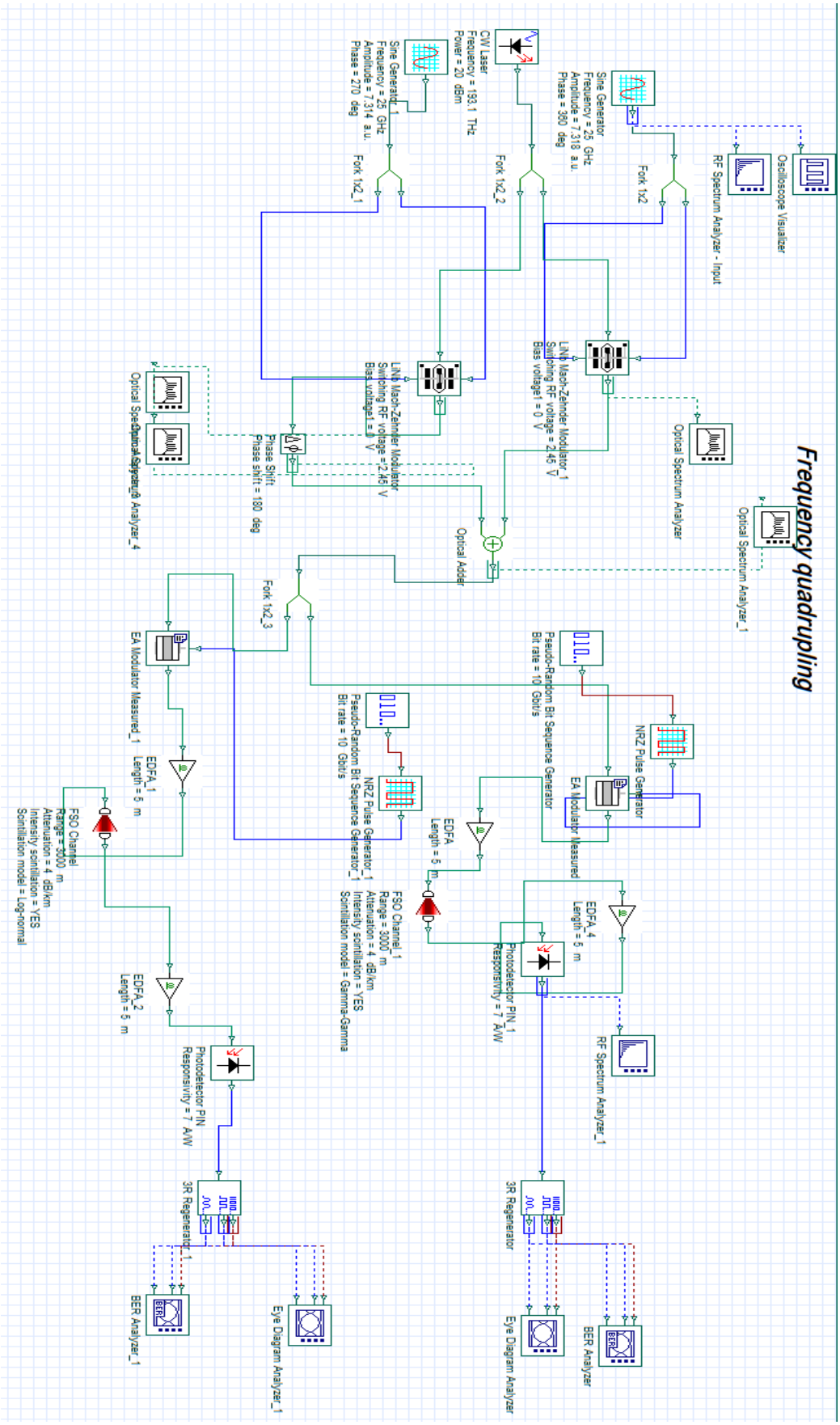

Appendix 13: The performance of 300 GHz over FSO channel at a different attenuation level.